FIRAT UNIVERSITY
GRADUATE SCHOOL OF NATURAL AND APPLIED SCIENCES
TÜRKİYE

INFLUENCE OF GRAPHITE OXIDE ON THE THERMAL AND ELECTRICAL PROPERTIES OF 4-METHYL-2-OXO-2H-CHROMEN-7-YL METHACRYLATE AND METHYL METHACRYLATE COPOLYMERS

AbdulHaleem AbdulKareem AHMAD

Master's Thesis

DEPARTMENT OF CHEMISTRY
Program of
Division of Physical Chemistry

JULY 2021

FIRAT UNIVERSITY
GRADUATE SCHOOL OF NATURAL AND APPLIED SCIENCES
TÜRKİYE

Department of Chemistry

Master's Thesis

INFLUENCE OF GRAPHITE OXIDE ON THE THERMAL AND ELECTRICAL PROPERTIES OF 4-METHYL-2-OXO-2H-CHROMEN-7-YL METHACRYLATE AND METHYL METHACRYLATE COPOLYMERS

Author
AbdulHaleem AbdulKareem AHMAD

Supervisor
Prof. Dr. Kadir DEMİRELLİ

JULY 2021
ELAZIG

FIRAT UNIVERSITY
GRADUATE SCHOOL OF NATURAL AND APPLIED SCIENCES
TÜRKİYE

Department of Chemistry

Master's Thesis

Title:	Influence of Graphite Oxide on the Thermal and Electrical Properties of 4-methyl-2-oxo-2H-chromen-7-yl methacrylate and Methyl methacrylate Copolymers
Author:	AbdulHaleem AbdulKareem AHMAD
Submission Date:	01 June 2021
Defense Date:	02 July 2021

THESIS APPROVAL

This thesis, which was prepared according to the thesis writing rules of the Graduate School of Natural and Applied Sciences, Fırat University, was evaluated by the committee members who have signed the following signatures and was unanimously approved after the defense exam made open to the academic audience.

Signature

Supervisor:	Prof. Dr. Kadir DEMİRELLİ Firat University, Faculty of Science	Approved
Chair:	Prof. Dr. Hülya TUNCER Firat University, Faculty of Science	Approved
Member:	Prof. Dr. Esin KAYA Muş Alparslan University, Faculty of Science	Approved

This thesis was approved by the Administrative Board of the Graduate School on

..... / ..... / 20 .....

Signature

Associate Prof. Dr. Kürşat Esat ALYAMAÇ
Director of the Graduate School

DECLARATION

I hereby declare that I wrote this Master's Thesis titled “Influence of Graphite Oxide on the Thermal and Electrical Properties of 4-methyl-2-oxo-2H-chromen-7-yl methacrylate and Methyl methacrylate Copolymers” in consistence with the thesis writing guide of the Graduate School of Natural and Applied Sciences, Firat University. I also declare that all information in it is correct, that I acted according to scientific ethics in producing and presenting the findings, cited all the references I used, express all institutions or organizations or persons who supported the thesis financially. I have never used the data and information I provide here in order to get a degree in any way.

02 July 2021

AbdulHaleem AbdulKareem AHMAD

PREFACE

In the name of Allah, the most beneficent, the most merciful.

This research presents details about coumarin polymers and their composites; their synthesis, and important applications in various fields for the benefit of man. Coumarin based polymers are generally linear polymers that have attracted great attention in the fields of polymer science and technology due to their fascinating electrical, thermal and optical properties. The effects of GO on the thermal and electrical properties of COUMA/ MMA copolymers have not been recorded in the literatures, therefore, this research is expected to fill obtainable gaps within the field of polymer science and technology. Thus, in this research, the effects of GO on the thermal and electrical behaviors, as well as the photodimerization of COUMA/ MMA copolymers have been studied. Coumarin based polymers are applied in photo-optical devices for information storage and management. Also, they are used in electronic devices for energy storage, optics, organic—inorganic hybrid materials and biomedical fields as antibacterial and antifungal agents.

For this purpose, all praises and thanks be to Allah, the Lord of the ‘Alamiin (mankind, jinns and all that exists). I would like to express my sincere gratitude to my research supervisor Prof. Dr. Kadir DEMİRELLI who has always been there for support, motivation, counsel, and exceptional guidance throughout the process of my research. I also wish to thank Prof. Dr. Hülya TUNCER for her invaluable support and immense knowledge she imparted to me.

I would like to pay special regards to my dear wife Maryam Ibrahim SA’AD and my daughters Nawal (Haleemah Sa’diyyah) and Amatullah for their support, prayers, patience and resilience.

My father, Dr. Abdulkareem AHMAD and my mother, Haj. Halima ALI deserve a special note of thanks. Their support, encouragement and prayers coupled with their confidence in me keep me scaling through what seems impenetrable. Also, the kind contribution of my siblings, friends and fellow lab mates is likewise well-acknowledged, with special thanks for Dr. Mustafa Ersin PEKDEMİR and Dr. Fatih BİRYAN. I hope this research contributes to general knowledge and proves beneficial to anyone who reads it.

This thesis was supported by the project number **FF.20.05** by Firat University Scientific Research Projects Coordination Unit (FÜBAP).

AbdulHaleem AbdulKareem AHMAD

ELAZIG, 2021

TABLE OF CONTENTS

ABSTRACT

Influence of Graphite Oxide on the Thermal and Electrical Properties of 4-methyl-2-oxo-2H-chromen-7-yl methacrylate and Methyl methacrylate Copolymers

AbdulHaleem AbdulKareem AHMAD

Master's Thesis

FIRAT UNIVERSITY
Graduate School of Natural and Applied Sciences

Department of Chemistry

July 2021, Page: xv + 77

The random copolymers of 4-methyl-2-oxo-2H-chromen-7-yl methacrylate (COUMA) and methyl methacrylate (MMA) P(COUMA8.9%, 24%, 36%, 49%, 65%-co-MMA) were prepared via the conventional free radical polymerization method. The copolymers were characterized by ^{1}H-NMR, FT-IR, UV-vis, TGA and DSC instruments. A kinetic study of the thermal decomposition of P(COUMA49%-co-MMA) COMCOP1 and P(COUMA49%-co-MMA)/ GO 16 wt.% COMCOP1/GO 16wt.% was investigated using thermogravimetric analysis with non-isothermal methods selected for analyzing solid-state kinetics data. The average activation energy values were calculated via FWO and KAS models in a period of α = 0.10 - 0.70. The average values of activation energy obtained from Kissinger method for COMCOP1 and COMCOP1/GO 16 wt.% were 94.5 kJ mol-1 and 101 kJ/mol, respectively. Whereas, those of estimated by FWO method were 103.5 and 87.0 kJ/mol. This study indicated that well-defined single chain polymer molecule (SCPM) via intramolecular cyclobutane formation could be obtained by the intrachain photodimerization of coumarin groups under UV irradiation at 365 nm diluted solution of COMCOP1. The photodimerization of coumarin groups in the copolymer was confirmed by UV-vis, FT-IR and ^{1}H-NMR instruments. Electrical and dielectric behaviors of the composites having a semi-conductor behavior filled with GO at various filler loadings were investigated. The activation energy values based on DC conductivity for COMCOP1 loaded GO 10 wt.% and 12 wt.% were decreased from 0.206 to 0.069 eV. Also, the E_a values estimated for COMCOP2 loaded GO 12 wt.% and 13.6 wt.% were 0.0580 eV and 0.0859 eV , respectively.

Keywords: Coumarin; Electrical investigation; Thermogravimetric analysis (TGA); Nanocomposites; Photodimerization.

ÖZET

4-metil-2-okso-2H-kromen-7-il metakrilat ve Metil metakrilat Kopolimerlerinin Termal ve Elektriksel Özellikleri Üzerine Grafit Oksitin Etkisi

AbdulHaleem AbdulKareem AHMAD

Yüksek Lisans Tezi

FIRAT ÜNİVERSİTESİ
Fen Bilimleri Enstitüsü

Kimya Anabilim Dalı

Temmuz 2021, Sayfa: xv + 77

4-Metil-2-okso-2H-kromen-7-yl metakrilat (COUMA) ve metil metakrilat (MMA)'ın [P(COUMA8.9%, %24, %36, %49, %65-co-MMA)] rastgele kopolimeleri geleneksel serbest radikal polimerizasyon yöntemi ile hazırlandı. Kopolimelerin yapısı ^{1}H-NMR, FT-IR, UV-vis, TGA ve DSC teknikleri ile karakterize edildi. P(COUMA49%-co-MMA) COMCOP1 ve P(COUMA49%-co-MMA)/ GO 16 wt% COMCOP1/GO 16wt% termal bozunmasına yönelik kinetik çalışma seçilen izotermal olmayan yöntemlerle termogravimetrik analiz kullanılarak araştırıldı. Ortalama aktivasyon enerji değerleri α = 0.10 - 0.70 aralığında FWO ve KAS modelleri kullanılarak belirlendi. COMCOP1 ve COMCOP1/GO 16 wt.% için Kissinger yönteminden elde edilen ortalama aktivasyon enerjisi değerleri sırasıyla; 94.5 kJ/mol ve 101 kJ/mol idi. Oysa FWO yöntemiyle hesaplanan aktivasyon enerji değerleri 103.5 ve 87.0 kJ/mol olduğu belirlend. D,ğer taraftan, kopolimer sisteminde moleküliçi siklobütan oluşumu iyi tanımlanmış tek zincirli polimer molekülün (SCPM) COMCOP1'in 365 nm tetrahidrofuranın seyreltik çözeltisinde UV ışığı altında kumarin gruplarının moleküliçi fotodimerleşme ile elde edilebileceği ortaya konuldu. Kopolimerdeki kumarin gruplarının fotodimerleşmesi UV-vis, FT-IR ve 1H-NMR cihazları ile doğrulandı. Grafit oksit ile farklı oranlarda hazırlanan kompozitlerin yarı iletken davranışa sahip olduğu elektriksel ve dielektrik davranışlardan belirlendi.r. 10 wt% ve 12 wt% GO katkılı COMCOP1 için DC iletkenliğinden hesaplanan aktivasyon enerji değerleri 0,206'dan 0,069 eV'ye azaldığı ortaya konuldu. Ayrıca, GO 12 wt% ve 13.6 wt% GO katkılı COMCOP2'in hesaplanan E_a değerleri sırasıyla 0.0580 eV ve 0.0859 eV olduğu anlaşıldı.

Anahtar Kelimeler: Kumarin; Elektriksel karakterizasyon,; Termogravimetrik analiz (TGA); Nanokompozitler; Fotodimerleşme.

LIST OF FIGURES

Page

LIST OF TABLES

Page

LIST OF APPENDICES

Page

SYMBOLS AND ABBREVIATIONS

Symbols

T_g : Glass transition temperature
T_i : Initial decomposition temperature
ε' : Dielectric constant
ε'' : Dielectric loss factor
ε_o : Permittivity of space
Tan δ : Tangent loss
σ_{ac} : Alternating electrical conductivity
σ_{dc} : Direct electrical conductivity
α : Activation energy conversion
E_a : Activation energy
C : Capacitance
s : Power law exponential
F : Frequency

Abbreviations

AIBN : Azobisisobutyronitrile
BPO : Benzoyl peroxide
COUMA : Coumaryl methacrylate
DMF : Dimethyl formamide
DSC : Differential scanning calorimetry
DTA : Differential thermal analysis
FRP : Free radical polymerization
FWO : Flynn-Wall-Ozawa (method)
GO : Graphite oxide
KAS : Kissinger-Akahira-Sunose (method)
MMA : Methyl methacrylate
PMMA : Poly methyl methacrylate
TGA : Thermogravimetric analysis

1. INTRODUCTION

The term "polymer" is derived from the classical Greek words "poly" (many) and "meres" (parts). Polymers, in other words, are long-chain molecules made up of a large number of repeating units with the same structure. Certain polymers, such as protein, cellulose, and silk, are found in nature, whereas many other polymers (such as polystyrene, polyethylene, and nylon) are synthesized artificially.

The birth of polymer products can be traced back to the mid-19th century in the 1830s. The plastics industry started in 1868, when John Wesley Hyatt synthesized nitrocellulose. Billiard manufacturers initiated a competition to accelerate the mass production of billiard balls. Hyatt mixed pyroxin and nitric acid with camphor and resulted in cellulose nitrate, which he called celluloid. Though in 1862, Alexander Perkes, seeking for better insulating material for the electrical industry, recognized that camphor was an efficient plasticizer for cellulose nitrate. Cellulose nitrate derives from cellulose – a natural polymer. 41 years after the discovery by Hyatt, Dr. Leo Hendrick developed phenol-formaldehyde plastics known as phenolics – applied in handles of electric iron and cookwares, grinding wheels and electric plugs. Other polymers such as cellulose acetate for toothbrushes, combs, cutlery handles, and eyeglass frames followed in the 1920s, as did urea-formaldehyde for buttons and electrical accessories, PVC for flooring, upholstery, wires, cable insulation, shower curtains, and nylon for stockings, surgical sutures, and toothbrush bristles. Despite the fact that the development of plastics slowed in the 1920s, it gained considerable momentum in 1930s and 1940s. Empirical activities resulted in the first generation of synthetic polymers. The primary emphasis was on chemical composition, with little attention paid to structure. Extensive organic and physical developments in the first half of the twentieth century led to the first understanding of polymer structural concepts – as long chains or networks of covalently bonded molecules. The classic work of German chemist Hermann Staudinger on polyoxymethylene and rubber, and American Chemist W. T Carothers on nylon, stand out clearly in this regard. Staudinger was the first to propose that polymers were made up of massive molecules, and he coined the term macromolecule to describe them. Carothers discovered nylon, and his fundamental research through which nylon was discovered contributed considerably to the elucidation of the nature of polymers. He also classified polymers as addition and condensation, which still stands today.

1.1. Polymerization reaction

Polymerization is the chemical reaction that combines relatively small moieties known as monomers to form a very large network of molecules known as polymers. The monomers may be

identical in structure and properties, or they may be composed of two or more compounds. To form a polymer molecule with distinct physical properties, at least one hundred monomer molecules must be combined in most cases.

Polymerization reactions are carried out in reactors [1] or containers (polymerization tubes) under the influence of heat and various substituents. The processes of polymerization may be homogenous or heterogeneous [2], based on phases and kinds of medium that exist between the reactants.

1.1.1. Controlled radical polymerization

Controlled radical polymerization was first defined by Szwarc [3] as a chain growth process without transfer or termination. Controlled radical polymerization involves absolutely pure reactants incapable of causing termination. Controlled radical polymerization enables end group control and often used in the production of block copolymers. In controlled radical polymerization, termination occurs only when all the monomers have been used, and could continue when additional monomers are introduced. Currently, NMP, RAFT, and ATRP are the three most effective CRP methods.

ATRP was developed in 1995 [4] as an expansion of transition metal catalyzed atom transfer radical addition (ATRA). The origin is the Kharasch addition reaction; where a polyhalogenated alkene is added to an alkene, forming a 1:1 addition product. Figure 1.1 below shows the schematic representation of general ATRA reaction.

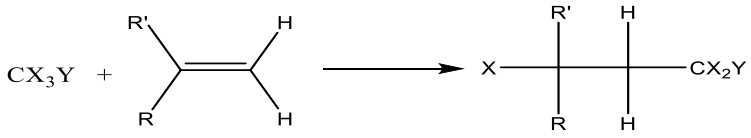

Figure 1.1. Schematic representation of general ATRA reaction

Radicals produced by light add to the double bond of the alkene. Transition metal complexes can also catalyze this reaction via a redox mechanism. Here, the radical addition and the halogen transfer is more efficient. Figure 1.2 below shows the mechanism for ATRA reaction.

$$M^n + CXCl_3 \rightleftharpoons [M_t^{n+1}]\,Cl + {*}CXCl_2$$
$${*}CXCl_2 + CH_2{=}CRR' \longrightarrow Cl_2XC\text{-}CH_2\text{-}CRR'$$
$$Cl_2XC\text{-}CH_2\text{-}CRR' + [M^{n+1}]Cl \rightleftharpoons Cl_2XC\text{-}CH_2\text{-}CRR'\text{-}Cl + M^n$$

Figure 1.2. Schematic representation of ATRA

ATRP is an accurate, efficient, and well-controlled technique for the preparation of different types of membranes [5]. Therefore, due to its unique properties, this technique is used widely by researchers for the preparation of temperature-responsive membranes. ATRP mechanism is given in Figure 1.3 below.

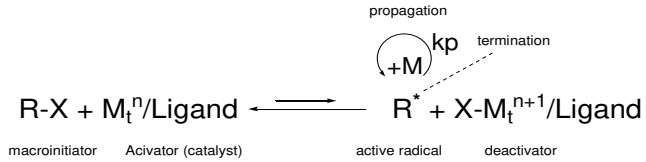

Figure 1.3. Mechanism of ATRP as reported by Matyjaszewski et al

In ATRP, a dynamic equilibrium is established between the metal complex and the corresponding ligand. The equilibrium is shifted towards the dormant species in order to allow for control of molecular weight and architecture of polymer, and to keep the concentration of the radical at a minimum, thereby suppressing the radical termination. Polymerization in this case is self-regulating – persistent radical effect (PRE). Control over ATRP can be monitored by addition of small amounts of deactivator. ATRP polymers can be used as macroinitiators similar to alkyl halides used in the reaction, also, it is often used to produce star polymers, block copolymers.

Monomers in ATRP include acrylonitrile, tert-butyl methacrylate (t-BMA), benzyl methacrylate (BzMA), trimethylsilyl methacrylate (TMSMA) and so on. Initiators in ATRP include 3-bromoprop-1-ene, 2-bromobutanenitrile, 2-cyanoacetamide and so on.

1.1.2. Free radical polymerization (FRP)

FRP is one of the most important synthesis routes for obtaining vinyl polymers [6]. The polymerization starts off with a molecule called initiator. Common initiators are benzoyl peroxide (BPO) and 2,2'-azo-bis-isobutyrylnitrile (AIBN). Both molecules have a strong tendency to fall apart in a rather unusual way; that is, when they split, the pair of electrons in the bond which is broken, will separate. The two fragments with unpaired electrons are called free radical initiators. Following its generation, the initiating free radicals react with a monomer unit thereby creating growing polymer chains. FRP mechanism is given in Figure 1.4 below.

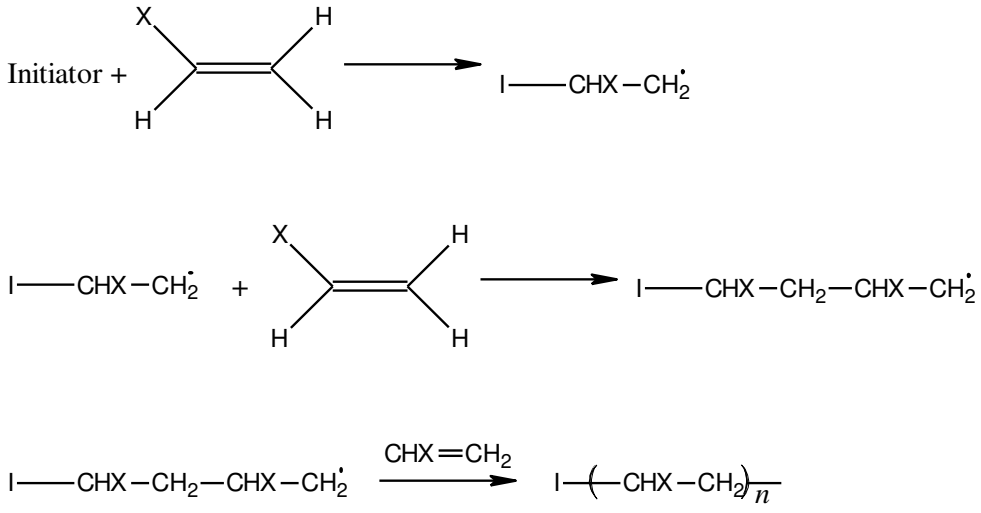

Figure 1.4. Schematic representation of FRP

Where X is a substituent which could be any of the following: C_6H_5, Cl, Br, $OCOCH_3$, COOR or H. The mechanism also includes disubstituted monomers such as vinylidene chloride and methyl methacrylate.

1.2. Coumarin (2H-chromen-2-one) containing monomers

Coumarin is a lactone compound formed by a benzene ring fused to an α-pyrone. Compounds of coumarin possess conjugated systems having high electron density and reasonable charge transport behaviors.

Coumarin, depicted in Figure 1.5, was first synthesized in 1868 and used in the pharmaceutical industry as a precursor in the synthesis of anticoagulant pharmaceutical products [7]. The molecule is made up of a benzene molecule having two adjacent Hydrogen atoms replaced by a lactone chain. The result is a six membered heterocycle sharing two carbon atoms with the benzene ring. The oxygen containing heterocycle of coumarins makes the compounds important in the field of medicinal chemistry.

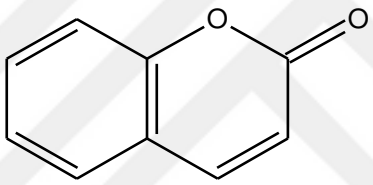

Figure 1.5. Structure of coumarin

Quite a lot of investigations have proven coumarin to show different behaviors under acidic and basic conditions, making it a monomer with enormous potential. Polymers based on coumarin monomer are used as fluorescent sensors for metal ion detection showing reasonable sensitivity towards Cu(II) and Hg(II). A wide range of other applications of coumarin based polymers are seen in the building of electronic devices and photo-responsive polymers. The photo-reactive coumarin ring attached to homopolymers or copolymers containing acrylic and methacrylic moieties allows the formation of thermo- and photo-responsive polymers through a [2 + 2] cycloaddition. This property indicates the applicability of coumarin based polymers in drug delivery [8] based on light cross linkable and pH de-cross-linkable units. Also, incorporating coumarin units on linear silicon polymer chains formed silicon polymer networks exhibiting thermoplastic elastomer properties in absence of covalent cross-links whose properties depend on the concentration of the coumarin compound [9].

1.3. Synthesis of Coumarins

The origin of coumarins may be dated back to 1820 when Vogel [7] extracted the compound from Tonka bean plant. However, coumarins were first chemically synthesized by W.

H Perkin in 1868; a sodium salt of salicylaldehyde was heated in acetic acid – a process termed as Perkin reaction. Furthermore, Stecker, Fittig and Tiemann first proposed the structure of coumarin as 1-benzopyran-2-one, which was universally accepted in 1872, and the crystal structure investigated firstly in 1941 by Swamy [10]. Currently, coumarins are synthesized through several methods, generally based on condensation reactions, and solvent-free reactions such as irradiation. Two among the various methods are discussed below.

1.3.1. Synthesis of Coumarin by Pechmann Condensation

Pechmann condensation involves synthesizing coumarins by the reaction of phenols with β-keto esters as given in Figure 1.6 below.

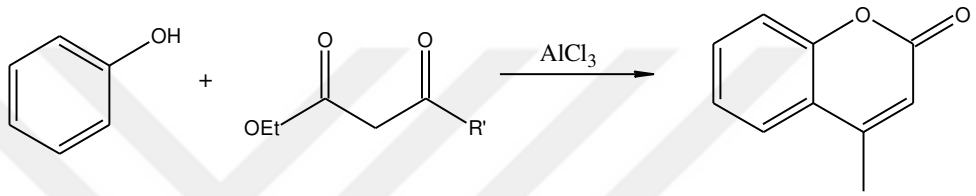

Figure 1.6. Pechmann condensation for the synthesis of coumarins

Mechanism of Pechmann condensation

The reaction is carried out with a strong Bronsted-Lowry or Lewis acid (such as methane sulfonic acid and $AlCl_3$ respectively) which catalyzes transesterification and keto-enol tautomerization. Subsequently, coumarin skeleton is formed by Michael addition, followed by rearomatization. Finally, acid-induced elimination of water gives the final coumarin compound, as illustrated in Figure 1.7 below.

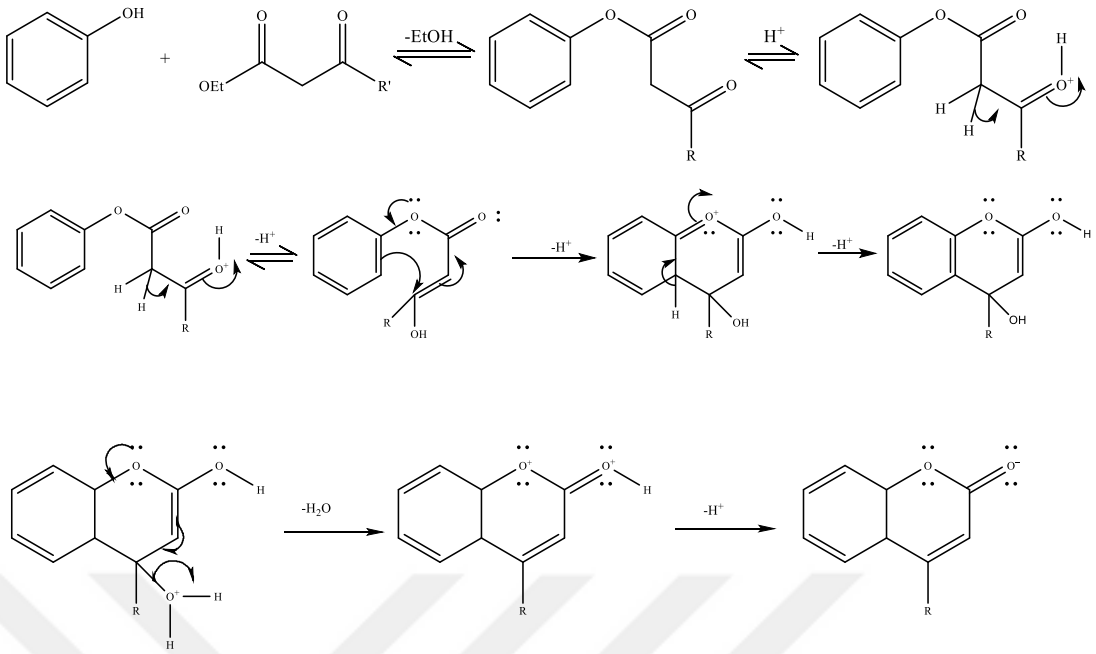

Figure 1.7. Mechanism of Pechmann condensation

1.3.2. Synthesis of Coumarin by Knoevenagel Condensation

In a study by Melita et al (2020), the synthesis of coumarin was carried out by Knoevenagel condensation [11], where a deep eutectic solvent (DES) was used. DES was prepared by mixing choline chloride (ChCl) and zinc chloride at 100°C [12]. As given in Figure 1.8 below, the coumarin derivatives were prepared by reaction of simple or substituted salicylaldehydes and methylene compounds. In the reaction, DES was used both as solvent and as catalyst.

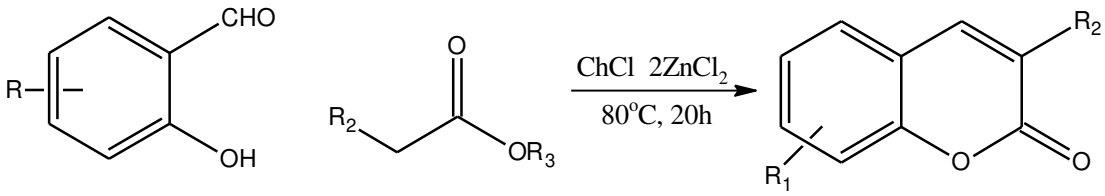

R_1 (H, OH, Br), R_2 (COOMe, CN, COPh), R_3 (Me, Et)

Figure 1.8. Knoevenagel condensation

1.4. Synthesis of 7-hydroxy-4-methyl-2H-chromen-2-one

Synthesis of 7-hydroxy-4-methyl coumarin was carried out by dissolving 1g resorcinol and 1.15mL ethyl acetoacetate in 6 mL trifluoroacetic acid at ambient temperature [13]. The reaction is represented in Figure 1.9. The mixture was quenched with ice cold water, the precipitate was filtered, washed with water and dried under vacuum. The product was collected as a white solid.

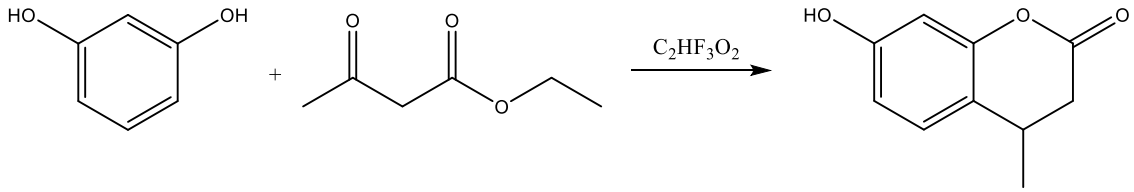

Figure 1.9. Schematic representation for production of 7-hydroxy-4-methyl-2H-chromen-2-one

1.5. Modification of coumarin bearing monomers with methacryloyl chloride

Synthesis [14] of 7-methacryloyloxy-4-methylcoumarin (MAOMC) was carried out by Pechmann condensation, described as follows; A three-necked round-bottom flask fitted with a thermometer, a stirrer, and a dropping funnel containing 5g (0.028 mol) 7-hydroxy-4-methyl coumarin, 6.9 mL (0.049 mol) Triethylamine and 300 mL ethylmethylketone was cooled between −5 °C to 0 °C. 3.87 mL (0.039 mol) Methacryloyl chloride in 25 mL ethylmethylketone was added dropwise into the flask maintained between −5 °C to 0 °C. The reaction is shown in Figure 1.10. The reaction was allowed to proceed for 1 h at 0°C −5°C with constant stirring, then another 2 h at room temperature. The reaction mixture was washed with water followed by 1% NaOH solution to remove the traces of methacryloyl chloride. The organic layer was dried in anhydrous sodium sulphate. The product was purified by recrystallization from methanol and obtained as white crystals.

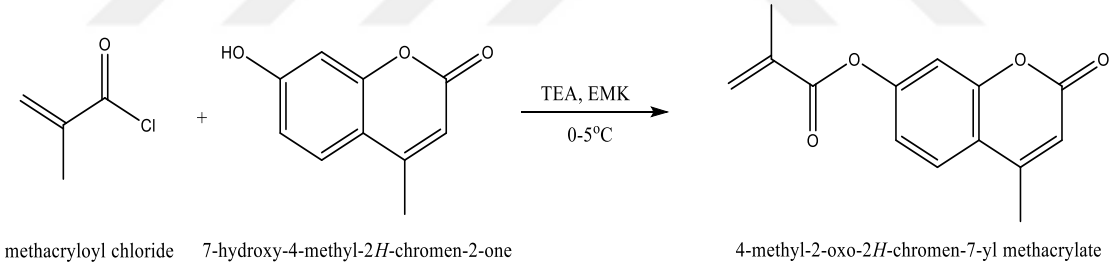

methacryloyl chloride 7-hydroxy-4-methyl-2*H*-chromen-2-one 4-methyl-2-oxo-2*H*-chromen-7-yl methacrylate

Figure 1.10. Synthesis of 7-methacryloyloxy-4-methyl coumarin

1.6. Polymers Bearing Coumarin Pendant Group

Coumarin based polymers are also known as ‘antenna’ or ‘light-harvesting’ polymers [15]. They are extensively studied as a result of their several interesting properties. Polymers based on coumarin side chains are reported [16] to be generally linear polymers with the coumarin group as a pendant or terminal group on the polymer chain. Fig 1.11 below shows an illustration of free radical copolymerization of MMA and COUMA depicting the linear structure of the polymer compound under specific conditions.

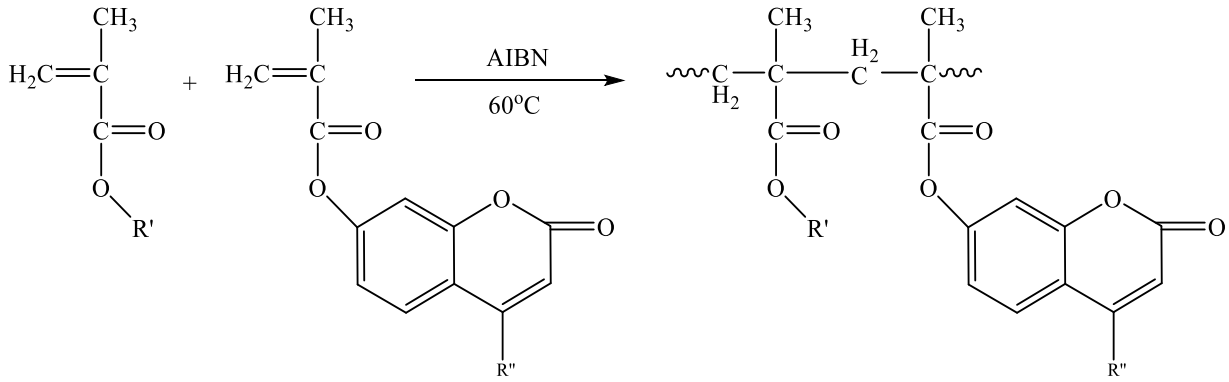

Figure 1.11. Synthesis of P(COUMA-co-MMA) via FRP

Coumarin polymers are applied in various fields such as electronics, liquid-crystal materials, optics [17], biomedical applications, organic-inorganic hybrid materials. Coumarin derivatives such as thiazole, azetidinone and oxazole are also found to be effective against bacterial and fungal infections [14].

As a result of their fascinating photochemical and photophysical properties [18, 19], the analogues of coumarin are used in photo-optical devices for information storage and management. Some derivatives of coumarin are able to undergo a photo-induced cyclodimerization to produce a dimer of cyclobutane upon UV irradiation at ≥ 300 nm, and reverse photo-cleavage of the dimer can be induced by UV irradiation of higher energy photons at >250 nm. Figure 1.12 below gives the scheme for the photodimerization of coumarin polymers.

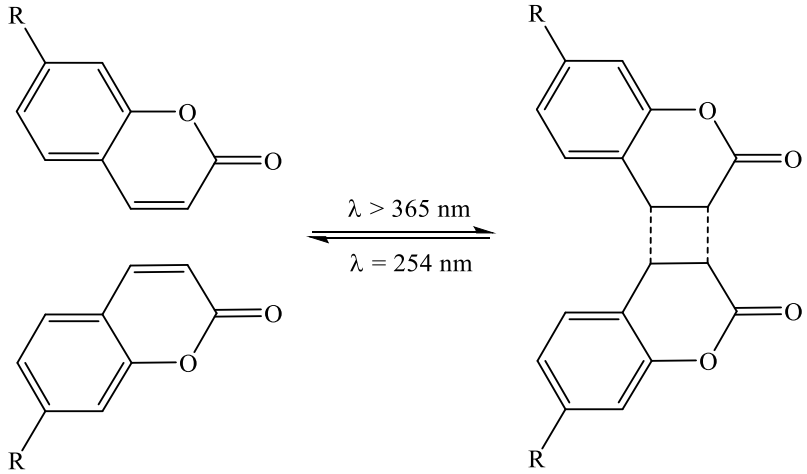

Figure 1.12. Intramolecular photocyclization of coumarin-based polymers

1.7. Nanocomposites

Nanocomposites are materials that incorporate nanosized particles into the matrix of a standard material. They are broad range of materials consisting of two or more components with at least one component having dimensions in nanometer region (between 1-100nm).

Nanocomposites consists of two phases (nanocrystalline and matrix phase). The phases may be composed in the following combination.

- Inorganic-inorganic
- Inorganic-organic
- Organic-organic

Nanocomposites are an amazingly acceptable option in contrast to regular composite materials due to their exceptional properties and are tracking down a wide scope of uses in different fields.

Nanocomposites consolidate nanosized particles into a grid of standard material like a polymer. Polymer nanocomposites are materials in which nanoscopic inorganic particles, regularly 10-100 A in at least one dimension, are dispersed in a polymer (organic) network to significantly improve the properties of the polymer.

The structure of nanocomposites generally comprises of the matrix material containing the nanosized reinforcement segments as particles, bristles, strands, nanotubes, etc. The viability of the nanoparticles is to such an extent that the measure of material added is ordinarily just somewhere in the range of 0.5 and 5% by weight.

Addition of nanocomposites to polymeric materials improves properties like sturdiness, mechanical strength, electrical and thermal conductivities [20]. Nanocomposites likewise significantly improve modulus and dimensional stability, diminished penetrability, substance opposition, surface appearance, and optical lucidity of the network materials.

Nanocomposite frameworks with carbon nanotubes have been a subject of late exploration and advancement since their revelation in 1991 and there has been a consistent and persistent expansion in a few distributions on this subject, including surveys and licenses every once in a while. Nanocomposites are additionally found in nature, for instance in the design of the abalone shell and bone. Nanocomposites vary from traditional composites because of the great surface territory to the volume proportion of the building up nanoparticles and their extraordinarily high angle proportion. The building up material can be comprised of particles (for example minerals, metallic nanoparticles, Carbon nanotubes), sheets (for example shed earth stacks, graphene), or filaments. The zone of the interface between the lattice and nano-support is regularly a significant degree higher than the customary composites. Clays are a gathering of nanofiller materials that have been widely utilized for the planning of polymer grid nanocomposites. Polymer/clay nanocomposites have been getting huge consideration in the scholarly world and enterprises because of their improved properties contrasted with regular composites.

Nanostructured carbon/polymer composites, because of their improved mechanical qualities, high heat resistance and sophisticated optical and electrical features, have acquired extensive consideration in the worldwide research communities for quite a long time. The

remarkable properties of carbon and its allotropes represent the wide assortment of their applications in numerous fields.

Generally, a greater part of polymers is insulating and have exceptionally low centralization of free charge carriers and conductivities ranging from 10-12 and 10-15 S/cm. They are named dielectrics and their electrical response is identified with relaxation phenomena that can be described through the real and imaginary parts of dielectric permittivity. Incorporating conductive considerations, such as carbon structures in a polymer grid, influence the subsequent electrical properties, and at a critical concentration, the composite's conductivity increments by significant degrees [21].

1.7.1. Classification of Nanocomposites

Nanocomposites can be classified into three according to the matrix and reinforcement materials used in their construction.

i. **Ceramic Matrix Nanocomposites**: ceramic matrix nanocomposites with a phase having nano dimension are another age of engineering and designing materials, having a wide scope of utilizations in the industrial sector. The microstructure of nanoceramic composites brings about remarkable electrical and mechanical properties. Generally, the regular methods utilized in microcomposites concepts are conventional powder method, polymer precursor method, spray pyrolysis, and chemical methods for example, sol-gel, colloidal and precipitation approaches and template synthesis. Al_2O_3/SiO_2, SiO_2/Ni, Al_2O_3/TiO_2 and Al_2O_3/SiC are common examples of ceramic matrix nanocomposites.

ii. **Metal Matrix Nanocomposites**: metal matrix nanocomposites are materials that consist of metal or alloy matrix filled with nanoparticles, and exhibit different physical, chemical and mechanical properties from those of the matrix material. Metal matrix nanocomposites are used in metals and alloys to improve behaviors such as wear resistance, dumping and mechanical properties. The nanomaterials serve as barriers in dislocation movements and hence improve the mechanical properties. Common methods for preparation of metal matrix nanocomposites are liquid metal infiltration, vapor techniques, rapid solidification, colloidal and sol gel techniques. Examples of metal matrix nanocomposites are Fe-Cr/Al_2O_3, Ni/ Al_2O_3, Fe/MgO, Al/CNT and Mg/CNT.

iii. **Polymer Matrix Nanocomposites**: Polymer nanocomposites are materials that have polymer as a lattice material and nanoadditives are utilized as reinforcement. The added substances can be one-dimensional in form of nanotubes and strands, two-dimensional in form of layered materials like clay or three-dimensional

(spherical particles). The other astounding properties of polymer nanocomposites are barrier resistance, flame retardancy, wear resistance, excellent electrical and optical properties.

An ordinary polymer composite is a blend of polymer (network) and a filler (reinforcement). Polyamide is a thermoplastic polymer, and carbon and glass fibers are for the most part utilized as reinforcement materials. In the aeronautic industry, carbon filaments are broadly utilized as reinforcement materials. The choice of reinforcement material relies upon the applications. The polymer matrix and fillers are generally bonded by weak intermolecular forces, notwithstanding, chemical bonding is often utilized. To achieve improvements on chemical, electrical and mechanical properties, the nanoparticle must be dispersed on atomic or molecular (nanoscale) levels within the matrix, thus remarkable improvements on chemical, electrical and mechanical properties can be accomplished.

1.7.2. Techniques of manufacturing polymer matrix nanocomposites

The following pathways are employed for preparation of polymer matrix nanocomposites;

• **Sol-gel polymerization method**: Is a method that involves colloidal suspension or dispersion of solid nanoparticles in a solution of monomer. The mixture forms interconnecting 3D network phases through polymerization reaction and hydrolysis. The 3D polymer network extends throughout the solution. The polymer serves as a nucleating agent promoting the growth of layered crystals, which grow and, the polymer is seeped between the layers forming a nanocomposite.

• **Melt intercalation method**: This method involves mixing of nanofillers and polymer matrix at molten temperature. The mixture of the polymer and the nanofiller is heated and cooled statically or in parts. Melt intercalation method is encouraging and widely used in industries. The method is consistent with injection and extrusion molding and it allows the use of polymers that are not suitable for in situ polymerization and solution blending.

• **In situ polymerization method**: This involves the swelling of the nanofillers in a solution of monomer. The low molecular weight of the monomer allows it to easily seep in between layers within the solution and causing swelling. The mixture is then polymerized via heat, radiation, diffusion or organic initiation. The polymerization is carried out within the interlayers forming exfoliated or intercalated nanocomposites. The nanofillers are synthesized in presence of polymer chains. Both solutions (polymer matrix and nanofillers) are dissolved in an aqueous solution and reflux at elevated temperatures. The polymer chains are confined within the fillers, and nucleation and growth of the nanofiller layers take place at high temperatures.

• **Direct mixing of polymer and nanofiller**: This method is suitable for manufacturing polymer matrix nanocomposites. It involves two (2) general methods of polymer/ nanofiller mixing.

o Melt compounding: This involves addition of nanofillers to the polymer matrix above the glass transition temperature of the polymer in the absence of solvent. In melt compounding method, the hydrodynamic force is effected in the polymer melt through viscous drag. This breaks down the total nanofiller content and hence results in a homogenous nanofiller dispersion within the matrix.

o Solvent method: In solvent method, nanoparticles are dispersed in a solvent and the polymer in a co-solvent. The resulting nanocomposites are evaporated through solvent coagulation method. In solvent method, the hydrodynamic force is lowered compared to melt compounding method. Nanofillers are pre dispersed in a solvent by sonication in order to breakdown the total nanofiller content.

Polymer composites prepared through either of the above techniques are finally processed by standard methods such as casting, calendaring, injection molding, thermoforming and other typical nanocomposite processing methods.

1.7.3. Uses of polymer nanocomposites

The outstanding qualities of polymer nanocomposites such as high elastic stiffness and strength, wear and barrier resistance, excellent magnetic as well as improved optical and electrical properties make the materials applicable in the (among others) following fields;

i. Automobiles
ii. Aerospace
iii. Injection Molded Products
iv. Coatings
v. Adhesives
vi. Fire-retardants
vii. Packaging Materials
viii. Microelectronic Packaging
ix. Optical Integrated Circuits
x. Drug Delivery
xi. Sensors
xii. Membranes
xiii. Medical Devices
xiv. Consumer Goods

1.8. Graphite

Graphite – derived from the Greek verb *graphein* (to write) – also called Plumbago or black lead is an allotrope of carbon having a structure in layers consisting of six carbon atoms arranged in horizontal planes.

Graphite naturally forms by the sedimentation and metamorphosis of carbonaceous substances on reaction of carbon compounds with hydrothermal or volcanic fluids, or by crystallization of large masses of crystalline rocks.

Contrary to the element Carbon (which crystallizes in tetrahedral or octahedral arrangement), graphite crystallizes in hexagonal arrangement. Graphite is a very soft (hardness about 1½ on Mohs scale), opaque substance, with a dark grey to black color and a greasy feel when touched. Graphite leaves a black mark on surfaces and thus the Greek verb *graphein*.
Graphite is used in pencils, lubricants, crucibles, brushes for electric motors, cores of nuclear reactors.

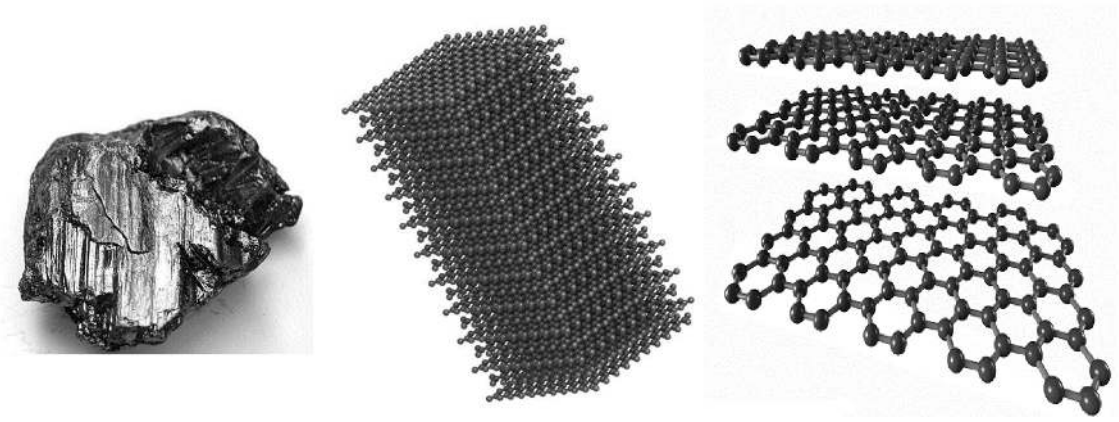

Figure 1.13. Forms of graphite

Graphite, shown in Figure 1.13 above converts to diamond under influence of high temperature and pressure. The conductivity of graphite is high, thus, suitable for electronic parts such as batteries, electrodes and solar panels.

1.9. Graphite oxide

Graphite oxide, (graphitic oxide or graphitic acid), is a compound of carbon, oxygen, and hydrogen in variable proportions, obtained by treating graphite with strong oxidizing agents [22], [23].

1.9.1. Structure of Graphite oxide

Graphite oxide retains the structure of graphite, however, with much larger and irregular arrangement and presence of oxygenated groups. The basic structure of graphite as well as other

allotropes of carbon such as charcoal, carbon nanotube and fullerenes is graphene. Graphite on the other hand is formed by stacked layers of graphene, one on top the other with an interplanar spacing of 0.335 nanometers. Structure of GO is given in Figure 1.14 below.

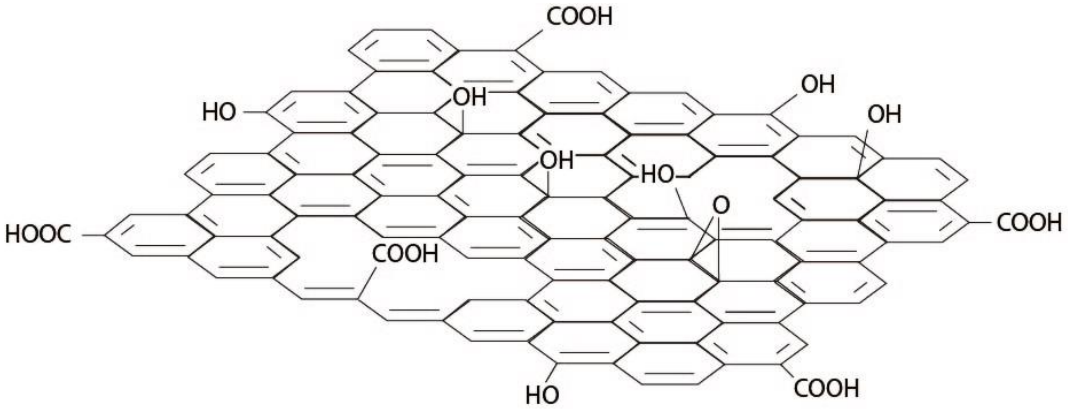

Figure 1.14. Structure of graphite oxide

The bulk product freely disperses in bases or can be dispersed by sonication in polar solvents to yield monomolecular sheets, known as graphene oxide by similarity to graphene, the single-layer type of graphite.

1.10. Thermal analysis of polymers

Thermal analysis refers to a set of techniques in which the property of a sample is measured against time or temperature while the sample's temperature is programmed in a controlled environment. The principal techniques employed are differential thermal analysis (DTA), differential scanning calorimetry (DSC), thermogravimetry (TGA), thermomechanical analysis (TMA), dynamic mechanical analysis (DMA), and dielectric analysis (DEA).

1.10.1. Differential thermal analysis

Differential thermal analysis measures the thermal behavior of a sample by analyzing its chemical compositions and how it responses to heat. As a substance is heated, it undergoes phase transitions involving absorption and emission of energy (heat). In DTA, the temperature of the substance is measured in relation to an inert reference material. The procedure employs the use of a thermocouple which detects any change in temperature within the test substance and the reference. The results of DTA are recorded as peaks on a moving chart. In addition to its application in polymer analysis, DTA is likewise widely used in the identification of minerals and mixtures [24]. Figure 1.15 shows the block diagram of a DTA machine.

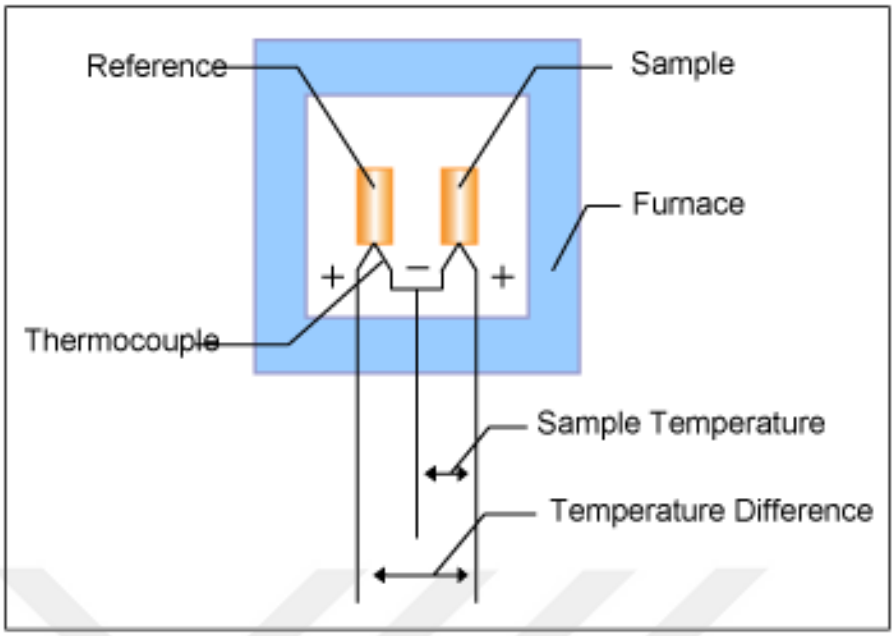

Figure 1.15. Block diagram of DTA instrument

1.10.2. Thermogravimetric analysis

Thermogravimetric analysis is another essential technique for material characterization, carried out by an instrument called thermogravimetric analyzer (TGA). The procedure is applicable in areas such as environmental, food, petrochemical and pharmaceutical industries.

Thermogravimetric analysis monitors the mass of a substance as a function of temperature or time as it is heated in a controlled environment. Upon heating a substance, it gains or loses its mass. An inert or occasionally a reactive gas is purged through the instrument, and flows over the sample. The gas controls the sample atmosphere and exits through an exhaust. The set-up is made up of sample holder, sensors and a computer set which displays the result as a moving sketch and collected for examination.

1.10.3. Differential scanning calorimetry

This instrument directly measures energy and allows exact measurements of heat capacity of a substance [25]. The technique of differential scanning calorimetry estimates the amount of energy required to increase the temperature of a sample and reference material as a function of temperature. DSC is used to study fusion, crystallization and oxidation of substances. In polymers, DSC is employed to study the glass transition (T_g) temperatures, melting and boiling points as well as thermal degradation of polymers. The machine consists of a compartment for measurement and a computer set. The test sample is placed in a container usually made of aluminum or platinum, and the reference in another cell (usually empty). The instrument is programmed by the computer to observe and control the rate of change of temperature of the

sample and the reference. The result is obtained as a curve of heat flow versus temperature (T) or time, generated by the instrument and displayed on the computer screen. The block diagram for DSC machine is given in Figure 1.16 below.

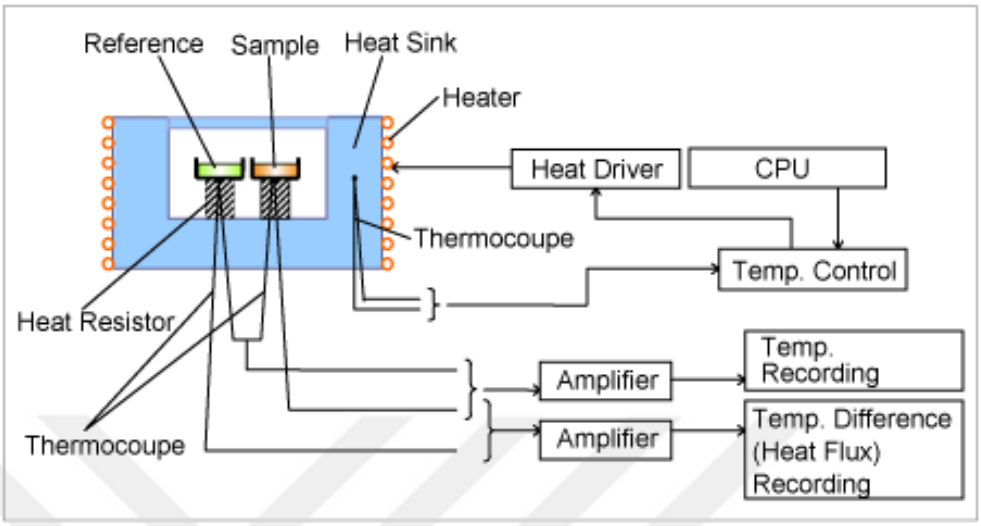

Figure 1.16. Block diagram of DSC instrument

1.11. Electrical investigation of polymers

Polymers are known to be insulating, having very low concentration of free charge carriers, and used quite often for insulating electrical devices and cables. Notwithstanding, quite a number of several other polymers conduct electricity. The conductivity of such polymers is centered on the conjugated double bonds on the polymer backbone. The conjugation results in the electrical conductivity of polymeric materials [26]. Moreover, doping the polymers with free charge carriers creates available spaces within the conduction bands, thus allowing for free movement of charges through the material.

1.12. Electron microscope analysis of polymers

Presently, several characterization procedures are available to examine and describe materials, and they help with perceiving the end-uses of the materials by giving intensive information on the design (structure) and property correlations. Microscopy procedures direct an extraordinary position in studying numerous characteristics such as morphology, chemical composition and structure, topology, interfacial properties, atomic, microstructure, and micromechanical properties. An electron microscope uses an electron beam to illuminate the sample and generate an enlarged image. The electron microscope can reach 0.05 nm resolution and a magnification of about 10,000,000 times.

1.12.1. Scanning electron microscopy

SEM provides a high magnification and resolution image by using high-energy rays of electrons. The electron beams generate certain signals with information about the homogeneity, morphology, crystalline structure and chemical composition of the sample. In polymer composite systems, SEM is used mainly to determine the distribution and dispersion of nanofillers within the polymer matrix [27].

The main components of SEM instruments are the source of electrons, lenses, sample (analyte) chamber, detectors and output devices. Set-up is shown in Figure 1.17 below.

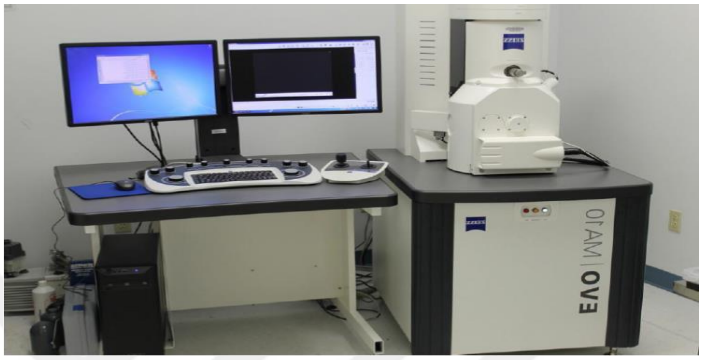

Figure 1.17. Set-up of SEM device

1.12.2. Scanning electron microscope/ Energy-dispersive x-ray spectroscopy (SEM/ EDX)

EDX is an accessory integrated in SEM, used to investigate the elemental composition and chemical characteristics of a sample.

Using a primarily focused scanning electron beam, images of high resolutions and outstanding depth are made. The primary electrons pass on a surface with energy and create many secondary electrons with lower energies. The intensity of the secondary electrons is seen by the surface topography of the sample. An image of the sample is generated by estimating the secondary electron's intensity to the primary scanning electron beam position.

1.12.3. Transmission Electron Microscopy (TEM)

TEM is one of the most powerful microscopes used as an analytical tool for visualization and analysis of samples in nanoscale range [28]. The principles of TEM and light microscopy are similar, however, TEM uses electrons instead of light, and images obtained by TEM have considerably higher optical resolution that those of light microscope. This is due to the small wavelengths of electron compared to those of light. This enables TEM to produce the minutest details of the analyte, even as small as individual atoms.

TEM is applied in areas such as material science, nanotechnology, biological, medical and biomedical [29] as well as semiconductor research. In polymeric systems, TEM analysis enables

for in-depth analysis of the internal structure, spatial distribution of different phases, and dispersion of nanoparticles within a polymer matrix.

1.13. X-ray Diffraction analysis of polymers

Also called x-ray powder diffraction, XRD, is a technique used to examine crystalline structures and atomic spacing of materials. The technique is based on constructive interference between monochromatic x-rays and the crystalline sample [30], when electrons are accelerated and bombarded against the sample, with energy sufficient to displace the inner shell electrons of the material. Thus, x-ray spectra are produced. The interaction is based on Bragg's law.

$$n\lambda=2dSin\theta$$

The Bragg's law relates the wavelength of the electromagnetic radiation to the diffraction angle and atomic spacing of the material. The irregular structural orientation of the powdered sample allows for the formation of possible diffraction angles.

x-ray diffractometer contains three (3) fundamental parts, namely;

- An x-ray tube
- Detector
- Sample holder

While generating x-rays, similarly, electrons are produced by heating a filament in the cathode ray tube – electrons that are bombarded against the sample in the holder which is rotated along with the detector. The intensity of the reflected x-rays is recorded as a signal peak, which is converted to a count rate and displayed on a computer monitor.

Some applications of the x-ray diffractometer are listed below;

i. Material characterization
ii. Determination of unit cell dimensions
iii. Measurement of sample purity
iv. Identification of fine-grained materials

1.14. Aims and objectives

The key purpose of this research is to synthesize a series of copolymers of 4-methyl-2-oxo-2H-chromen-8-yl methacrylate and methyl methacrylate via free radical polymerization technique (FRP). The thermal, electrical and dielectric properties of the p(COUMA-co-MMA) copolymers will be investigated, depending on varying amounts of graphite oxide. Monomer reactivity ratios will be investigated by Kelen-Tudos and Finemann-Ross methods.

The objectives of this research are;

i. To synthesize p(COUMA-co-MMA) copolymers and characterize using FT-IR, ^{1}H-NMR, UV-VIS.

ii. To investigate the thermal, electrical and dielectric behaviors of the p(COUMA-co-MMA) copolymer composites in relation to the pure copolymer systems.

iii. To investigate the photodimerization of P(COUMA-co-MMA) copolymers using UV irradiation at ≥365 nm

iv. To estimate the activation energies (E_a) of COMCOP1 and COMCOP1/ GO using FWO and KAS methods

1.15. Literature review

Coumarins have recently gained quite a lot of attention in the fields of research due to their physiological and fluorescent properties. Polymer derivatives of coumarins possess high photo stability and quantum yield of photo and electroluminescence [17]. The chemical modification of coumarins allows for variation of emission wavelength continuously throughout the visible spectrum.

Various coumarin based monomers and polymers have been synthesized and characterized by different authors through different methods [31]. Coumarin bearing monomers are generally synthesized by condensation reactions [32], however, polymers of coumarin base are synthesized by controlled radical polymerization techniques such as anionic, cationic, free radical and atom transfer radical polymerization techniques [33]. Among the polymers are polyamides derived from 6-ethynylphenyl coumarin dicarboxylic acid and aliphatic diamines, polyesters based on 6-(3'-hydroxy)-phenylcoumarin-3-carboxylic acid and 6,6'-biscoumarinyl-3,3'-dicarboxylic acid which showed good emission properties with reasonable solubility in volatile solvents such chloroform.

F. Serguei et al (1998) examined the design and synthesis of novel hyper branched and comb-like coumarin containing polymers in which a mixture of 7-hydroxy-4-methyl coumarin, 1,2-dichloroethane, N-methylpyrrolidone were stirred in the presence of K_2CO_3 [34]. The mixture was poured in 5% HCl, and the precipitate was filtered and crystallized from ethanol. According to the studies, the polymers were prepared by the high temperature transesterification in melt.

In a similar study, K. Demirelli (2011) examined the thermal stabilities, dielectric behaviors and monomer reactivity ratios of methacrylate bearing coumarin copolymers prepared by free radical polymerization [35], [36, 37]. In the studies, MAOC was polymerized in 1,4-dioxane solvent, and AIBN initiator at 60 ^{o}C. The polymer was recrystallized in ethanol, purified in petroleum ether and dried for 24 h at 40 ^{o}C.

Moreover, free radical copolymerization of MAOC with BMA, MMA, EMA and IBMA were carried out in 1,4-dioxane, in the presence of AIBN, and the mixture was degassed for about

10 min with Argon gas. After 24 h, the copolymers were precipitated in excess ethanol, purified by reprecipitation, and dried for 24 h at 40 ºC.

In this study, the thermogravimetric analysis of the copolymers revealed that as the amount of BMA increased, the thermal decomposition temperature decreased, the dielectric constant decreased sharply up to 100 Hz and then gradually decreased, and the dielectric constant and dielectric loss factors increased with temperature as well.

Photo-crosslinking of coumarin-based polymers is reported in various studies, as described by Sangho et al (2019). The study investigated the synthesis, characterization and dielectric properties of photo-crosslinkable coumarin polymers. In their studies, PVBMC was polymerized via FRP in the presence of AIBN, DMF as solvent and 80 ºC temperature for 48 h. Subsequent to characterization, the photodimerization and crosslinking of the coumarin units was examined by UV-vis and FT-IR analysis. Spectrum of the PVBMC without irradiation showed a strong absorption peak at λ=319 nm, attributed to the C=C bond of the benzopyrone ring and compared to the absorption band of PVBMC after irradiation. The peak intensity of the spectra showed a considerable drop, which is attributable to the dimerization of the coumarin units. The steady drop in peak intensity and estimated percent conversion as a function of time indicate the degree of photodimerization of the coumarin units. The dielectric properties of the crosslinked polymer were investigated by measuring leakage current density by sweeping voltage between -40 and 40V in MIM-type capacitor, fabricated by sandwiching the film between bottom ITO and Au electrode. The leakage current was found to be 10^{-4} A/mm^2 at electrical field 0.2 MV/cm. This result was compared against the pure PVBMC measured under similar conditions. According to the findings, the photocrosslinking reaction resulted in high-density polymer chain packing, which reduced the passage of electric current through the material. The cross-linked polymer exhibited a steady capacitance within the range of observed frequencies in the capacitance against frequency response of the MIM device [38].

Literature investigations have shown little or no information related to the effects of graphite oxide on the thermal and electrical behaviors such as dielectric constants, dielectric loss factor, DC conductivity, refractive index (n), current (I), voltage (V) of P(COUMA-co-MMA) composites. Likewise, monomer reactivity ratios of P(COUMA-co-MMA) have not been recorded in literature. However, in a study, Guzin et al (2019) examined the dielectric behaviors of P(CUMAC-co-BA); dielectric measurements were carried out using impedance analyzer as a function of temperature and frequency. Side group elimination was observed to be higher in the coumarin unit, reducing activation energy and accelerates degradation. Additionally, a significant decrease in the dielectric behaviors was observed at 320ºC, thought to be the result of the breakdown of Cl-Coumarin unit in the structure [37].

The effects of graphite oxide particles on the electrical and thermal properties of P(COUMA-co-MMA) composites has not been systematically studied. Therefore, in this study, it is expected that GO will increase or decrease the thermal decomposition rate of the copolymer systems. Graphite oxide possessing polar functional groups such as C=O, OH and C-O, affords to its compatibility with P(COUMA-co-MMA). As contents of graphite oxide increase in the systems, a P(COUMA-co-MMA)/ Graphite oxide composite system will show the behavior of a semiconductor material.

2. MATERIALS AND METHODS

2.1. Materials

- Monomers: 7-hydroxy-4-methyl-2H-chromen-2-one (4-methylumbelliferone) (COUMA), methyl methacrylate (MMA), and Methacryloyl chloride (MAC)
- Solvents: Dichloromethane (DCM), Tetrahydrofuran (THF), 1,4-Dioxane, and ethanol
- Initiators: Azobisisobutyronitrile (AIBN)
- Precipitants: Ethanol, Methanol, Diethyl ether
- Other chemicals: Triethylamine (TEA), N,N-Dimethylformamide (DMF), triethylammonium Bromide (TEABr), Chloroform-D
- Polymers: PMMA, PCMA and p(COUMA-co-MMA)

2.2. Instrumentation

- Weighing measurements: Avery Berkel VA304-1AAZM13AAE digital weighing balance
- Stirring/ Mixing: BioSan MS-3000 magnetic stirrer
- Reaction heat supply: VELP Scientifica ARE heating magnetic stirrer
- Sonication: FY-US-01 FYtronix digital ultrasonic homogenizer
- Sample drying: Nuve EV-018 vacuum oven
- Solvent evaporation: BUCHI Heating Bath B-490/ BUCHI R-200 Rotary evaporator
- Thin film coating: VTC-100 vacuum spin coater
- High-temperature oven for polymer degradation: NEYO 2-525 Series II vacuum oven
- FT-IR analysis: Perkin Elmer Spectrum One FT-IR spectrophotometer
- Calorimetric analysis: SHIMADZU DSC-50 Differential Scanning Calorimeter
- Thermogravimetric analysis: SHIMADZU TGA-50 Thermogravimetric Analyzer
- 1H and 13C-NMR analysis: Avance III Bruker 40 MHz NMR spectrometer
- The QuadTech 7600 LRC Impedance Analyzer for dielectric measurements from 100 Hz up to 2 kHz was used.
- The electrical characterization measurements were carried out using the FY Tronix Electric Characterization device.
- UV-vis spectrophotometric analysis: SHIMADZU UV-mini 1240 spectrophotometer
- UV irradiation: FY Tronix AS UV irradiator
- Other materials: polymerization flasks, beakers, reaction flasks, automatic pipet, funnel, pestle and mortar, thermometer, aluminum and platinum caps for DSC and TGA measurements

2.3. Experimental

2.3.1. Purification of methyl methacrylate monomer

To purify MMA monomer prior to modification, 10 mL MMA was dissolved in a mixture of 25 mL diethyl ether and 5 mL 5% NaOH in a separation funnel. The contents were thoroughly mixed, and separated. The procedure was repeated severally to ensure adequate partition of the constituents. Furthermore, the same procedure was carried out with H_2O – in order to neutralize NaOH. Dried $MgSO_4$ was added to the mixture and filtered after thorough mixing. Finally, DE-Et was evaporated and purified MMA was recovered from the residue. All purifications were carried out at room temperature.

2.3.2. Modification of 7-hydroxy-4-methyl-2H-chromen-2-one with methacryloyl chloride

The synthesis of 4-methyl-2-oxo-2H-chromen-7-yl methacrylate (COUMA) monomer was carried out from the reaction of methacryloyl chloride and 7-hydroxy-4-methyl coumarin according to the usual method [39]. The monomer, 4-methyl-2-oxo-2H-chromen-7-yl methacrylate (COUMA), is a yellow viscous solution. The reaction pathway is illustrated in Figure 2.1. Structure of the compound was characterized by FT-IR and ^{1}H-NMR techniques.

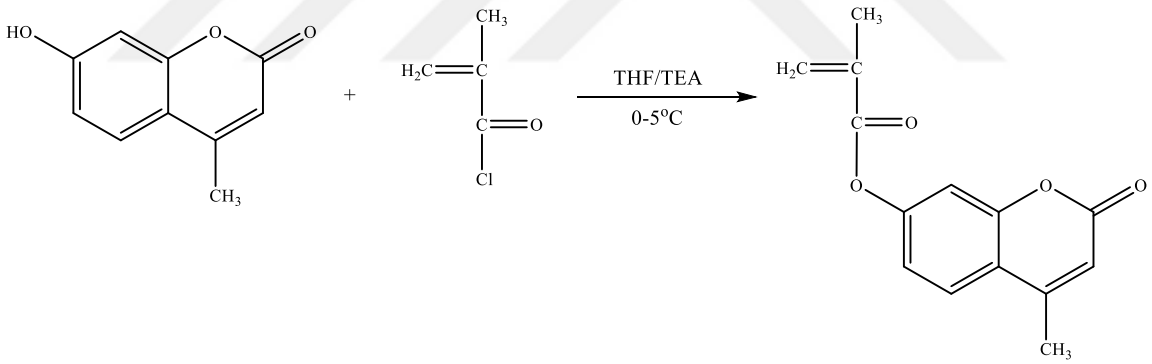

Figure 2.1. Synthesis of 4-methyl-2-oxo-2H-chromen-7-yl methacrylate via monomer modification

2.3.3. Synthesis of PCOUMA via Free Radical Polymerization

Subsequent to monomer modification, 0.8g 4-methyl-2-oxo-2H-chromen-7-yl methacrylate was dissolved in 3 mL 1,4-Dioxane in a polymerization tube. 1% (0.008 g) AIBN was introduced into the mixture and argon gas was passed through for 15 min. The mixture was stirred for 24 h at 60 °C. After cooling, the solution was precipitated in ethyl alcohol, and filtered. The product was dried under vacuum for 48 h at 45°C. The illustration of this reaction is shown in Figure 2.2 below.

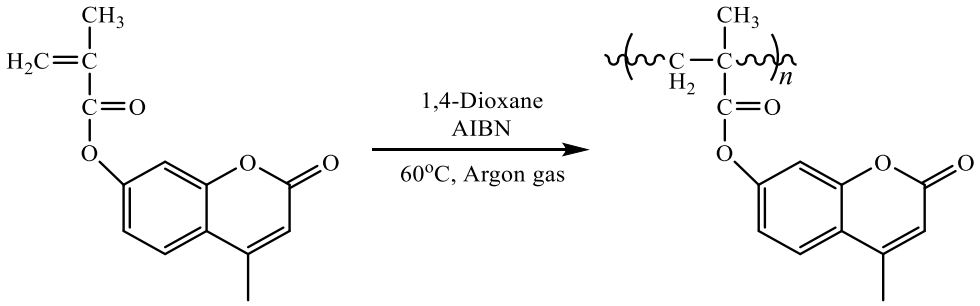

Figure 2.2. Synthesis of PCOUMA

2.3.4. Synthesis of PMMA via Free Radical Polymerization

In a 3 mL 1,4-dioxane solution, 1g of purified MMA was added followed by 1% (0.01 g) AIBN, and argon gas was injected into the solution for 15 min. The mixture was stirred for 24 h at 60 °C. Afterwards, the solution was precipitated within ethyl alcohol. The precipitate was filtered; residue was dried under vacuum for 48 h at 45 °C. Figure 2.3 illustrates the pathway for the synthesis of PMMA.

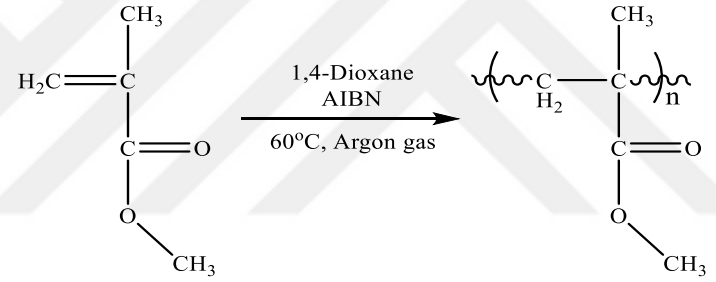

methyl methacrylate PMMA

Figure 2.3. Synthesis of PMMA

2.3.5. Free Radical Copolymerization of COUMA and MMA

The methyl methacrylate (MMA), methacryloyl chloride and 7-hydroxy-4-methyl coumarin were provided from Sigma-Aldrich. MMA was used after distillation under vacuum. The 2,2'-azobisisobutyronitrile (AIBN) was recrystallized within methanol by dissolving within chloroform. Tetrahydrofuran, ethyl alcohol and dichloromethane were used as received.

The coumarin-containing copolymers were prepared by free radical copolymerization method and the synthetic procedure was as follows. To five different polymerization flasks, 0.06 g (0.25 mmol), 0.3 g (1.23 mmol), 0.6 g (2.45 mmol), 1.2 g (4.91 mmol), 1.7 g (6.95 mmol) of COUMA, 0.8 g (7.93 mmol), 0.7 g (6.95 mmol), 0.51 g (5.126 mmol), 0.49 g (4.9 mmol), 0.123 g (1.23 mmol) of MMA and 1% AIBN (0.008 g, 0.009 g, 0.01 g, 0.017 g, 0.03 g respectively) to each of the monomer compositions were dissolved in 8 mL 1,4-dioxane in a 20.0 ml polymerization flasks. The reaction mixture was passed with argon gas for 10 min. The

polymerization flasks were then placed in a preheated oil bath at 60 ºC for 24 hours. Because olefinic C=C band (at 1634 cm^{-1}), which is a characteristic for units of COUMA and MMA in FT-IR spectrum was considerably decreased, the polymerization reaction was stopped, and it was cooled to room temperature. The copolymer was collected after two times of precipitation in ethyl alcohol, and dried under vacuum at 40 ºC for 24 h. From the ^{1}H-NMR spectrum (in $CDCl_3$), composition of COUMA and MMA were calculated to be 8.9%, 24%, 36%, 49% and 65% (by mol), respectively. In this regard, it was used to estimate composition of copolymer the resonance signals of =CH next to C=O group in the COUMA unit and the –OCH_3 groups of MMA at 6.23 ppm and 3.61 ppm, respectively. The copolymerization of COUMA and MMA is illustrated in Figure 2.4.

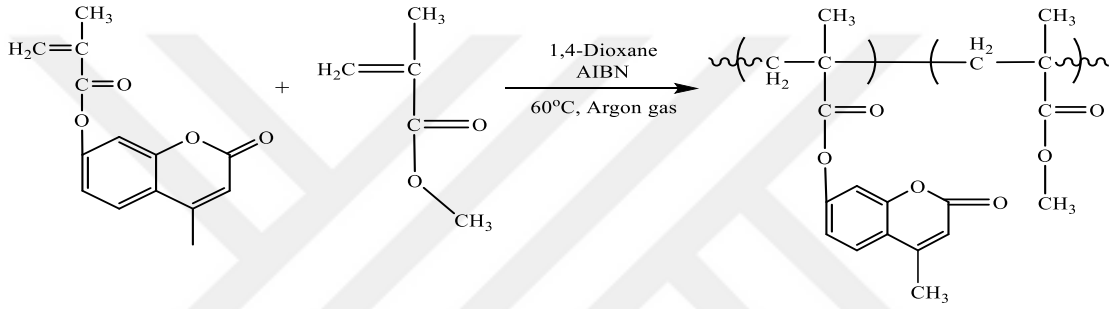

Figure 2.4. Synthesis of P(COUMA-co-MMA)

2.4. Synthesis of Graphite oxide

Graphite oxide was prepared by chemical oxidation of graphite flakes (supplied by Sigma Aldrich) by Staudenmaier method (Sali et al 2019), based on the Brodie method [40, 41]. 5g graphite was treated with a mixture of HNO_3:H_2SO_4 in a 1:3 ratio (v/v; 25 mL). The mixture was refluxed for 10 min with dynamic evolution of NO_2 gas. The mixture was cooled for 2 h, filtered and finally rinsed with water. The residue (GO) was dried for 12 h at 85ºC. reaction is given in Figure 2.5 below.

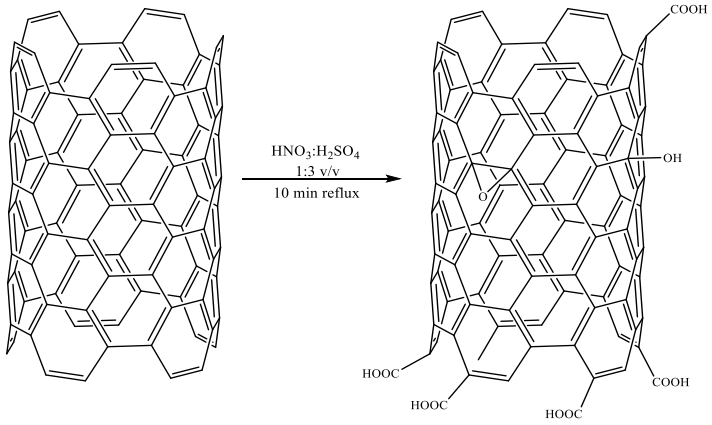

Figure 2.5. Synthesis of Graphite oxide

2.4.1. Preparation of P(COUMA-co-MMA)/Graphite oxide composite systems

To prepare composites of COMCOP1 and COMCOP2 with GO, the copolymers were first dissolved in dichloromethane in a beaker at room temperature. On the other hand, the dispersed GO powder in dichloromethane in a separate beaker was sonicated for 7 h at 25°C. Then, COMCOP1 solution was poured to dispersed GO solution at distinct amounts to get desired composition. The mixed solutions were further sonicated for a few time at 25°C. Subsequently, every solution was precipitated within methyl alcohol and filtered. The composites were dried under vacuum, and they were treated for at least 30 minutes with agate mortar to fine powder. The amounts of GO in the COMCOP1/GO were 10, 12 and 16 wt.%. Also, the amounts of GO in the COMCOP2/GO were 12, 13.6 and 15 wt.%. All the tablets prepared under 4-ton pressure were about thickness of 0.60 mm and area of 1.32 mm^2.

2.5. Photodimerization of (COMCOP1) (P(COUMA0.49-co-MMA))

The dimerization of coumarin in the COMCOP1 was carried out by irradiation of a THF solution of copolymer at 365 nm for 240 hours in presence of 15W UV light at 365 nm. In this regard, the photodimerization of the coumarin group in the prepared dilute solution of the copolymer bearing the coumarin group was followed by UV-vis spectroscopy. The Schematic representation of the formation of single chain polymer molecule possessing the head-to-head cis cyclobutane structure with the photodimerization of coumarin in the COMCOP1 structure with 365 nm UV light is shown in Figure 2.6.

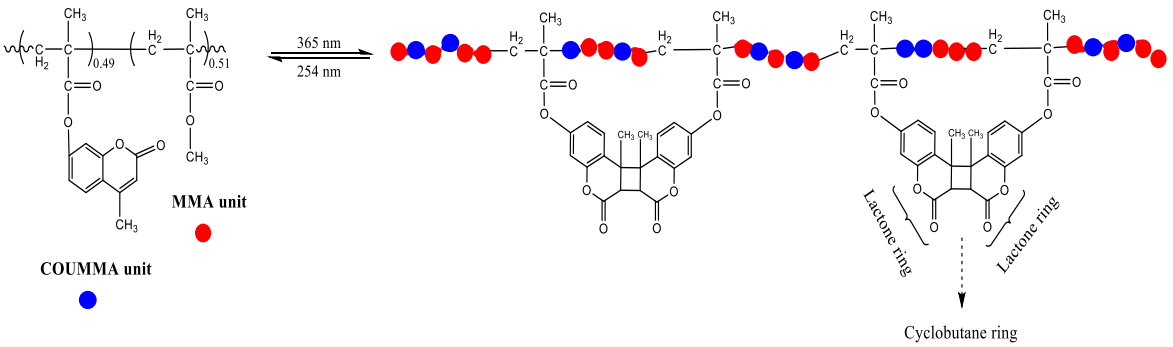

Figure 2.6. Schematic representation of the formation of single chain polymer molecule possessing the head-to-head cis cyclobutane structure with the photodimerization of coumarin in the COMCOP1 structure with 365 nm UV light

3. RESULTS

3.1. PCOUMA

PCOUMA was purified by precipitation in ethanol. The polymer was dried under vacuum for 24 h at 45 ºC, and characterized using FT-IR and ^{1}H-NMR techniques.

3.1.1. Characterization of P(COUMA)

The IR spectrum of PCOUMA is shown in Figure 3.1, and the evaluation is given in Table 3.1 below.

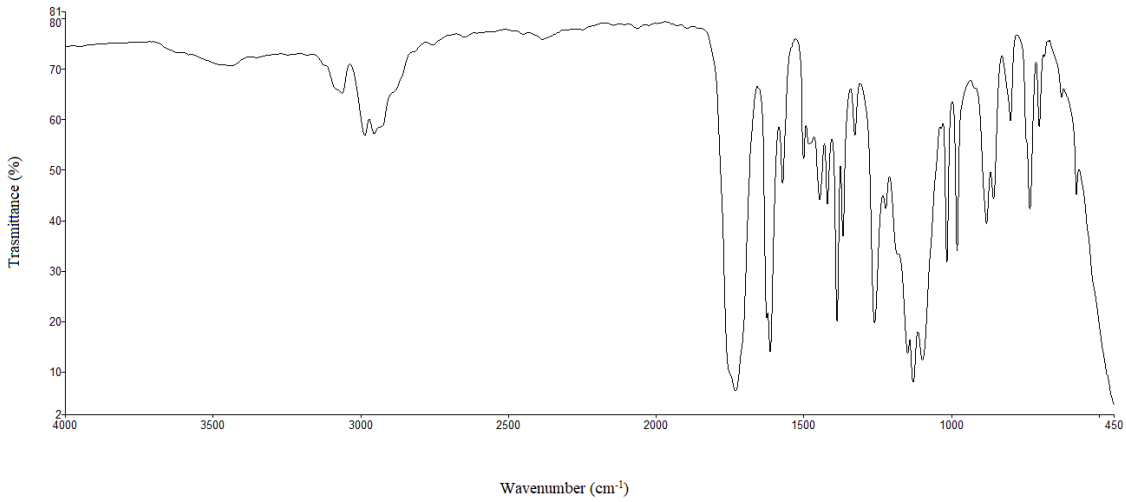

Figure 3.1. FT-IR spectrum of PCOUMA

Table 3.1. FT-IR evaluation of PCOUMA

Wavelength (cm^{-1})	**Vibration type**
1572	C=C stretching
1614	Aromatic C=C
1732	C=O Stretching
2850	C - H Stretching
1490 - 1385	C – H bending

3.1.2. Thermal analysis of PCOUMA

The TGA and DSC curves of PCOUMA are given in Figures 3.2 and 3.3 respectively. The curves are evaluated in Table 3.2.

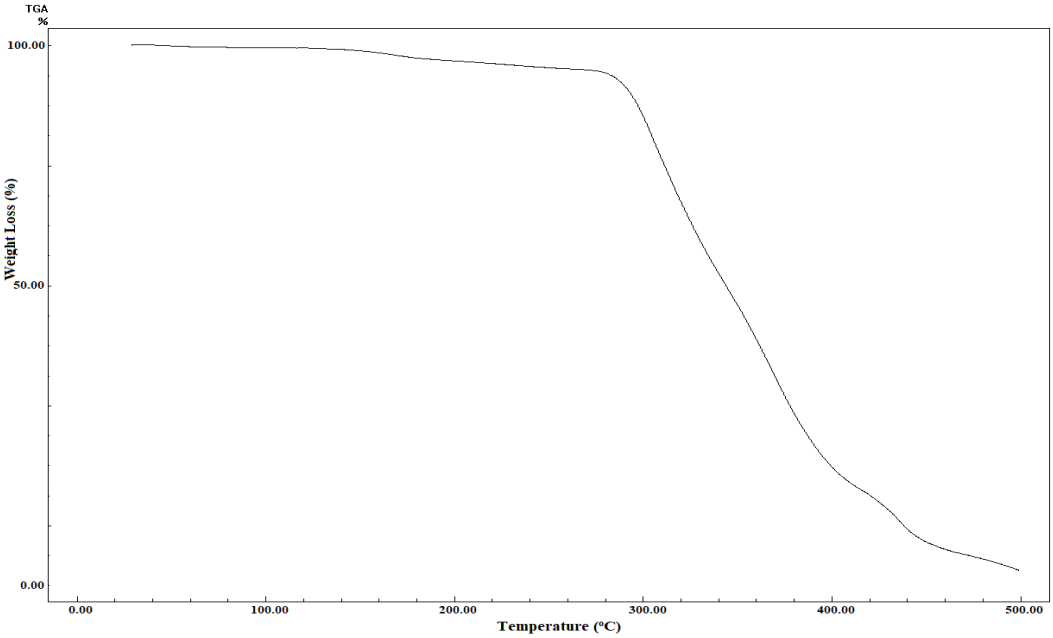

Figure 3.2. TGA Curve of PCOUMA

Table 3.2. TGA and DSC evaluation of P(COUMA)

Samples	T_g (°C)	T_i (°C)	$T_{max\ 50\%}$ (°C)	Total Weight Loss (%)	Residue (%)
PCOUMA	150	215.67	354.83	96.1	3.986

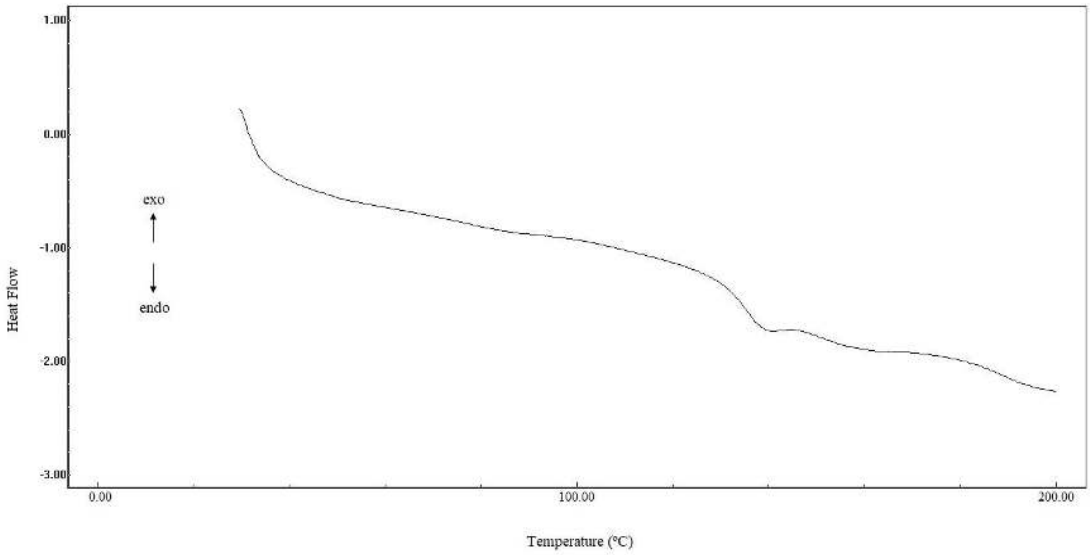

Figure 3.3. DSC Curve of PCOUMA

3.2. PMMA

PMMA was purified by precipitation in ethanol. The polymer was dried under vacuum for 24 h at 45°C. The homopolymer was characterized using FT-IR and ^{1}H-NMR techniques.

3.2.1. Characterization of PMMA

The IR spectrum of PMMA is shown in Figure 3.4 and evaluated in Table 3.3 below.

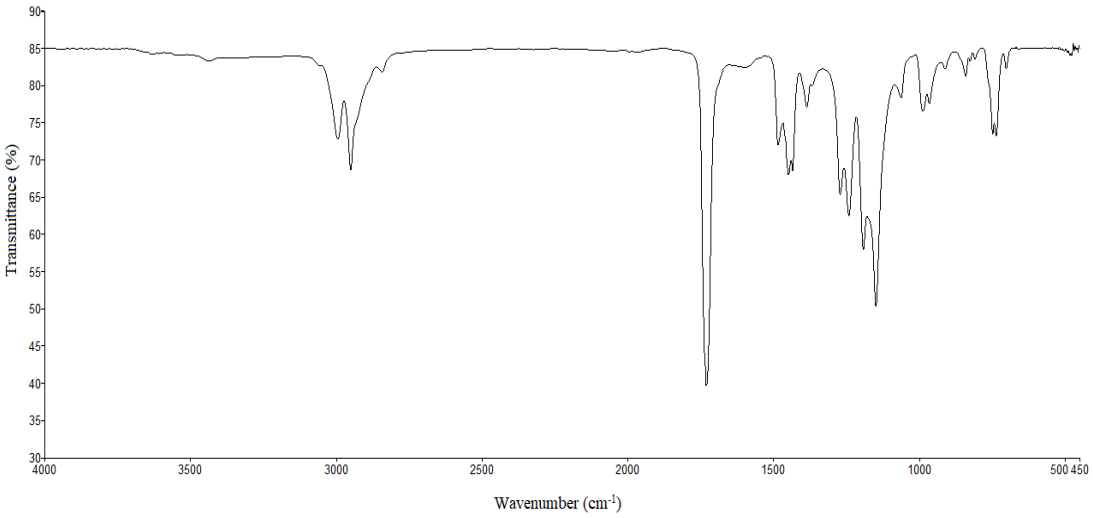

Figure 3.4. FT-IR Spectrum of PMMA

Table 3.3. FT-IR evaluation of PMMA

Wavelength (cm^{-1})	**Vibration type**
1718.3	C=O stretching
1150	-C-O
1063.6	C-O-C Stretching
2841.6	O-CH_3
1435.3	-CH_3 asymmetric bending

3.2.2. Thermal properties

The TGA and DSC curves of PMMA are given in Figures 3.5 and 3.6, respectively. The curves are evaluated in Table 3.4.

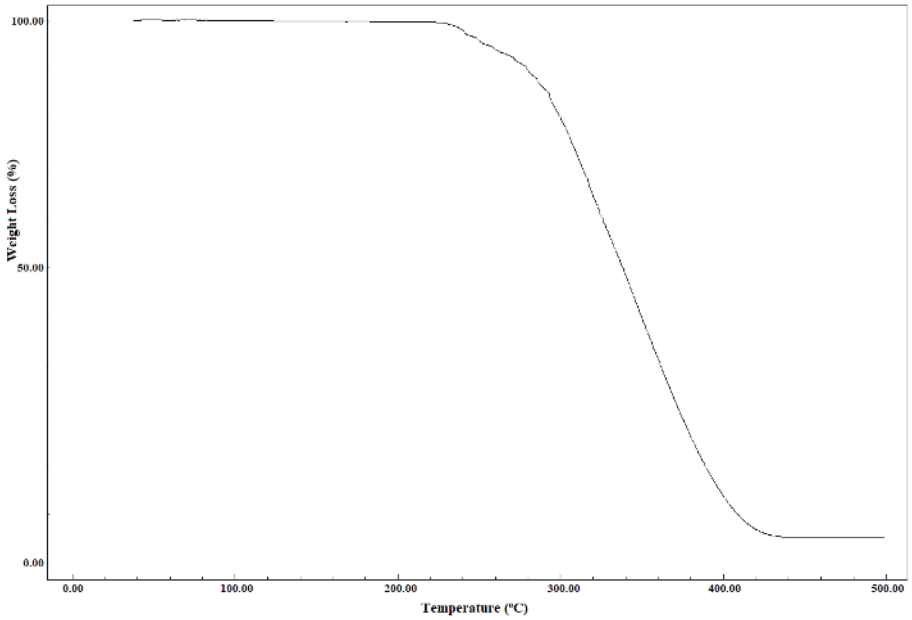

Figure 3.5. TGA Curve of PMMA

Table 3.4. TGA and DSC evaluation of PMMA

Samples	T_g (°C)	T_i (°C)	$T_{max\ 50\%}$ (°C)	Total Weight Loss (%)	Residue (%)
PMMA	110	210.18	341.88	94.74	5.25

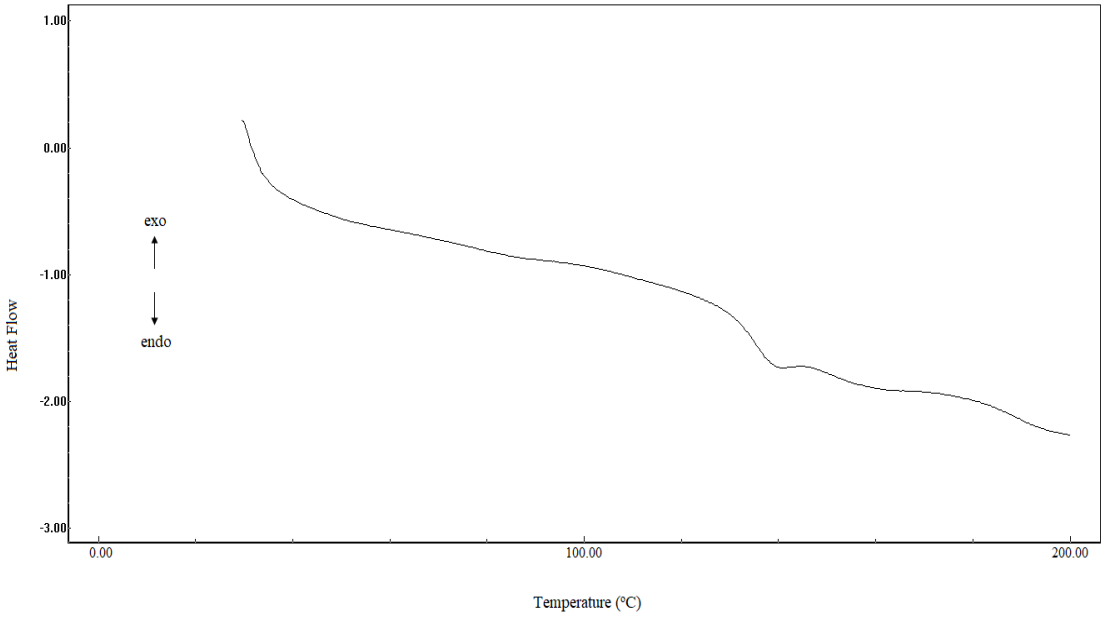

Figure 3.6. DSC Curve of PMMA

3.3. Free radical copolymerization of COUMA and MMA

A series of copolymer systems at different compositions of COUMA and MMA monomers were prepared by free radical copolymerization method at 60 °C. The copolymers were purified by precipitation in ethanol and dried under vacuum at 40 °C for 24 h. The copolymers of [P(COUMA-co-MMA)] were characterized by FT-IR and ^{1}H-NMR. Thermal investigations were carried out using TGA and DSC techniques, and UV-vis analysis was carried out as well. All measurements were evaluated in the given Tables.

3.3.1. Characterization

The FT-IR spectra of P(COUMA-co-MMA) for different compositions of COUMA and MMA monomers are given in Figure 3.7 and evaluated in Table 3.5.

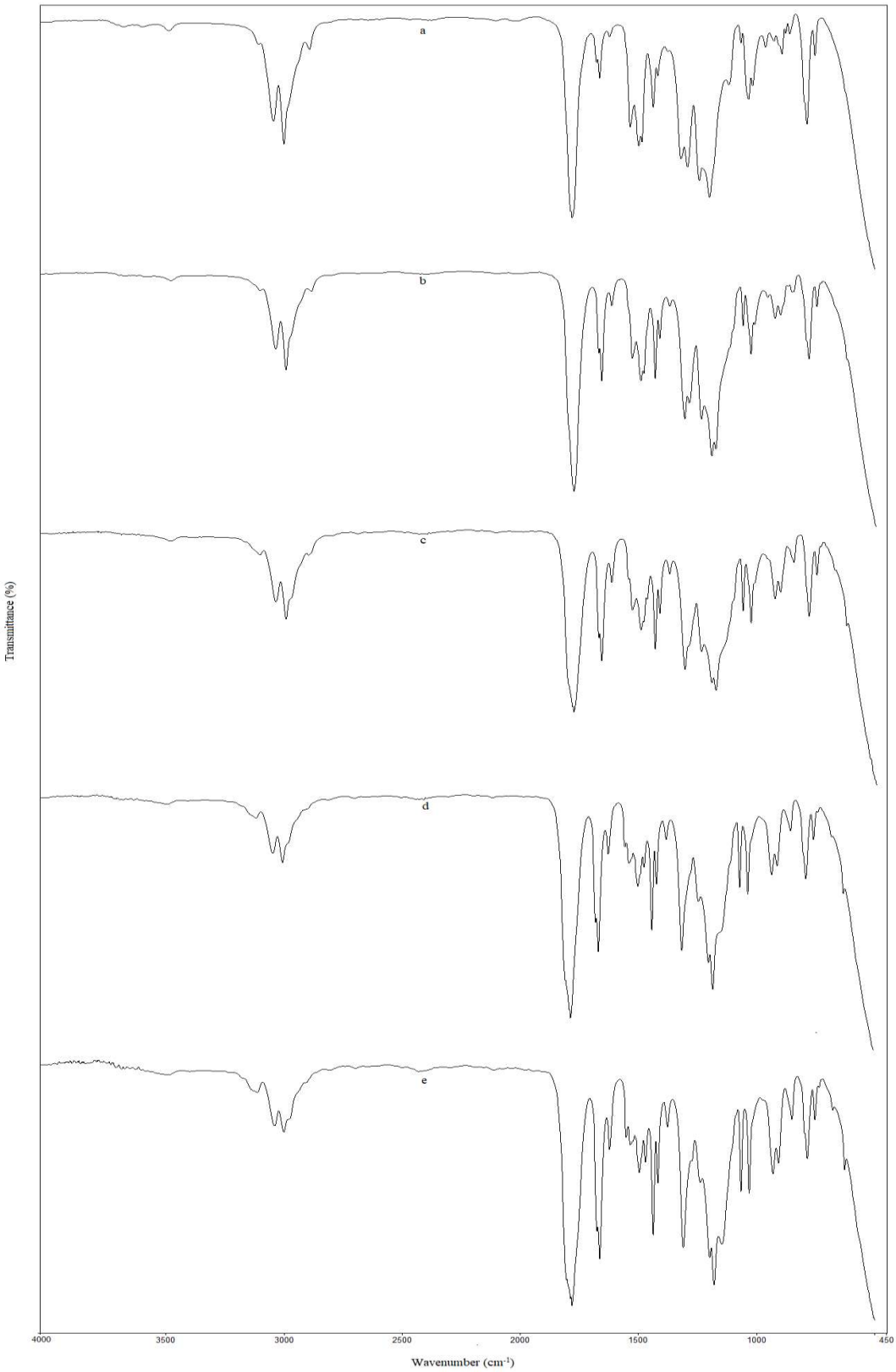

Figure 3.7. FT-IR Spectra of (a) P(COUMA8.9%-co-MMA) (b) P(COUMA24%-co-MMA) (c) P(COUMA36%-co-MMA) (c) P(COUMA49%-co-MMA) (e) P(COUMA65%-co-MMA)

Table 3.5. FT-IR evaluation for copolymers of P(COUMA-co-MMA) at different compositions of COUMA and MMA monomers

Wavelength (cm^{-1})	**Vibration type**
1730	C=O stretching
2993	$-CH_2-$
2923	Aliphatic -C-H bending
1624-1572	C=C
1261	Ar-O-C symmetric
1131	Ar-O-C asymmetric

The ^{1}H-NMR spectra of P(COUMA-co-MMA) for variable composition of COUMA and MMA monomers, percentage conversion of monomers and theoretical and experimental ^{1}H-NMR values of copolymers are given in Figure 3.8 and evaluated in Tables 3.6, 3.7 and 3.8, respectively.

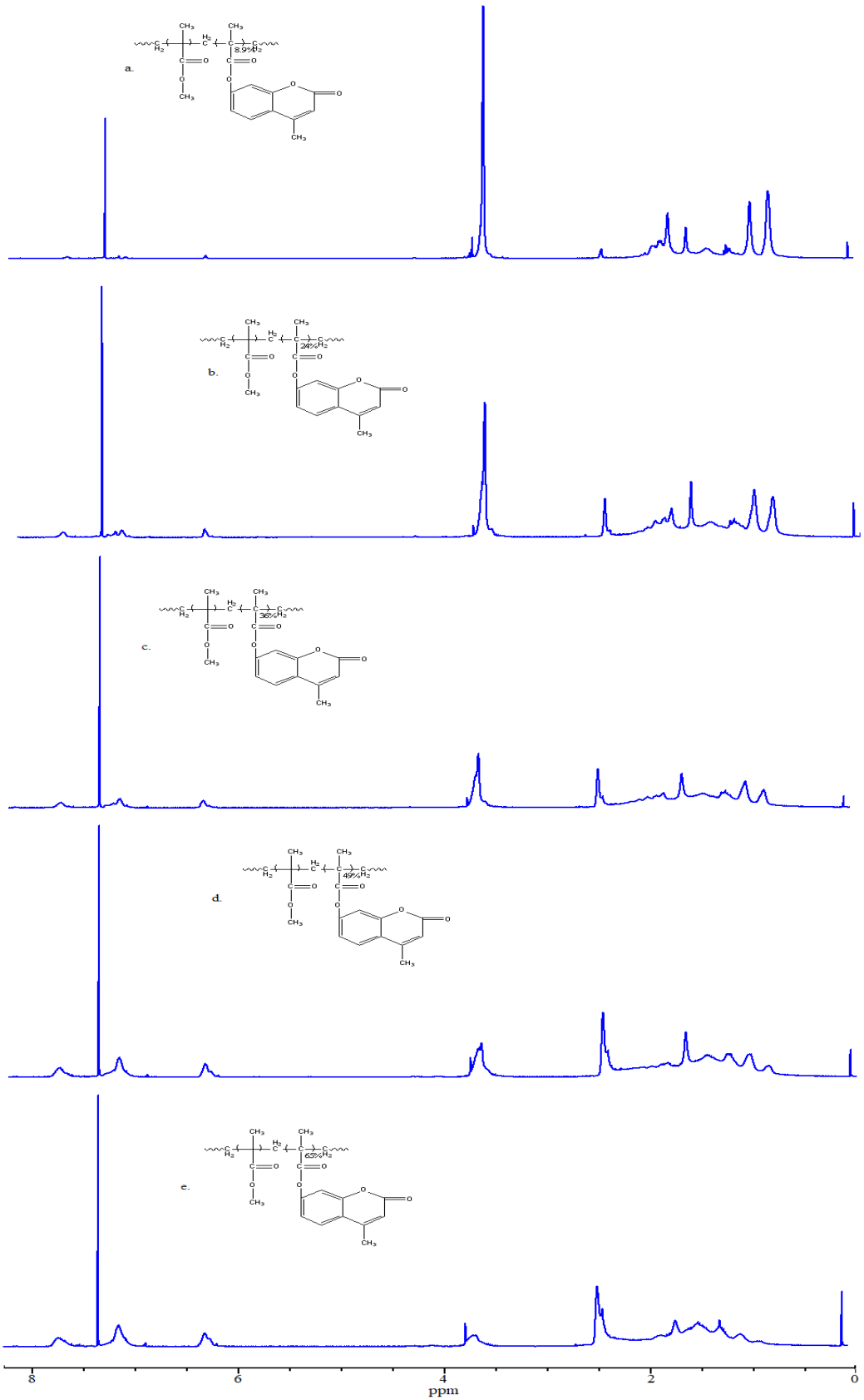

Figure 3.8. ^{1}H-NMR Spectra of a) P(COUMA8.9%-co-MMA) b) P(COUMA24%-co-MMA) c) P(COUMA36%-co-MMA) d) P(COUMA49%-co-MMA) e) P(COUMA65%-co-MMA)

Table 3.6. ^{1}H-NMR Spectra evaluation of P(COUMA8.9%, 24%, 36%, 49%, 65%-co-MMA) in $CDCl_3$

Chemical shift (ppm)	Signal type
2.46	$-CH_3$
6.23	-C=CH
2.0 – 2.5	$-CH_2-$
0.91 – 1.90	CH_3-
3.61	$-CH_3O-$

Table 3.7. Conversion (%) of monomers

Sample	% by weight	% by mol
P(COUMA8.9%-co-MMA)	32	7.03
P(COUMA24%-co-MMA)	35	30
P(COUMA36%-co-MMA)	58	51
P(COUMA49%-co-MMA)	59	71
P(COUMA65%-co-MMA)	24	93

Table 3.8. Summary of theoretical and experimental NMR Values for copolymers of COUMA and MMA at different monomer compositions

Sample	Theoretical	Experimental
P(COUMA8.9%-co-MMA)	2.9	8.9
P(COUMA24%-co-MMA)	14	24
P(COUMA36%-co-MMA)	30	36
P(COUMA49%-co-MMA)	50	49
P(COUMA65%-co-MMA)	84	65

3.3.2. Thermal properties

The TGA and DSC curves for different compositions of P(COUMA-co-MMA) copolymers are given in Figures 3.9 and 3.10 respectively, and evaluated in Tables 3.9 and 3.10, respectively.

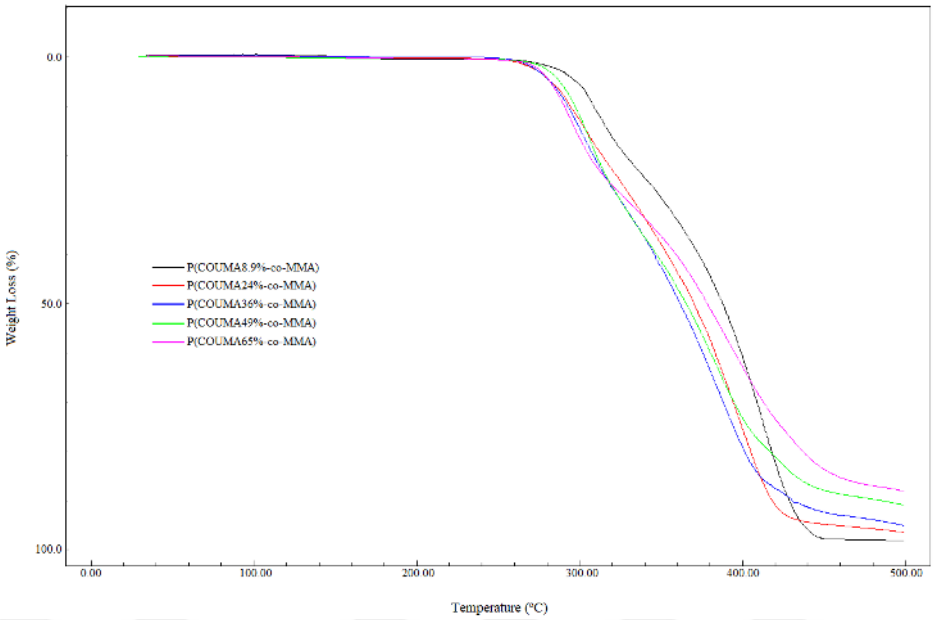

Figure 3.9. TGA Curves of P(COUMA-co-MMA) for different monomer compositions

Table 3.9. TGA evaluation of P(COUMA-co-MMA) for different monomer compositions

Samples	T_i (°C)	$T_{max,\ 50\%}$ (°C)	Total Weight Loss (%)	Residue (%)
P(COUMA8.9%-co-MMA)	255.05	387.18	97.5	2.5
P(COUMA24%-co-MMA)	234.5	366.75	94.4	5.6
P(COUMA36%-co-MMA)	242.8	356.7	92.4	7.6
P(COUMA49%-co-MMA)	233.6	356.8	88.5	11.5
P(COUMA65%-co-MMA)	235.6	366.5	85.8	14.2

Table 3.10. DSC evaluation of P(COUMA-co-MMA) at different compositions of COUMA and MMA monomers

Samples	T_g (°C)
P(COUMA8.9%-co-MMA)	135
P(COUMA24%-co-MMA)	131
P(COUMA36%-co-MMA)	130
P(COUMA49%-co-MMA)	129
P(COUMA65%-co-MMA)	125

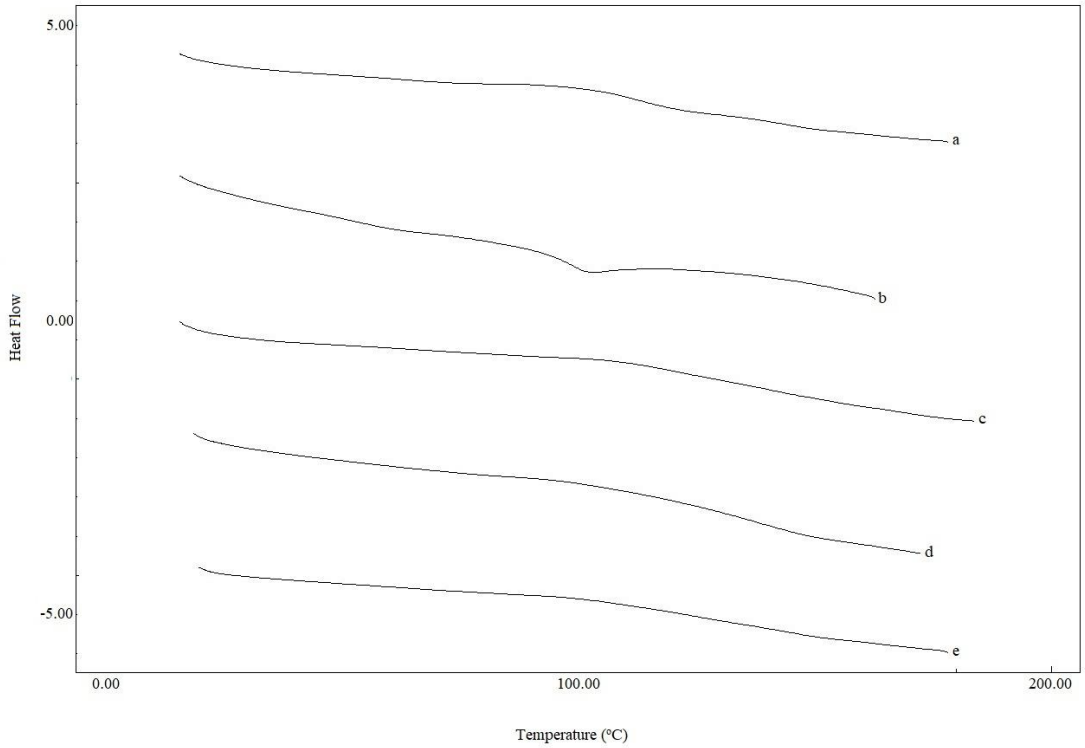

Figure 3.10. DSC Curves of P(COUMA-co-MMA) at different compositions (8.9%, 24%, 36%, 49% and 65%) of COUMA and MMA monomers

3.4. P(COUMA-co-MMA)/GO

3.4.1. Thermal and UV-vis Spectroscopic analysis of COMCOP1 and COMCOP2

The TGA and DSC curves of P(COUMA49%-co-MMA)/ GO 16 wt.%, 12 wt.% and 10 wt.% (COMCOP1) and P(COUMA36%-co-MMA)/ GO 15 wt.%, 13.6 wt.% and 12 wt.% (COMCOP2) are given in Figures 3.11 and 3.12, respectively. The curves are evaluated in Tables 3.11 and 3.12 respectively.

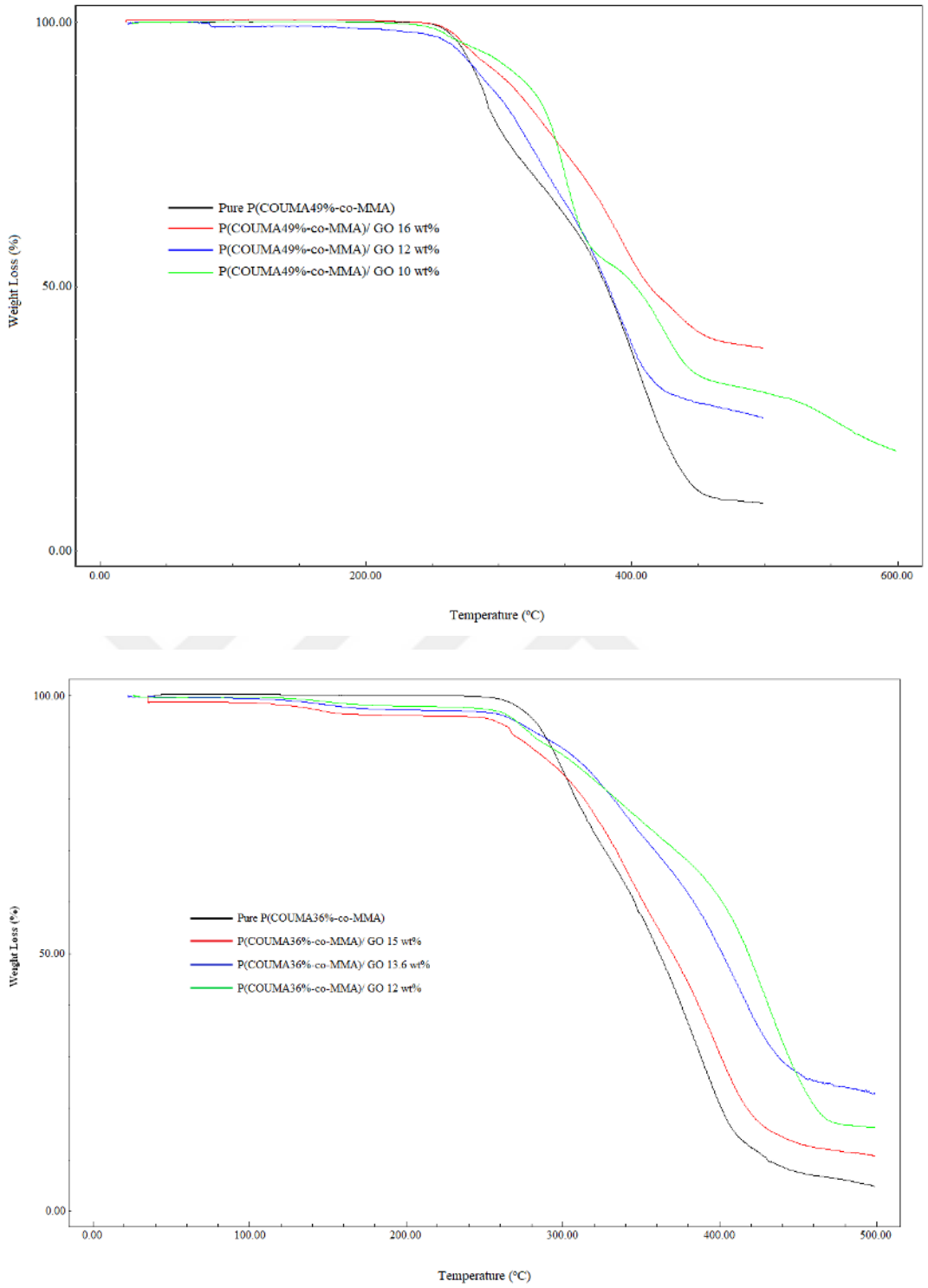

Figure 3.11. TGA curves of A] a) pure COMCOP1 b) composites loaded GO 16 wt%, c) 12 wt% and d) 10 wt%; B] a) pure COMCOP2 b) composites loaded GO 15 wt%, c) 13.6 wt%, d)12 wt %

Table 3.11. TGA evaluation of COMCOP1 and COMCOP2 for variable GO loadings

Samples	T_i (°C)	$T_{max,\ 50\%}$ (°C)	Total Weight Loss (%)	Residue (%)
COMCOP1/ GO 16 wt.%	187.22	368.32	62.21	37.79
COMCOP1/ GO 12 wt.%	178.44	359.32	74.104	25.896
COMCOP1/ GO 10 wt.%	176.93	361.68	72.582	27.418
COMCOP2/ GO 15 wt.%	240.22	364.17	85.30	14.663
COMCOP2/ GO 13.6 wt.%	237.76	384.33	74.264	25.736
COMCOP2/ GO 12 wt.%	247.1	408.30	81.40	18.608

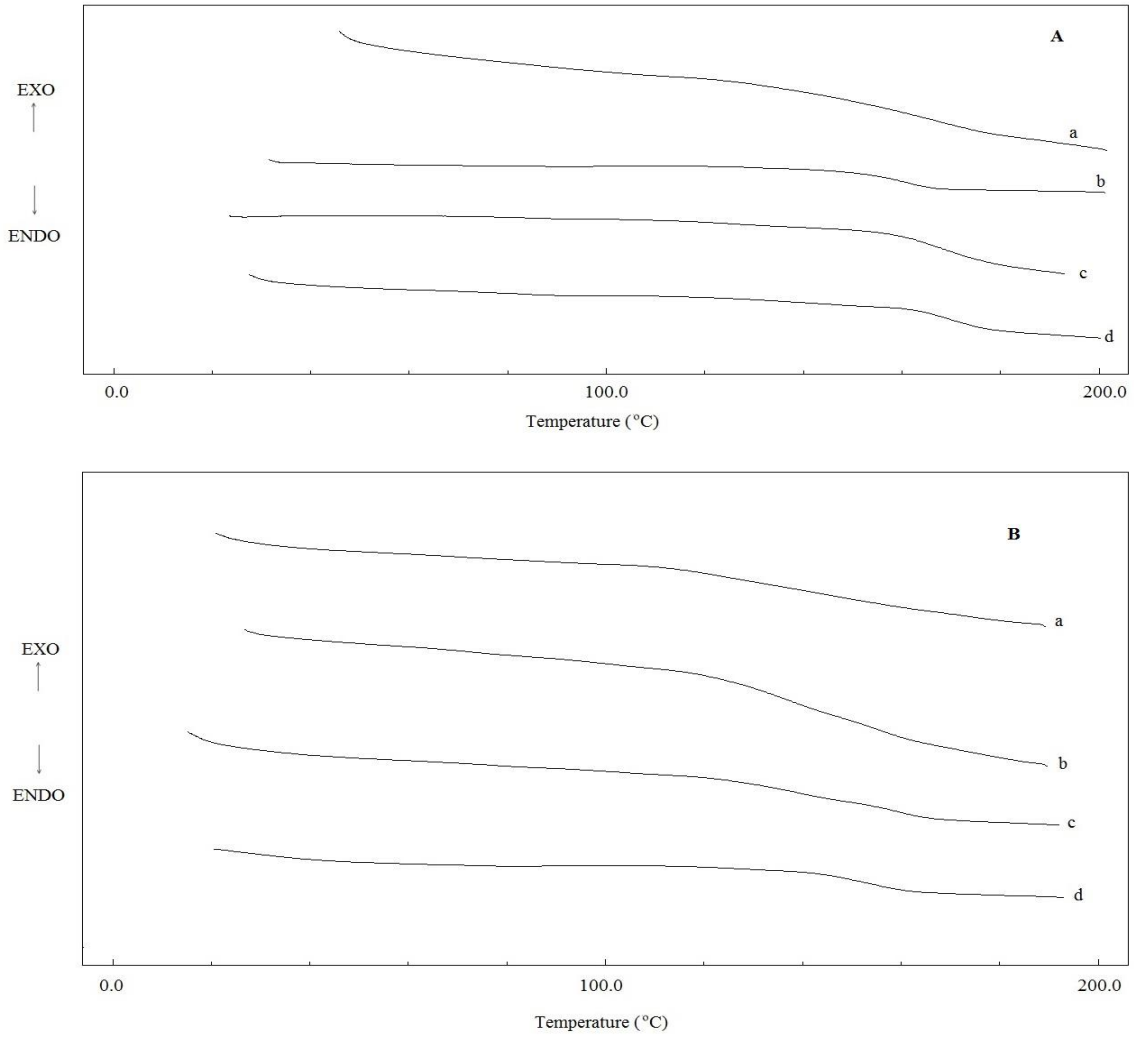

Figure 3.12. DSC curves of A] a) pure COMCOP1 b) composites loaded GO 16 wt%, c) 12 wt% and d) 10 wt%; B] a) pure COMCOP2 b) composites loaded GO 15 wt%, c) 13.6 wt%, d)12 wt %

Table 3.12. DSC evaluation of COMCOP1 and COMCOP2 at different GO loadings

Samples	T_g (ºC) 16% GO	T_g (ºC) 12% GO	T_g (ºC) 10% GO	T_g (ºC) 15% GO	T_g (ºC) 13.6% GO	T_g (ºC) 12% GO
COMCOP1	173	169	162	-	-	-
COMCOP2	-	-	-	170	150	143

The ^{1}H-NMR spectra of COMCOP1 and COMCOP2 are given in Figure 3.13 and evaluated in Table 3.13.

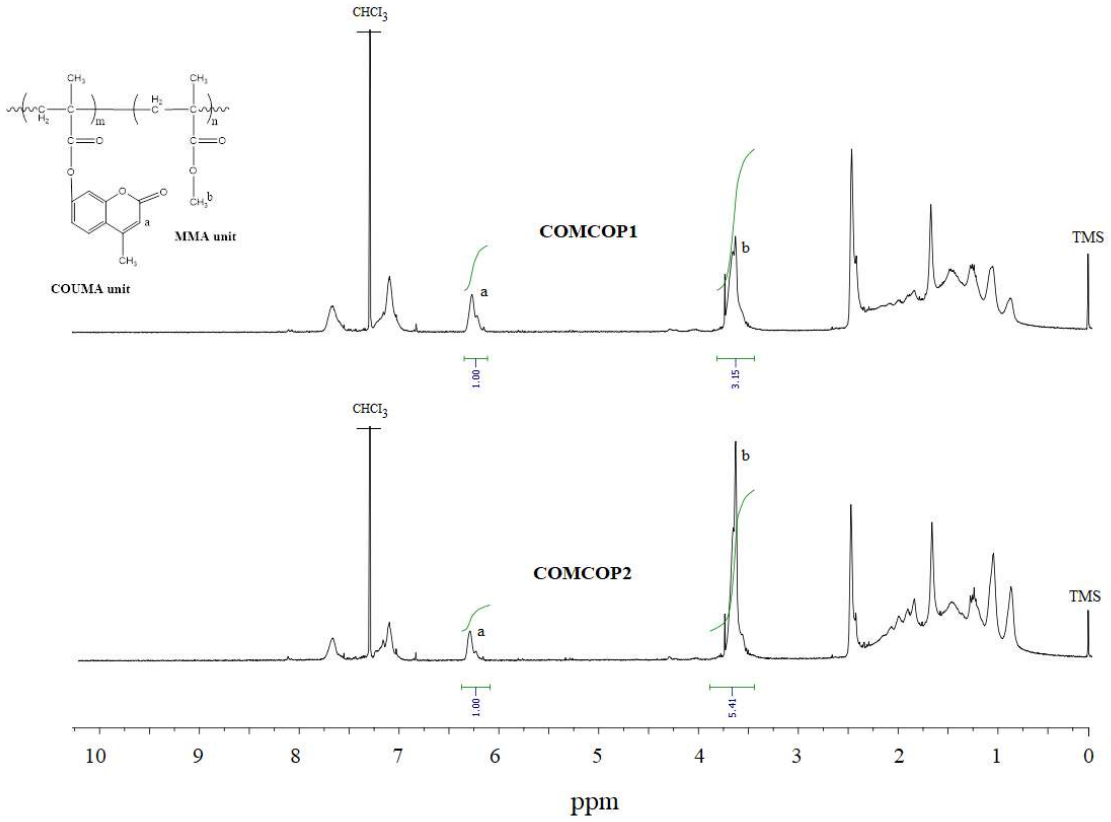

Figure 3.13. ^{1}H-NMR spectra of COMCOP1 and COMCOP2 (in $CDCl_3$)

Table 3.13. ^{1}H-NMR evaluation for COMCOP1 and COMCOP2 (in $CDCl_3$)

Chemical shift (ppm)	Signal type
0.91 – 1.90	$-CH_3$
2.0 – 2.5	$-CH_2-$
2.46	$-CH_3$
6.23	-C=CH

3.4.2. UV-vis spectroscopy analysis of COMCOP1

Figure 3.14 shows the UV-vis spectra of P(COUMA49%-co-MMA) (COMCOP1) in dilute solution of THF measured after 365 nm UV light irradiation at different time intervals of 0-240 hrs.

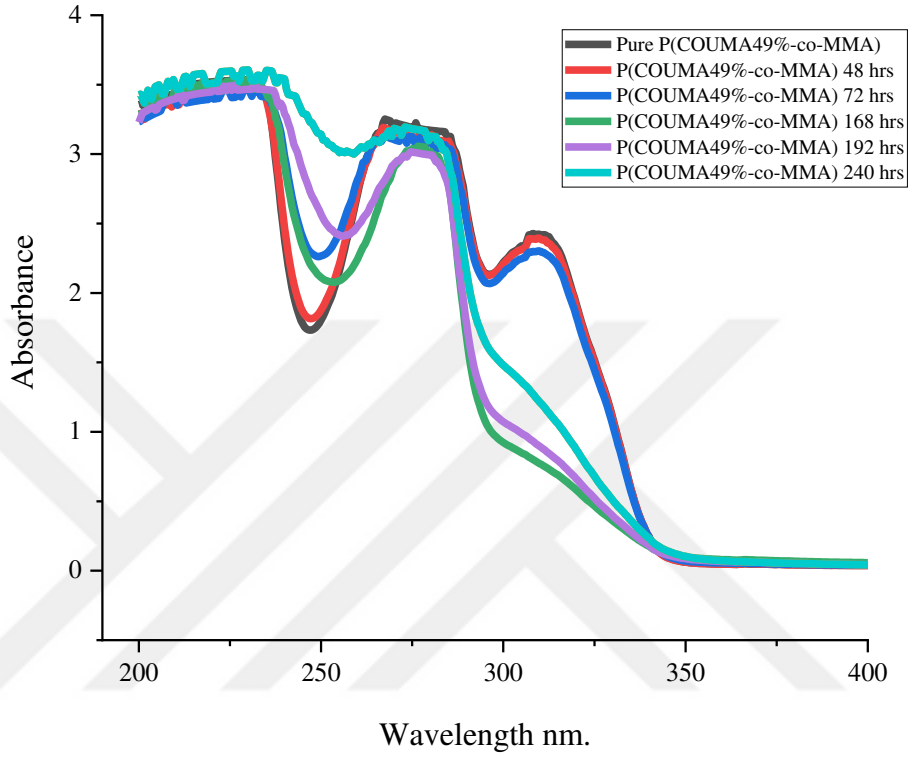

Figure 3.14. UV-vis spectra of COMCOP1 in dilute solution of THF

Subsequent to UV irradiation, COMCOP1 copolymer was characterized using FTIR and ^{1}H-NMR techniques in order to confirm the occurrence of photodimerization in the copolymer. Figure 3.15 shows the FTIR spectra pure COMCOP1 and UV irradiated COMCOP1 at 365 nm after 240 hours. The IR spectra is evaluated in Table 3.14. ^{1}H-NMR spectra of pure COMCOP1, and COMCOP1 after UV irradiation at different time intervals (120 h, 168 h and 240 h) are shown in Figure 3.16, and evaluated in Table 3.15. Figure 3.17 on the other hand shows the degree of photo-initiated dimerization of COMCOP1 copolymer in relation to time. This was carried out in a dilute solution of $CDCl_3$ and recorded after UV irradiation at 365 nm.

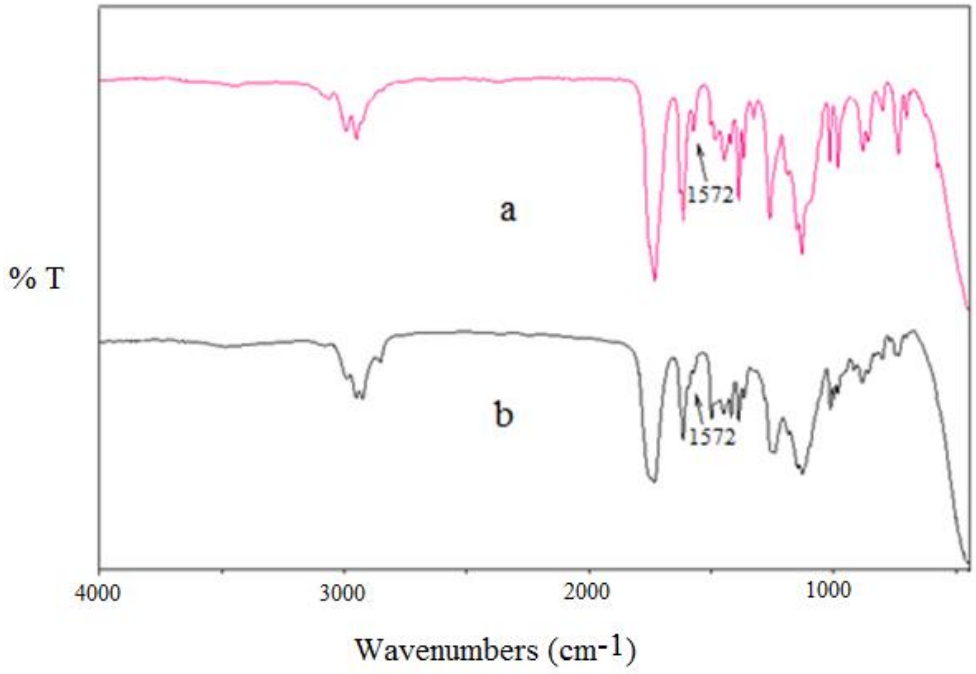

Figure 3.15. FT-IR spectra of a) pure COMCOP1 and b) COMCOP1 irradiated with UV light at 365 nm for 12 days

Evaluation of the FT-IR spectra of pure COMCOP1 and UV irradiated COMCOP1 at 365 nm for 12 days are given in Table 3.14 below.

Table 3.14. FT-IR evaluation of a. COMCOP1 b. COMCOP2

Wavelength (cm^{-1})	**Vibration type**
1572	C=CH
1419-1497	C-H
N/A due to overlapping of 6 membered lactone and ester C=O	C=O

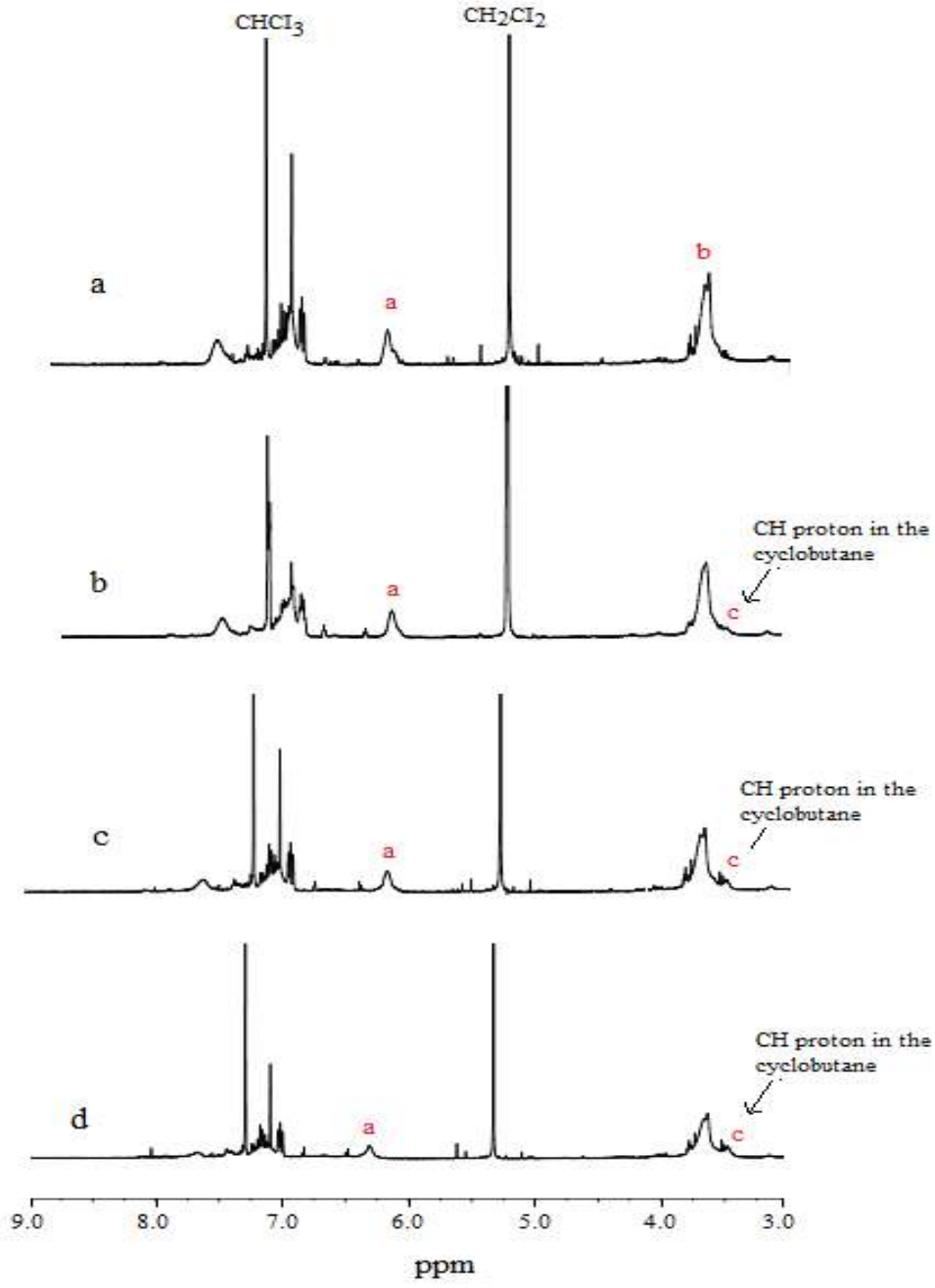

Figure 3.16. ^{1}H-NMR spectra in $CDCl_3$ of a) COMCOP1 before UV light and b) 5 days c) 7 days d) 12 days after UV light at 365 nm

Table 3.15. ^{1}H-NMR Spectra evaluation of a. COMCOP1 before UV light irradiation and b. 5 days c. 7 days d. 12 days UV light at 365 nm

Chemical shift	**Signal type**
3.61	-OCH3
6.23	HC=CH
3.45	CH over cyclobutane ring

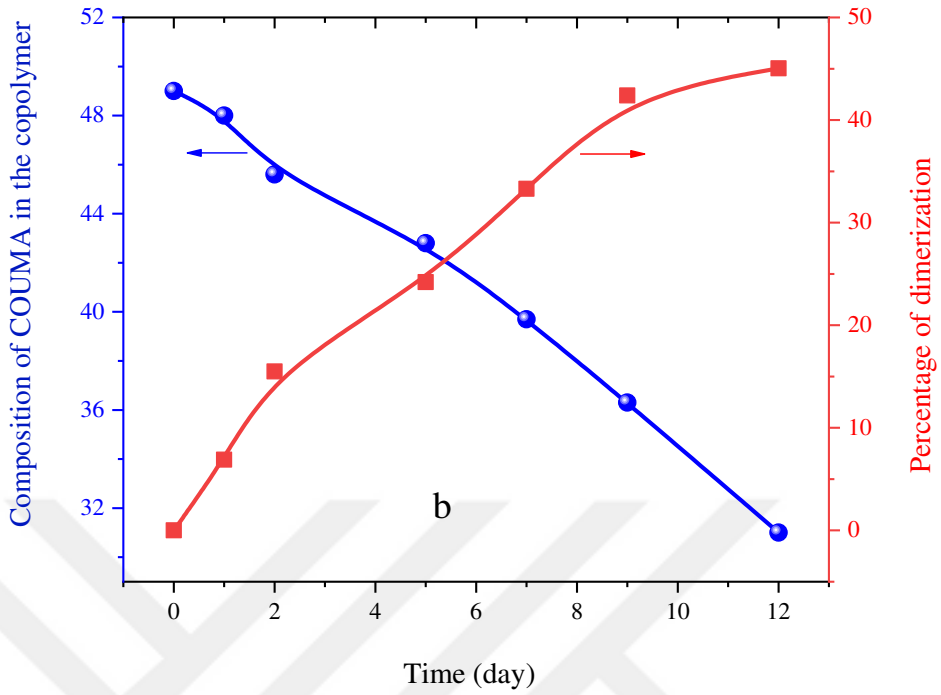

Figure 3.17. Composition of COUMA in the copolymer system and percentage dimerization depending on time of COMCOP1 in dilute solution of $CDCI_3$ recorded after UV irradiation showing photodimerization upon at 365 nm irradiation

3.4.3. Kinetic analysis of P(COUMA49%-co-MMA)/GO 16 wt.% (COMCOP1)

The kinetic studies of thermal degradation of pure COMCOP1 and P(COUMA49%-co-MMA)/GO 16 wt.% (COMCOP1/ GO 16 wt.%) was carried out by thermogravimetric analysis using non-isothermal methods. The TGA curves for the kinetic studies of pure and 16 wt.% GO doped COMCOP1 are given in Figure 3.18. The thermal degradation was performed at different temperature ranges from room temperature to 500 °C under nitrogen gas flow (in the flowing rate of 10 ml/min) at different heating rates of 5, 10, 15, 20 and 30 °C. The average activation energy values were calculated via FWO and KAS models in a period of α=0.10–0.70. FWO and KAS models for E_a measurement for pure COMCOP1 and COMCOP1/ GO 16 wt.% are shown in Figures 3.19 and 3.20 respectively. Variation of activation energy with conversion (α) for pure COMCOP1 and COMCOP1/ GO 16 wt.% are given in Figure 3.21.

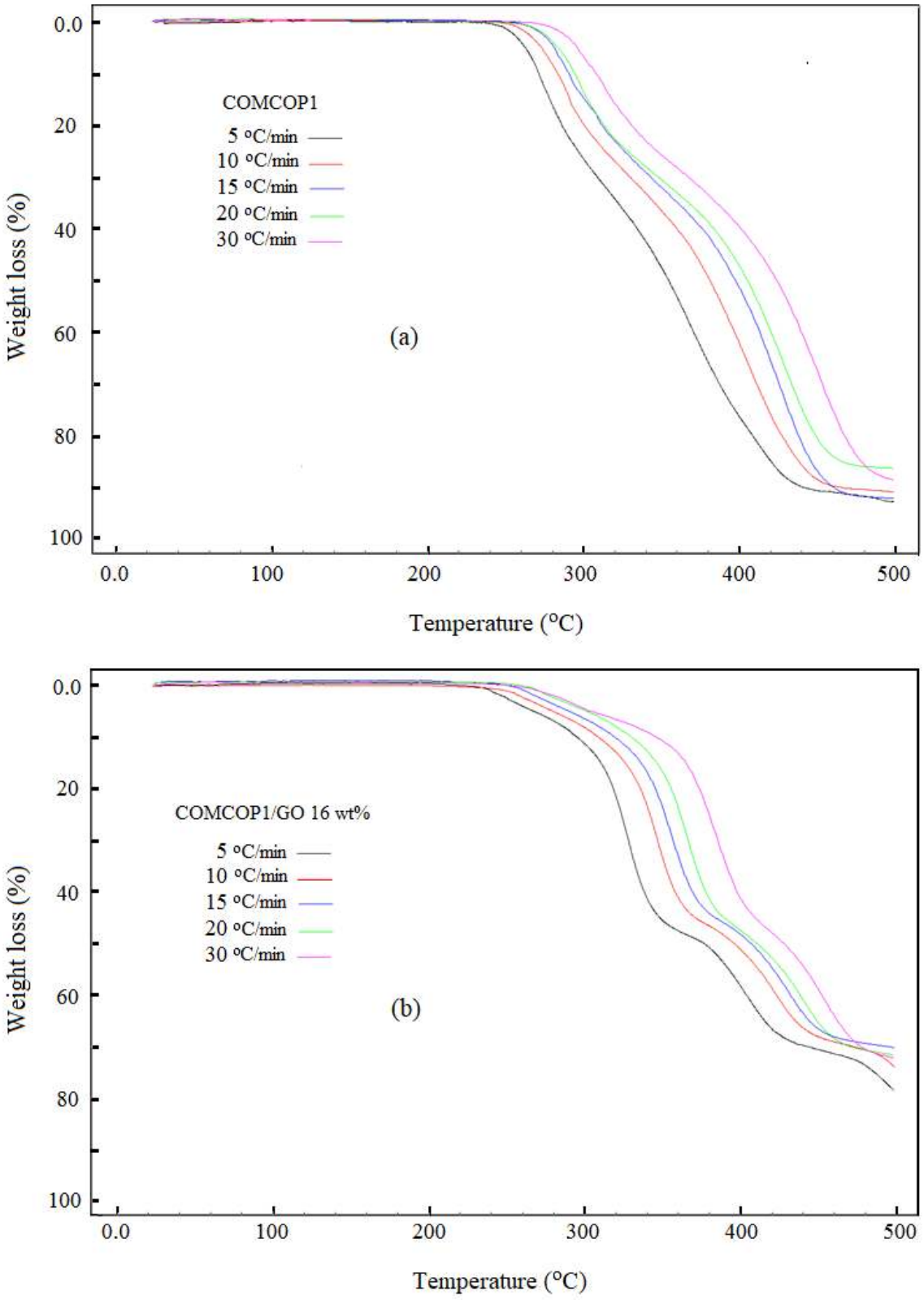

Figure 3.18. TGA curves of a) COMCOP1 and b) COMCOP1/GO 16 wt.% for heating rate of 5, 10, 15, 20 and 30 °C under argon gas flow of 10 ml min^{-1}

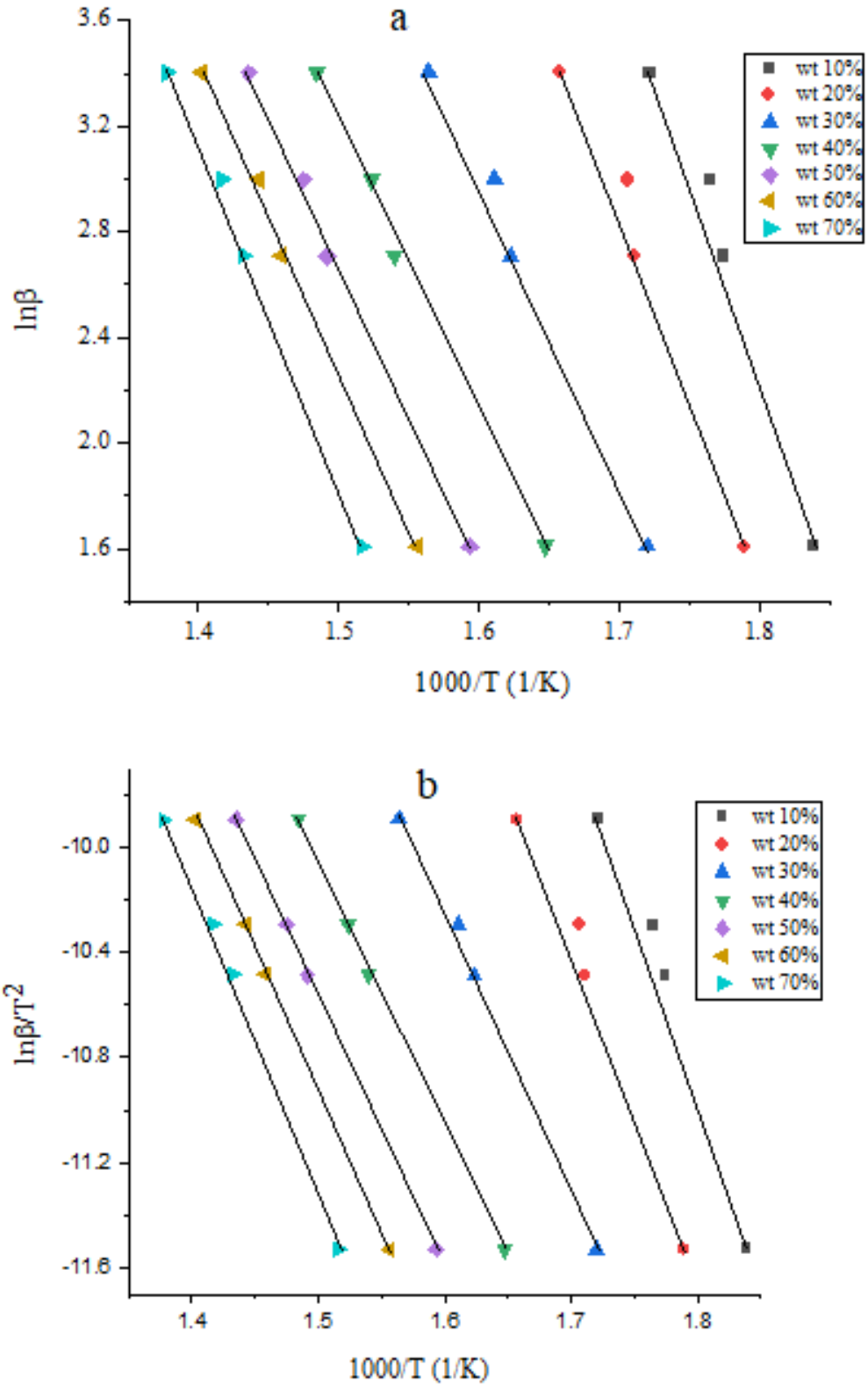

Figure 3.19. (a) FWO and (b) KAS plots of COMCOP1 for different values of conversion

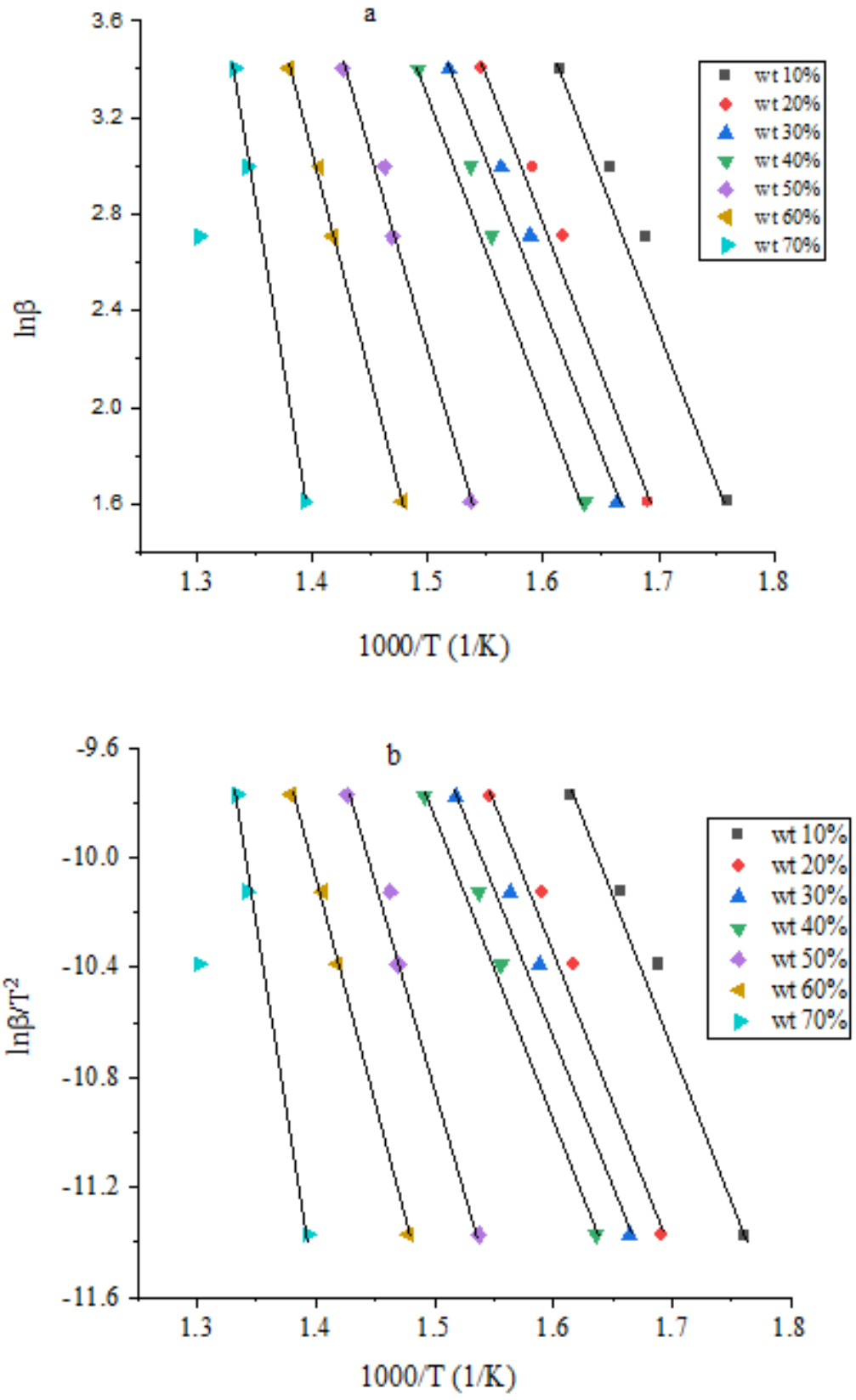

Figure 3.20. (a) FWO and (b) KAS plots of COMCOP1/GO 16 wt.% for different values of conversion.

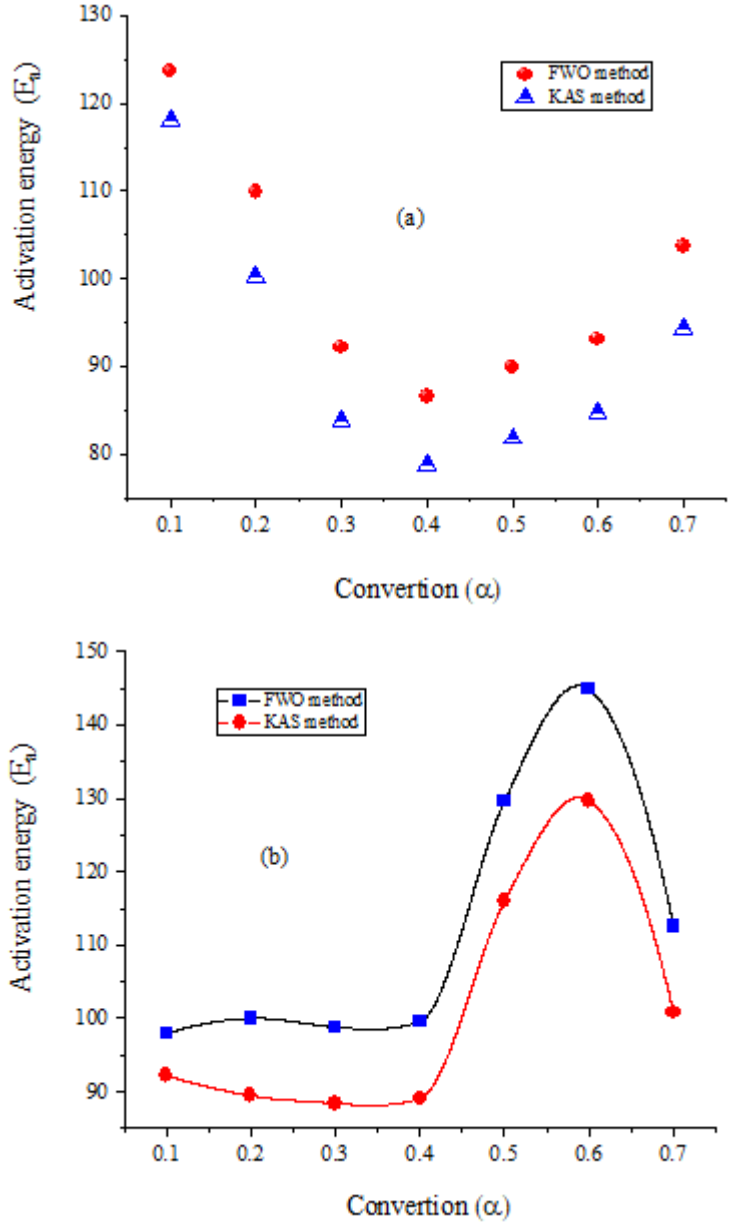

Figure 3.21. Activation energy variation with conversion, for a) pure COMCOP1 and b) COMCOP1/GO 16 wt% composite, estimated from FWO method and KAS method

3.4.4. Electrical investigation of COMCOP1/ GO and COMCOP2/ GO composite systems at different temperatures

Variation of dielectric constant, dielectric loss factor, tangent loss versus frequency, I-V and DC conductivities versus temperature (K) of COMCOP1 and COMCOP2 are shown in Figure 3.22-3.28. Detailed graphs of dielectric investigations of COMCOP1 and COMCOP2 are given in Appendices 1 and 2, respectively.

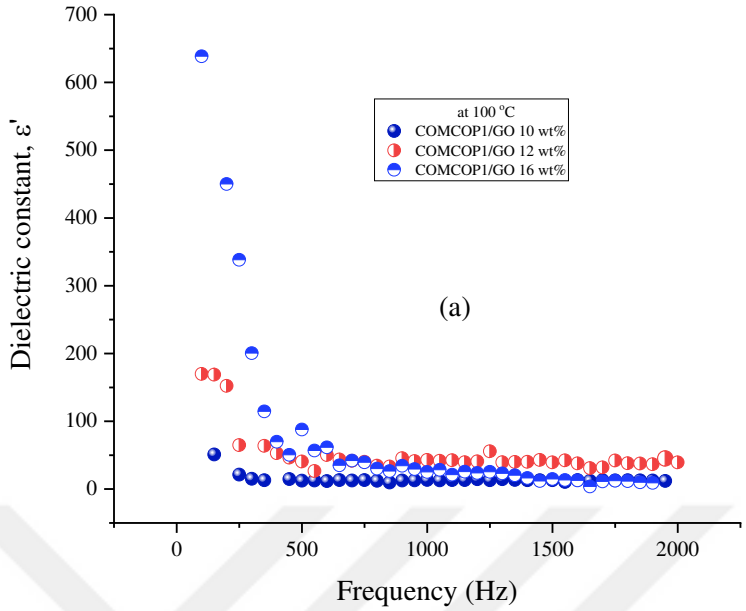

Figure 3.22. Dielectric constant dependence on frequency for COMCOP1 composites loaded with GO 10 wt.%, 12 wt.% and 16 wt.% at 100 °C

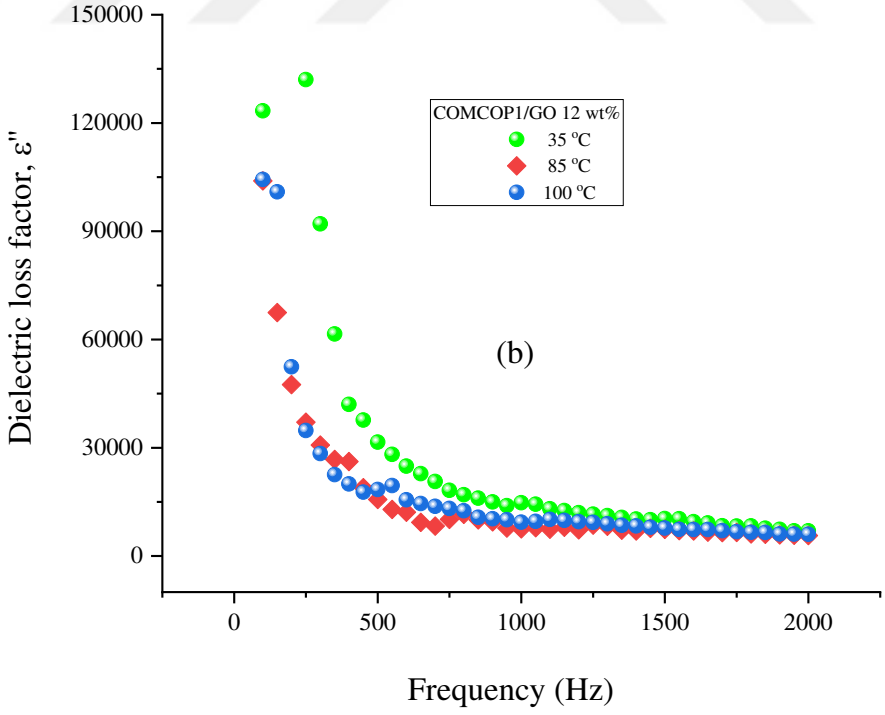

Figure 3.23. Dielectric loss factor dependence on frequency for COMCOP1/GO 12 wt.% composite at various temperatures

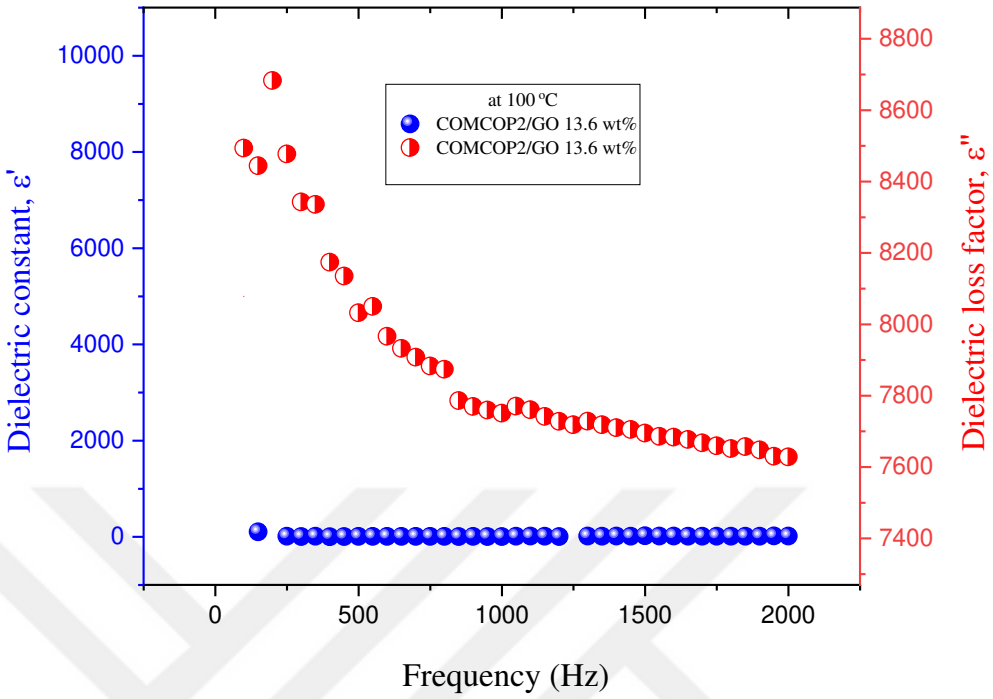

Figure 3.24. Dependence of ε´and ε´´ as a function of frequency for COMCOP2 filled with GO 13.6 wt.% at 100 °C

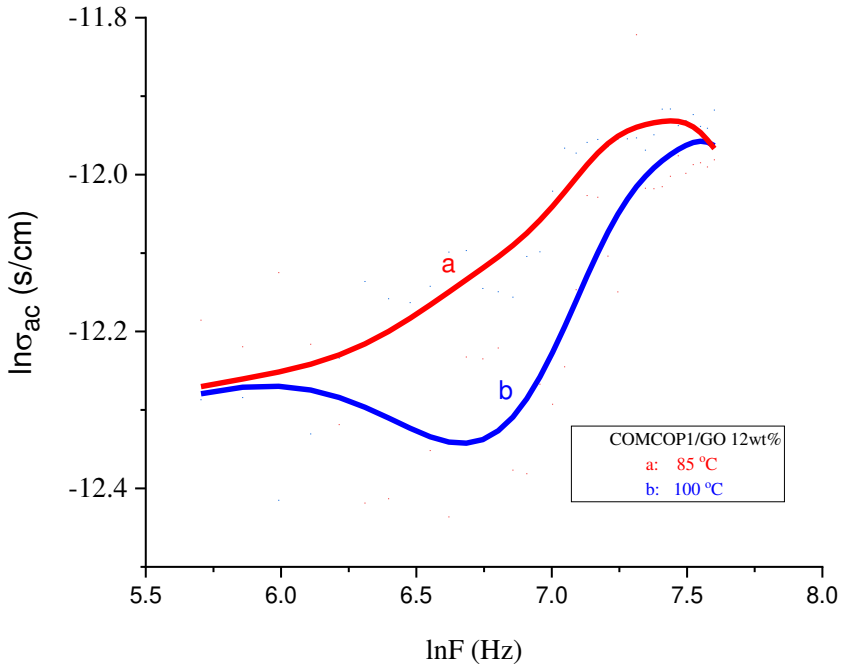

Figure 3.25. Dependence of $\ln\sigma_{ac}$ (S/cm) as a function of lnF for COMCOP1/GO 12 wt.% composite at 85 °C and 100 °C

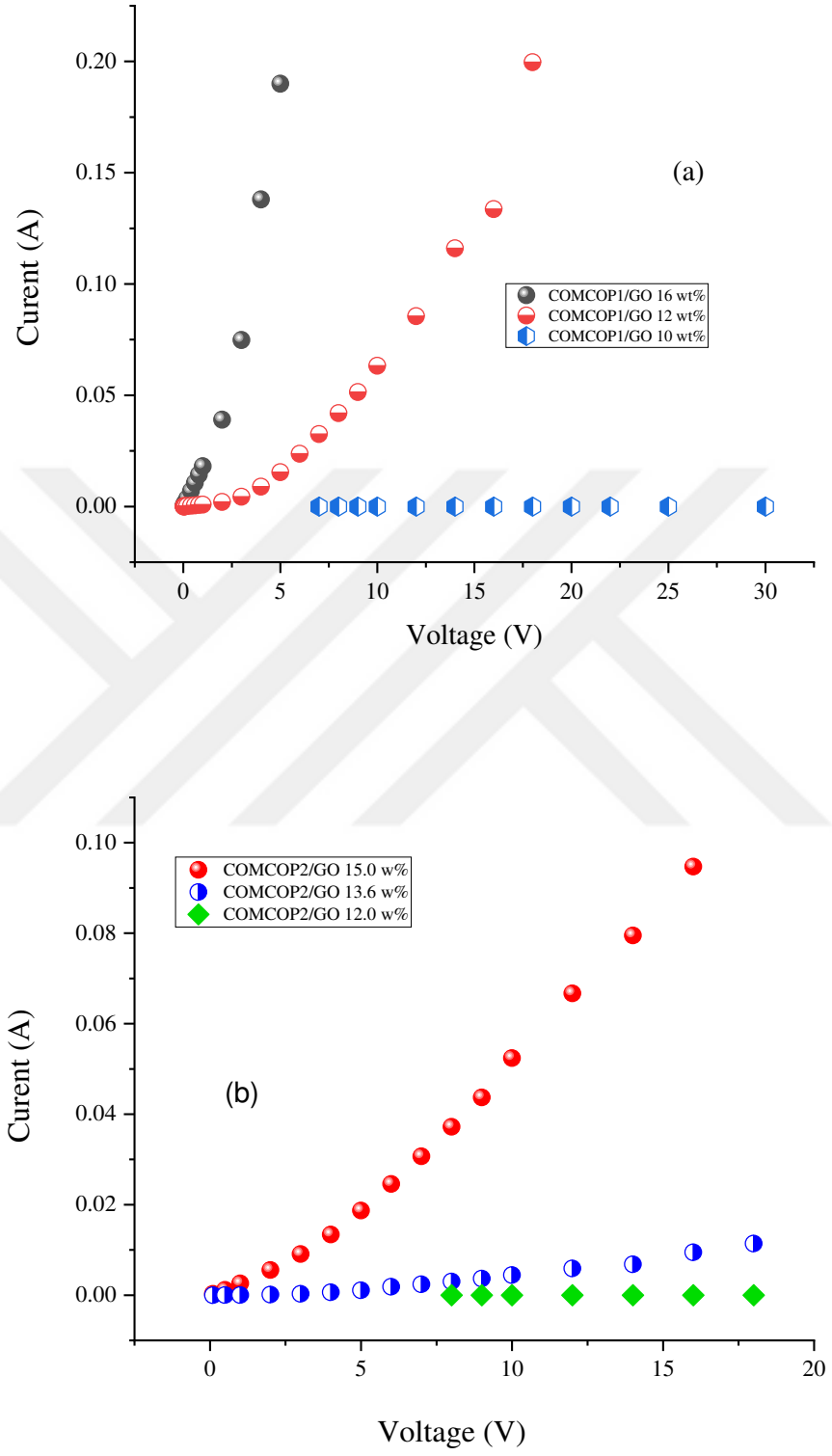

Figure 3.26. Current (I) - Voltage (V) characteristics of a) COMCOP1 and b) COMCOP2 composites (for various concentrations of GO)

For all the samples, $\ln\sigma_{dc}$ -1000/T graphs were drawn, from which the activation energies corresponding to the degrees of decomposition were calculated.

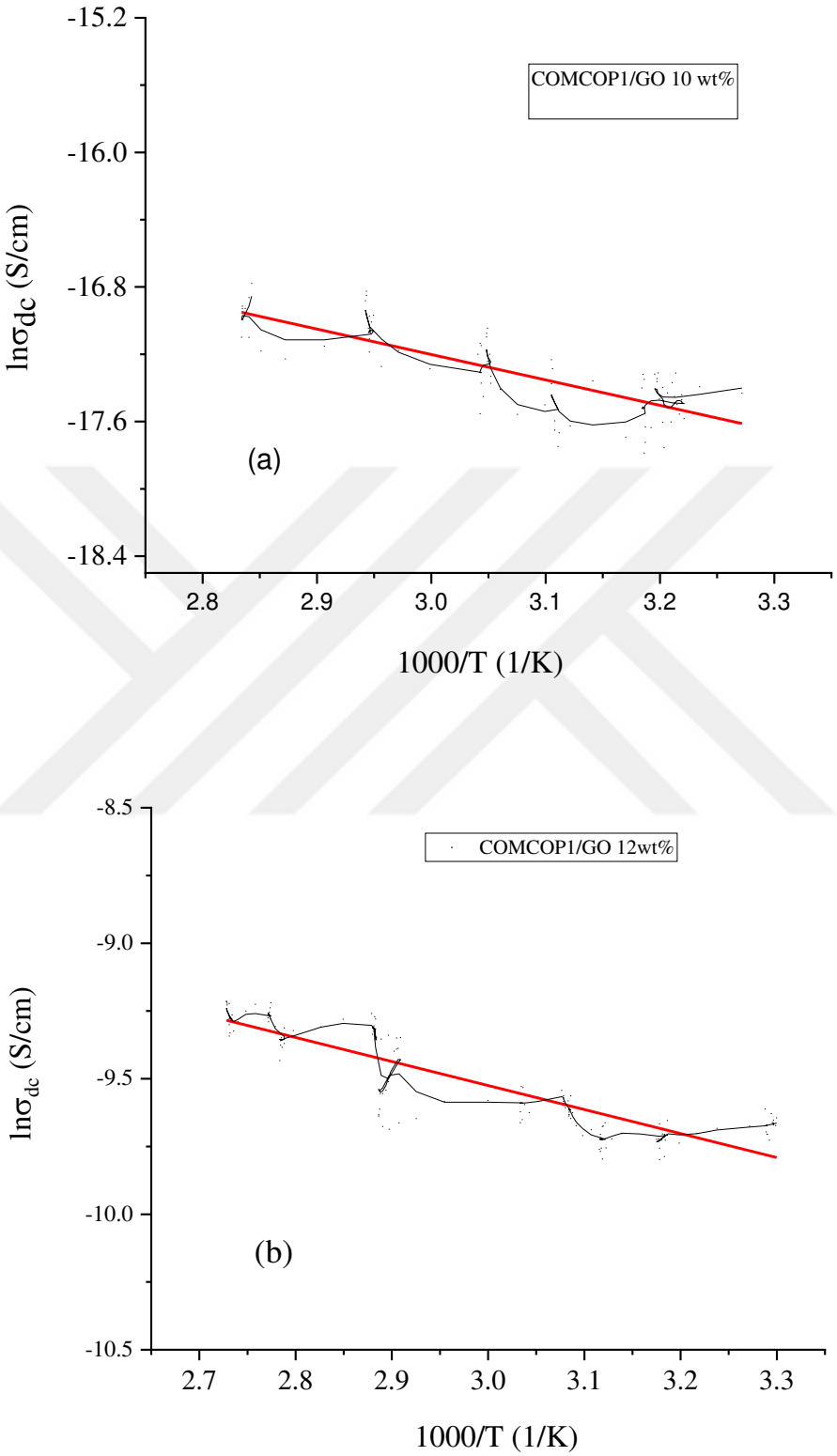

Figure 3.27. DC conductivity dependence on temperature for a) COMCOP1/GO 10 wt.% and b) COMCOP1/GO 12 wt.% composites

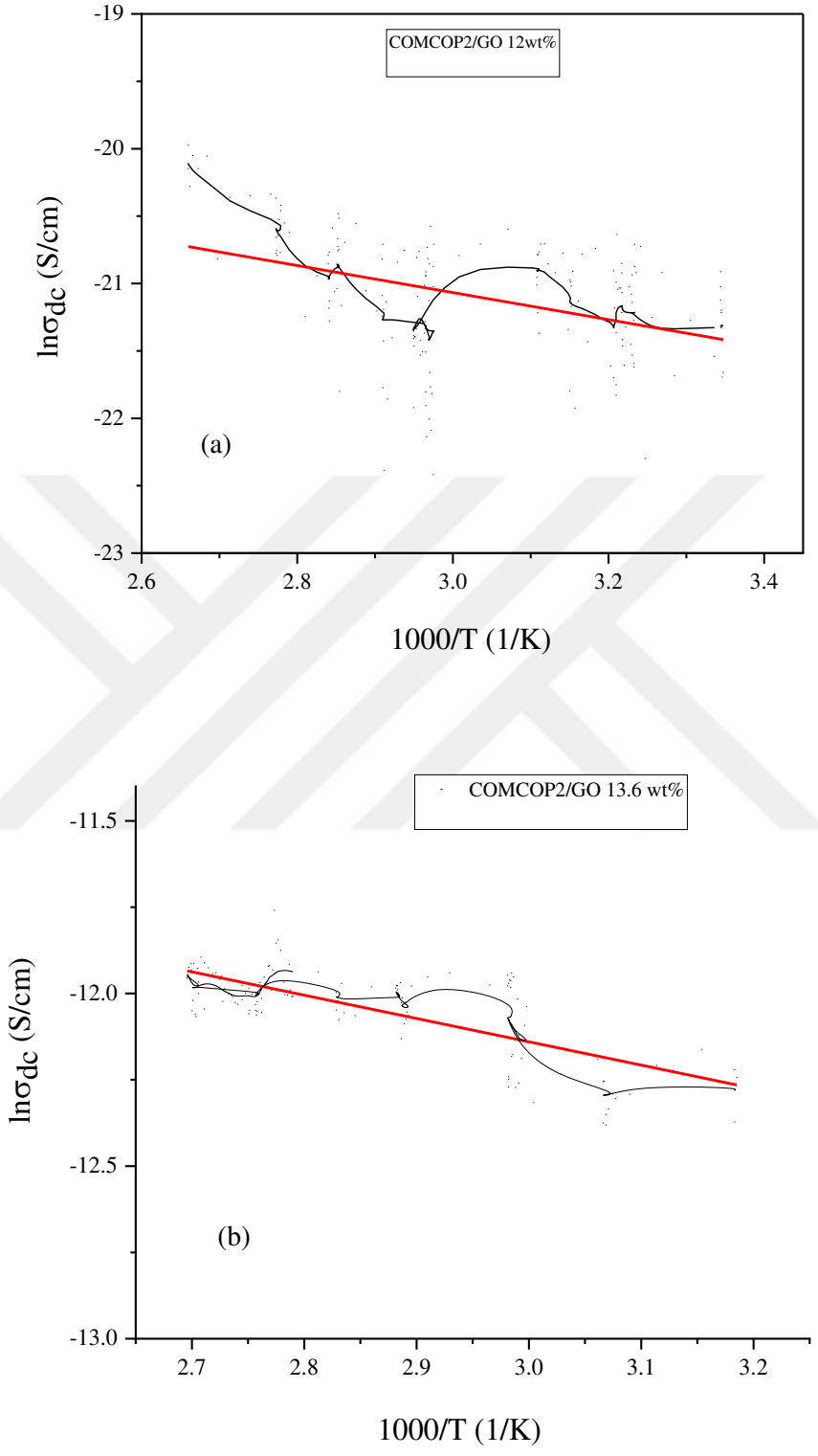

Figure 3.28. DC conductivity dependence on temperature for a) COMCOP2/GO 12 wt.% and b) COMCOP2/GO 13.6 wt.% composites

4. DISCUSSION

The structure of COUMA and MMA copolymers were confirmed by ^{1}H-NMR spectra as indicated in Fig. 3.8. While methyl and olefinic protons (−CH_3 and C=CH next to ester and on the ring of COUMA) appeared at 2.46 and 6.23 ppm, the methyl and methylene protons (−CH_3- and CH_2-) in the copolymer backbone contributed to the signal around 0.91–1.90 and 2.0–2.5 ppm, respectively. The peaks at 3.61 ppm indicated chemical shifts of the methoxy (CH_3O-) protons of MMA units. The characteristic peaks of the protons of COUMA and MMA showed the linking of COUMA and MMA moieties to the polymer backbone. The composition ratio of COUMA and MMA in the copolymers were estimated from integration heights of ^{1}H-NMR spectra as indicated (see Fig. 3.8). For this purpose, the copolymer composition ratio of COUMA and MMA in the copolymers was estimated by integrating to 1H (C=CH- next to ester oxygen) revealed at 6.23 ppm in COUMA unit the total number of 3 protons belonging to 3.61 (CH_3O- protons) of MMA unit. For example, the integration value per an olefinic hydrogen in COUMA moiety is 1 unit, total integration heights for 3H (-CH_3O- next to ester oxygen) of MMA unit is 3.15 unit, that is, integration value per hydrogen is 1.05 unit. Here, because the total number of protons is 2.05 units, the mole fraction of COUMA in the COUMA-MMA copolymer was estimated as 0.487 (49%). With similar calculation, the mole fraction (%) of COUMA unit incorporated in the other copolymers were calculated to be 9%, 24%, 36% and 65%. The FT-IR spectra of P(COUMA8.9%, 24%, 65%-co-MMA) as well as COMCOP1 (49%) and COMCOP2 (36%) showed the most characteristic bands of COUMA and MMA units at 1730 cm^{-1} (C=O stretching) and 1624-1572 cm^{-1} (C=C stretching), respectively. Comparing to each other, the absorption band around 1647 cm^{-1} of COUMA increased. Main assignments of absorption bands of the copolymer are as follows: 2993 cm^{-1}, (-CH_2-) C-H bending; 2923 cm^{-1}, (CH_3-) C-H bending; 1755 cm^{-1} C=O in the ester functional group of methacrylate in COUMA unit 1730 cm^{-1} C=O in the ester functional group in MMA; 1624 cm^{-1}, 1615 cm^{-1} and 1572 cm^{-1} (C=C stretching), a sharp band at 1261 cm^{-1} and a broad band at 1131 cm^{-1} are assigned to Ar–O–C symmetric and asymmetric stretching vibration of the ester group, respectively.

Fig. 3.2 and 3.5 show the TGA thermograms of PCOUMA and PMMA respectively. The weight loss temperatures were measured up to 500°C at the rate of 10°C/min. The weight loss (%) of the pure PCOUMA and PMMA homopolymers are 96.1% and 95% respectively. Fig. 3.9 indicate TGA thermograms of the pure copolymers. The weight loss temperatures of the copolymers were measured up to 500°C at 10°C/min. The weight loss temperatures of the copolymers were measured at 97.5, 94.4, 92.4, 88.5 and 85.8 (%) respectively. Fig. 3.10 indicates the DSC thermograms of the pure copolymers P(COUMA8.9-65%-co-MMA) consecutively. The glass transition temperatures of the copolymers at different amounts of monomer substituents

were measured up to 200 ºC at heating rate of 20 ºC/min. The T_g values of the copolymers are 135.55ºC, 131.02ºC, 130.15ºC, 129.73ºC and 125.53ºC respectively.

Fig. 3.12a and 3.12b indicate DSC thermograms for the pure COMCOP1, COMCOP2 and their composite filled with GO, respectively. After full curing, the glass transition temperatures (Tg's) of COMCOP1 and COMCOP2 were measured at 20 ºC/min by a second scan as the temperature of the halfway point of the heat capacity transition when the material was converted from glass to rubber. The T_g values of neat COMCOP1 and COMCOP2 are 166 ºC and 137 ºC, respectively. The T_g of PMMA has been recorded as 109.5 ºC in the literature [42]. With an incorporation of 49 mol % COUMA content, the T_g of COMCOP1 increased to 166 ºC, which was higher 56.5 ºC than that of the control PMMA. However, T_g of COMCOP2 decreased with the decrease of COUMA content in the copolymer system, for example, when the content of COUMA in the copolymer system have reached to 36 mol %, the T_g drops to 137 ºC. In this regard, T_g values of copolymers increased by the incorporation of COUMA units to the copolymer system. In the literature, it has been recorded that the glass transition temperature of copolymers in different ratios of increasing COUMA unit for coumarin based copolymers containing butoxyethyl methacrylate have increased [43]. When GO content in the COMCOP1 increased from 10% to 16%, the T_g value increased from 162 ºC to 173 ºC. In this regard, we think that movement ability of the chain is limited due to the strong effect of strong dipole–dipole interaction between coumarin group, which is a bulk group and GO may be another factor that affects the T_g temperature. On the other hand, while the T_g of neat COMCOP2 is 137 ºC. T_g values of COMCOP2 composite containing GO 12, 13.6 and 15 wt% was relatively 143, 150 and 170 ºC, respectively. The reason for such an interesting behavior can be attributed to the fact that the graphite oxide particles in the the copolymer reflects the movement ability of the chain.

The transition of n or π electrons to the π* excited state of the UV-Vis region at wavelengths ranging from 200 to 400 nm is the main characteristic of electronic absorption spectroscopy of organic compounds. Thus, UV spectra provide important information on energy difference between boundary molecular orbitals, conjugation and aromaticity. The dimerization of coumarin in the COMCOP1 was carried out by irradiation of a THF solution of copolymer at 365 nm for 240 hours in presence of 15W UV light. In this regard, the formation of photodimerization of the coumarin group in the prepared low dilute solution of the copolymer bearing the coumarin group was followed by UV-vis spectroscopy. UV-vis spectra of copolymer recorded over irradiation time are shown in Fig. 3.14. It shows UV-vis spectra given in comparison with each other and recorded in the tetrahydrofuran solution at different time intervals for COMCOP1.

The absorption peaks are observed at 310 and 278 nm without the aid of additional catalysts. It can be deduced that these peaks imply to the n→π* and π→π* transitions, respectively. The maximum peak intensity of the n→π* transition in the coumarin group at 310

nm decreases depending on the ongoing irradiation time, indicating an increase in the degree of dimerization. The polarity of solvent during photochemical processes has recently been shown to play an important role where excited-state, otherwise inversion is possible. As seen in Fig. 3.14, as time increases, the maximum peak intensity decreases, the peaks reflect the contribution of π-π * transitions of conjugated benzene and pyrone groups in the 4-methylcoumarin chromophores in the copolymer structure. Since the double bonds of the 4-methylcoumarin in the copolymer structure gradually dimerize to form cyclobutane ring and dilactone under 365 nm UV light, the conjugation between the double bonds and the phenyl ring can be significantly reduced as a result of homolytic cleavage of the C = C bond adjacent to the ester C = O group (see Fig. 2.6). As a result, the intensity of absorbance bands becomes more and more weaker. According to literature studies, four isomeric structures of coumarin dimers have been recorded [44, 45]. This reversible process provides reversible state networks in supramolecular architectures [46], this behavior creates a useful reaction pathway in the polymer field from photodimerization of coumarin based structures. Similar behavior was also observed for COMCOP1 prepared in this study. Photo-cycloaddition of coumarin derivatives [2πs + 2πs] with the photo-cyclobutane derivatives themselves even another double bond in the reaction medium upon irradiation with UV light (> 300 nm) is widely used in the synthesis of polymeric networks [47, 48].

Fig. 3.15a and 3.15b indicate comparatively the FT-IR spectra of COMCOP1 irradiated at 365 nm and pure COMCOP1. The 1572 cm^{-1} (C=CH) band, which appears to be moderate in Fig. 3.15a, but weakened in Fig. 3.15b and aliphatic C-H stretching at 1419-1497 cm^{-1} were important changes for photodimerization of coumarin units. In addition, the lactone C=O band couldn't be observed due to overlapping in the same region as both the C=O band of six membered lactone ring and ester C=O band in the methacrylate unit. The ^{1}H-NMR spectrum was very informative to follow dimerization of coumarin in the COMCOP1. Fig. 3.17 shows cyclobutane conversion depending on time. The spectrum revealed the presence of methoxy group (at 3.61 ppm) and the proton (at 6.23 ppm) over carbon-carbon double (π) bonds next to ester C=O group in the COMCOP1. The intensity measurements showed that the ratio of proton (at 6.23 ppm) over carbon-carbon double (π) bonds in the COUMA units to methoxy protons in MMA units of copolymer indicated both conversion of cyclobutane and composition of copolymer. The intensity of this signal (6.23 ppm) decreased upon time. In this regard, when solution in $CDCI_3$ of the copolymer was irradiated with UV light at 365 nm for 7 days, integral intensities of protons at 6.23 ppm and 3.61 ppm were 0.22 unit (1H) and 1.0 unit (3H or per hydrogen is 0.333 unit), respectively. Hence, the composition of copolymer and conversion to cyclobutane were 39.7% and 33.3%, respectively. After 12 days, the COUMA units in the COMCOP1 copolymer system were decreased from 49% to 31% (by mol). Also, a new resonance peak appears at 3.45 ppm, which is characteristic for formation of cyclobutane ring. As photodimerization of coumarin

increases, the intensity of peak at 3.45 ppm increased. This increase in resonance signal was another important evidence of photodimerization. The molecular interactions should arise mainly from the interaction between COUMA units within the same copolymer chain. Therefore, this behavior indicates the formation of a single chain polymer molecule (SCPM) with intramolecular dimerization and without cross link. From the ^{1}H-NMR measurements of every irradiated copolymer solution, the composition of moieties having coumarin in the copolymer was estimated. It can be concluded that the coumarin moieties present are the control factors for photoreversibility at 365 nm UV light. Although coumarin moieties at high diluted copolymer have decreased from 49% to 31% (by mol) at 365 nm UV light, no crosslinked networks were observed in the copolymer solution within the $CDCI_3$. The ability to record the ^{1}H-NMR spectrum of the very dilute solution in $CDCl_3$ irradiated for up to 12 days at 365 nm is another proof that the copolymer was not cross-linked. This behavior indicates that the photodimerization tendency of interchain coumarin groups is more difficult than that of intrachain coumarin groups, as the coumarin-containing copolymer was highly diluted in $CDCI_3$. For this reason, cross-linked polymers cannot be formed in the solution. Hence, as seen in Fig. 2.6, we suggested that dimerization occurs within the copolymer chains, not between the copolymer chains of the coumarin units. All of these results indicated that the formation of cyclobutane due to the intramolecular dimerization of coumarin moieties in the copolymer confirms the successful formation of the single chain polymer molecule. In addition, in our study, the photodimerization process of coumarin units in the dilute solution of both tetrahydrofuran (THF) and $CDCI_3$ of COMCOP1 indicated that the copolymer was not crosslinked up to 12 days.

All the isoconversional methods take their origins in the isoconversional principle, which states that the reaction rate in a certain constant conversion is only a function of temperature. The majority of kinetic methods used in thermal analysis field consider the rate depending upon temperature (T) and conversion (α) to be a function of only two variables:

$$d\alpha/dt = k(T)f(\alpha) \qquad (1)$$

The dependence of the process rate on temperature is denoted by the rate constant k and the transformation model f (α). The rate of a one-step process is described by equation (1). For the kinetic study of COMCOP1 and COMCOP1/GO 16 wt.% for seven conversion rates (α = 0.1–0.7) at the heating rates of 5, 10, 15, 20 and 30 °C min^{-1}, the TGA thermograms can be seen in Fig. 3.18. The kinetics of thermal degradation can be possible to estimate from the TGA curves using various methods. In this regard, the results obtained from thermogravimetric measurements are presented via model-free methods to estimate the kinetic parameters. A straight line whose slope was used in the calculation of E_a, it is derived from the logβ vs. 1/T plot from the data of a series of experiments performed at several heating rates, from which the E_a was calculated.

$$\ln(\beta) = \text{Constant} - 1.052\, Ea/RT \qquad (2)$$

In equation (2), R is a constant and β is the heating rate (°C/min). The Kissinger-Akahira-Sunose (KAS) model was used to estimate activation energy (E_a) more comprehensively than any other multiple heating rate technique due to its simplicity of usage. By considering Equation 3, the KAS method gives a relationship between heating rates and activation energy.

$$\ln(\beta/T^2) = \ln [(AR/Ea\ g\ (\alpha)] - (Ea/RT) \qquad (3)$$

The activation energy (E_a) required for a particular decomposition is calculated by the slope of the line obtained from graph of the $\ln(\beta/T^2)$ versus 1/T. On the other hand, the activation energy for a certain conversion point (α) is determined from the equation that the slope is equal to - E_a/R. In this regard, the FWO plot lnβ versus 1000/T K^{-1} for different values of conversion are shown in Fig. 3.19a, The KAS plot of $\ln\beta/T^2$ versus 1000/T (K^{-1}) for different values of conversion are shown in Fig. 3.19b. The FWO and KAS plots of COMCOP1/GO 16 wt.% were indicated in Fig. 3.20a and 3.20b, respectively.

The activation energy (E_a) values were estimated by FWO and KAS methods considering the conversion range studied (α=0.1-0.7). The average values of activation energy obtained from Kissinger method for COMCOP1 and COMCOP1/GO 16 wt.% were 94.5 kJ mol^{-1} and 101 kJ/mol, respectively. Whereas, those estimated by FWO method were 103.5 and 87.0 kJ/mol. Those data are consistent with the range of values obtained by the FWO and KAS methods. This behavior indicates that the models adequately describe the process of decomposition of the pure copolymer and its composite. In this regard, the activation energy during decomposition of neat copolymer and its composite had little variation in both methods used, which allows it to be adequately described as single-stage kinetic [49]. It has been recorded that the E_a value for the pure commercial PMMA decreased from 160 to 110 $kJmol^{-1}$ between α = 0.05 and 0.55 in the literature [50]. Laachachi et al. recorded similar results for the thermal degradation of PMMA in air [51].

Fig. 3.21a and 3.21b show the plots of activation energy as a function of conversion for α =0.1-0.7 COMCOP1 and COMCOP1/GO 16 wt.% composite based on two isoconversional methods. The estimated activation energy range is also clearly observed in Fig. 3.21a with a ‘‘V’’ shape between 86.6 and 123.6 $kJmol^{-1}$ (for FWO) and 78.7 and 118.0 $kJmol^{-1}$ (for KAS). As the thermal decomposition process proceeded in the COMCOP1 for FWO method, the activation energy slightly changed after the initial stage and decreased until α = 0.40, and the minimum activation energy was this point with 86.6 kJ/mol. After this point, an immediate increase in E_a was observed. Subsequently, there was an immediate increase to 103.7 kJ/mol (for α = 0.70). Similar trend was observed for KAS method until α = 0.40, and the minimum activation energy

was this point with 78.7 kJ/mol. On the other hand, as seen in Fig. 3.21b, the plot of activation energy as a function of conversion for COMCOP1/GO 16 wt.% composite was different from that of pure copolymer. The activation energies estimated for FWO and KAS methods did not change considerably up to $\alpha = 0.40$. The activation energies after this point increased giving a maximum 144.9 kJ/mol (for FWO) and 129.6 kJ/mol (for KAS method).

The complex permittivity ($\varepsilon*$) associated with free dipole swing can be studied according to the Debye equation as $\varepsilon* = \varepsilon' - i\varepsilon''$[52]. The real part ($\varepsilon'$) of complex permittivity is responsible for the electrical energy saving ability when an external electrical field is applied and the imaginary part for the power dissipation of the material. The ε' of the sample is a function of capacitance and it is estimated depending upon capacitance measurement as:

$$\varepsilon' = C.d/(\varepsilon_o A) \qquad (4)$$

In the above equation (4), A is the area of the electrode, C is the parallel capacitor, ε_o is the permeability of space and d is the thickness of the sample. It is known that with increasing frequency, the dielectric constant decreases due to its non-Debye behavior for the lower frequency range. Fig. 3.22 and 3.23 indicate the dielectric constant dependence on frequency for COMCOP1 composites loaded with GO 10 wt.%, 12 wt.% and 16 wt.% at 100 °C and dielectric loss factor dependence on frequency for COMCOP1/GO 12 wt.% composite respectively in various temperatures from 100 Hz to 2 kHz. Since the ε' is systematically decreased with increasing frequency due to the polarization effect, the charge accumulation in the prepared tablets also reaches constant values. The real part of complex permittivity is responsible for the electrical energy storage capability when an external electric field applied, and the imaginary part is responsible for the power dissipation of the material. In the prepared composite systems, filler GO as conductive component is polar due to possession of functional groups such as COOH, OH and epoxy groups, and furthermore matrix nature of the COMCOP1 also has a polar group. Therefore, with the addition of GO, dipolar and interfacial polarizations increase. Due to the addition of GO to COMCOP1 the conducting path is formed (GO particles contact each other and link with COMCOP1 chains) increasing conductivity, permittivity and polarization of composites. The value of dielectric constant measured at our laboratory for neat COMCOP1 for 1 kHz at 30 °C is 3.13. For COMCOP1/GO composites with 10 wt.% and 12 wt.% GO loading (see Fig. 3.23), the values of dielectric constant were 12.3 and 36.03 at 1 kHz and 30 °C, respectively. Whereas, the maximum values of dielectric constant were 13.42 and 42.95 at 1 kHz and 100 °C, respectively. That of COMCOP1 16 wt.% GO loading is 638.4 at 100 Hz and 100 °C. The π bond in the GO is loosely attached compared to the sigma bond, and it is easily polarized. So, it is revealed that with increasing temperature dielectric constant increases. This behavior indicated that polarization is higher at lower frequencies in the applied field when COMCOP1/GO composite contains more GO. It is clear that the value of dielectric constant decreases sharply up

to about 600 Hz and no changes are observed beyond this point. When the dielectric constant (ε′= 4.3 at 100ºC) of COMCOP1 compared to that of composites, it can be said that the dielectric constant of the composites increases with the increase in the amount of GO and the dielectric constant remains constant at high frequencies. The values of dielectric loss factor for COMCOP1/GO composites with 12 wt.% GO loading were measured at 35 °C, 85 ºC and 100 ºC for 1 kHz and are indicated in Fig. 3.23, and the values of dielectric loss factor were found as 1475.2, 7513.2 and 9368.5, respectively. Whereas, the maximum value of dielectric loss factor measured at our laboratory for neat COMCOP1 at 30 °C for 1 kHz is 0.333. The dielectric loss factor, ε″, increases depending upon increasing temperature while decreases with increasing frequency due to friction between dipoles. The frictional effect leads to a loss of energy named dielectric loss, which is dissipated as heat in the composite [52]. In this regard, dielectric loss factor, especially due to the limited chain movement of coumarin-based methacrylate and methyl methacrylate units with ester functional groups is less effective under the glass transition temperature of the polymer and slowly increases with temperature at low frequencies. Because dielectric loss factor is low at higher frequencies, it remains almost constant even if the temperature increases.

Fig. 3.24 shows the dependence of ε′and ε′′ as a function of frequency for COMCOP2 doped GO 13.6 wt.% at 100 ºC. From those figures, it is clear that the dielectric constant decreased monotonically with increasing frequency and attains a constant value at higher frequencies. The value of dielectric constant measured at 30 °C for 1 kHz is 4.67. Similar behavior was also observed for most polymers [53]. As the applied field is raised, it is known that the initial value of dielectric constant for polar materials is high depending upon the polarization effects, then it begins to drop, which could be due to the dipoles not able to follow the field variations at higher frequencies [54]. Frequency dependence of dielectric loss at 100 ºC for COMCOP2 doped GO 13.6 wt.% has been given in Fig. 3.24. The dielectric loss at 100 Hz for this composite was 8078.6. A moderate decrease in dielectric loss from 8078.6 to 2570.0 was observed. As the frequency increased from 100 Hz to 2 kHz, dielectric loss values decreased for this composite. Similar behavior has been recorded in the literature [55]. The exponential factor *s* is investigated as a function of temperature in order to determine the origin of the conduction mechanism. Values of *s* at two different temperatures such as 85 ºC and 100 ºC for the investigated COMCOP1/GO 12 wt.% were calculated from the slopes of linear part of the relation lnF-lnσac (Fig. 3.25). As seen in Fig. 3.25, *s* values estimated from slope of graph plotted for $\ln\sigma_{ac}$ (S/cm) versus lnF at 85 ºC and 100 ºC for COMCOP1/GO 12 wt.% are 0.518 and 0.288, respectively. As the temperature increases, it is understood that the plateau region of dc conductivity extends towards higher frequencies, while the charge carriers maintain their mobility even at these frequencies. The electrical conductivity follows the power law [56].

$$\sigma_{ac} = \sigma_{dc} + A\omega^{s} \qquad (5)$$

In equation (5), σ_{dc} is direct current conductivity, A is a constant and *s* is power law exponent. So, the ac conductivity data usage is fitted from the above equation. This event indicates that the correlated barrier hopping (CBH) conduction mechanism of this composite is predominant, as the *s* value decreases with increasing temperature. The conduction mechanism based on the nature of the variation of parameter with temperature is suggested by a few theoretical models. The small polaron (SP), the quantum mechanical tunneling (QMT), the overlapping large polaron (OLP) and the correlated barrier hopping (CBH) are known to be among the most applicable models [57]. In this regard, those theoretical models have different behaviors. Among these models, the QMT model has temperature independent behavior. In the SP model, it is based on the predominance of conduction due to increased temperature. It is important to realize that the CBH model takes into account that carriers jump over a potential barrier between two regions that separate them [58]. In the light of these information, the trend of COMCOP1/GO 12 wt.% can be said to be decreasing with temperature, the CBH model has a behavior closer to the conduction mechanism.

Fig. 3.26a and 3.26b show the current–voltage relationship of COMCOP1/GO and COMCOP2/GO composites at different temperature range 300K≤T≤ 370K, respectively. All the prepared composites showed a semiconducting behavior at all temperature ranges. The filling amount contained at least 10 wt.% GO for dc conductivity to occur in GO filled composites in the composites that we have prepared. Here, for all the samples, the current (A) increases linearly when the potential difference (V) applied as well as the % of GO incorporated into the polymer matrices were increased. In this regard, the conductivity increased from 300 K to 370 K showing semiconducting behavior depending upon the heating. The dc conductivity of composites is much greater than the pure copolymers and the magnitude of conductivity increases with increase in content of particles up to a certain weight percentage (16 wt.%). As shown in Fig. 3.26a, all the samples showed a linear variation of current–voltage (I–V), and this event indicates that the attachment of GO particles into the polymer exhibits an Ohmic conduction. The maximum current values for COMCOP1/GO 12 wt.% and 16 wt.% composites were estimated at 0.0181 A and 8.53x10-4 A at 1 V for 298 K, respectively. Whereas, those of COMCOP2/GO 13.6 wt.% and 15 wt.% composites as seen in Fig. 3.26b were $3.03x10^{-5}$ and 0.0026 A at 1 V for 298 K, respectively. So, the current increased with increase in the concentration of GO. It is suggested that the high electrical conductivity of the composite containing 16 wt.% GO is mainly due to the strong interface interaction between GO and the copolymer bearing polar groups. It is also known that the conductivity of a composite depends on the crystal structure and morphology [59].

In order to reveal the temperature dependence of the change in conductivity of composites prepared with the addition of GO, DC-temperature curves were obtained. The conductivity curves were formed with Arrhenius equation [60, 61].

$$\sigma_{dc} = \sigma_o \exp(-E_a/k_B T) \qquad (6)$$

From equation (6), σ_{dc} is direct current conductivity, k is Boltzmann constant, and E_a indicates activation energy. In the light of the data obtained, $\ln\sigma_{dc}$ -1000/T graphs were drawn for all samples, and activation energies corresponding to the decomposition degrees were calculated. Fig. 3.27 and 3.28 show $\ln\sigma_{dc}-1000/T$ graphs of the composite systems. From above equation (6), −Ea/kB, is equal to slope of plotted graphs. On the other hand, the activation energy is obtained by multiple of 0.086. Fig. 3.27 a and b indicate $\ln\sigma_{dc}-1000/T$ of COMCOP1 composites with 10 wt.% and 12 wt.% loading of GO particles, respectively. As seen in Fig. 3.27 a and b, the electrical conductivity of the samples increased with the addition of GO particles. The highest conductivity value was found in COMCOP1/GO 12 wt.% composite. In addition, it was clearly seen that the conductivity increased with increasing temperature. The E_a values estimated for COMCOP1 loaded GO 10 wt.% and 12 wt.% are 0.129 and 0.076 eV, respectively. These values can be said to have very low activation energies compared to those of some composites [62]. The low activation energies estimated suggest that both segmental motion of polymer molecules and the hopping mechanism contribute equally in coupled form of transportation for COMCOP1/GO composites. Also, this behavior may be due to the fact that the addition of more amounts of GO forms charge transfer complexes in the host lattice [62]. The charge transfer in the composite creates more electrical conductivity by providing additional loads in the lattice. In other words, this behavior means that the activation energy required for transmission decreases. Addition of GO increases carrier concentration and increases carrier mobility by possibly reducing the double Schottky barrier at the carrier boundaries, which provides a high electrical conductivity for composites [63]. Fig. 3.28a and b show the variation of activation energy as a function of GO wt.% for COMCOP2/GO composites. COMCOP2/GO 13.6 wt.% composite shows lowest activation energy (0.0580 eV) compared to other prepared composites. This behavior indicates that there may be more than one conduction center depending on the filler concentration in the composite. According to Jonscher [42], he emphasized that values greater than 0.8 eV may have ionic transport and below this value an electronic transmission mechanism. In addition, the excess of GO particles in the composite realizes the tendency to make direct contact from the formation of paths that provide more conductivity, and this behavior causes more electrical conductivity. The E_a values estimated for COMCOP2 loaded GO 12 wt.% and 13.6 wt.% are 0.0580 eV and 0.0859 eV, respectively.

CONCLUSION

This research is primarily concerned with the study of the effects of graphite oxide nanoparticles on the electrical and thermal properties of coumarin based copolymers. The copolymers; P(COUMA2.4%, 24%, 36%, 49% and 65%-co-MMA) were prepared by free radical polymerization method, and characterized by FT-IR, ^{1}H-NMR, UV-vis and thermal analysis techniques (TGA and DSC).

Among the series of copolymers, P(COUMA49%-co-MMA) (COMCOP1) and P(COUMA36%-co-MMA) (COMCOP2) were prepared and characterized using FT-IR, ^{1}H-NMR and UV-vis techniques. The photocycloaddition. thermal stabilities, thermal degradation kinetic studies and electrical investigations were carried out. Their composites loaded GO were prepared. In this research, we indicated that well-defined SCPM could occur via the intrachain photodimerization of coumarin groups upon UV irradiation at 365 nm diluted solution of COMCOP1. The photodimerization of coumarin moieties in the copolymer structure was confirmed by UV-vis, ^{1}H-NMR and FT-IR instruments. The new resonance peak appeared at 3.45 ppm, which are assigned to the formation of cyclobutane ring – another important evidence of dimerization. In this study, the photodimerization processes of coumarin units in the dilute solution within $CDCI_3$ of COMCOP1 indicated that the copolymer was not crosslinked. Thermal stabilities of the COMCOP1 and COMCOP2 and their composites loaded GO were studied using TGA and DSC, the results show that COUMA:MMA = 49:51 and 36:64 ratios is thermally more stable than their composites, also the T_g values increased with the increase in COUMA content in the COMCOP1 and COMCOP2. Thermogravimetric analysis and non-isothermal multiple heating rate methods were used to examine the thermal stability and thermal degradation kinetics of COMCOP1 and COMCOP1/GO 12wt.% after adding GO. Hence, it was observed that the thermal stability of COMCOP1/GO 12wt.% composites with different GO loadings has decreased as compared to COMCOP1. Activation energies and slopes were estimated using model-free methods. The activation energy values are consistent with the range of values obtained by the FWO and KAS methods and are very close to their average values equal to 93.47 and 87.07 kJ mol^{-1}, respectively; the values of the slope were also contained in a period of average value. The experimental results showed that the values of the kinetic parameters are good agreement, and FWO and KAS, which are the model-free methods satisfactorily defined the complexity of the decomposition process. Dielectric constant (ε') and dielectric loss factor (ε") have been measured on neat COMCOP1 and COMCOP1 containing different weight ratio of GO at different temperatures and frequencies. It has been found that both the dielectric constant and dielectric loss increases with the increasing amount of GO in the composite with the increasing content of filler. The activation energy values based on dc conductivity were decreased from 0.206 to 0.069

eV with the increasing amount of GO. In addition, the E_a values estimated for COMCOP2 loaded GO 12 wt.% and 13.6 wt.% are 0.0580 eV and 0.0859 eV, respectively.

REFERENCES

[1] Correa, R., Gonzalez, G., and Dougar, V. (1998). Emulsion polymerization in a microwave reactor, *Polymer*, Vol. 39 (6-7), pp: 1471-1474.

[2] Qiu, J., Charleux, B., and Matyjaszewski, K. (2001). Controlled/living radical polymerization in aqueous media: homogeneous and heterogeneous systems, *Progress in Polymer Science*, Vol. 26 (10), pp: 2083-2134.

[3] Jagur-Grodzinski, J. and Smid, J. (2002). Michael Szwarc, 1909–2000, *Journal of Polymer Science Part A: Polymer Chemistry*, Vol. 40 (13), pp: 2099-2100. doi: https://doi.org/10.1002/pola.10292.

[4] Patten, T.E. and Matyjaszewski, K. (1999). Copper (I)-catalyzed atom transfer radical polymerization, *Accounts of chemical research*, Vol. 32 (10), pp: 895-903.

[5] Ran, J., Wu, L., Zhang, Z., and Xu, T. (2014). Atom transfer radical polymerization (ATRP): A versatile and forceful tool for functional membranes, *Progress in Polymer Science*, Vol. 39 (1), pp: 124-144.

[6] Barthet, C., Hickey, A.J., Cairns, D.B., and Armes, S.P. (1999). Synthesis of novel polymer–silica colloidal nanocomposites via free-radical polymerization of vinyl monomers, *Advanced Materials*, Vol. 11 (5), pp: 408-410.

[7] Costa, T.M., Tavares, L.B.B., and de Oliveira, D. (2016). Fungi as a source of natural coumarins production, *Applied microbiology and biotechnology*, Vol. 100 (15), pp: 6571-6584.

[8] Cuevas, J.M., Seoane-Rivero, R., Navarro, R., and Marcos-Fernández, Á. (2020). Coumarins into Polyurethanes for Smart and Functional Materials, *Polymers*, Vol. 12 (3), pp: 630.

[9] Teixeira, E., Lima, J.C., Parola, A.J., and Branco, P.S. (2018). Incorporation of coumarin-based fluorescent monomers into co-oligomeric molecules, *Polymers*, Vol. 10 (4), pp: 396.

[10] Cao, D., Liu, Z., Verwilst, P., Koo, S., Jangjili, P., Kim, J.S., and Lin, W. (2019). Coumarin-Based Small-Molecule Fluorescent Chemosensors, *Chemical reviews*, Vol. 119 (18), pp: 10403-10519. doi: 10.1021/acs.chemrev.9b00145.

[11] Shaabani, A., Ghadari, R., Rahmati, A., and Rezayan, A. (2009). Coumarin synthesis via Knoevenagel condensation reaction in 1, 1, 3, 3-N, N, N′, N′-tetramethylguanidinium trifluoroacetate ionic liquid, *Journal of the Iranian Chemical Society*, Vol. 6 (4), pp: 710-714.

[12] Hong, S., Yuan, Y., Yang, Q., Chen, L., Deng, J., Chen, W., Lian, H., Mota-Morales, J.D., and Liimatainen, H. (2019). Choline chloride-zinc chloride deep eutectic solvent mediated preparation of partial O-acetylation of chitin nanocrystal in one step reaction, *Carbohydrate polymers*, Vol. 220 211-218.

[13] Palaniappan, S. and Chandra Shekhar, R. (2004). Synthesis of 7-hydroxy-4-methyl coumarin using polyaniline supported acid catalyst, *Journal of Molecular Catalysis A: Chemical*, Vol. 209 (1), pp: 117-124. doi: https://doi.org/10.1016/j.molcata.2003.08.006.

[14] Venkatesan, S., Ranjithkumar, B., Shanmugam, R., and Basha, K. (2014). Synthesis, characterization, thermal stability and antibacterial activity of coumarin based methacrylate copolymers, *Chinese Journal of Polymer Science*, Vol. 32. doi: 10.1007/s10118-014-1515-9.

[15] Ayaz, N., Bezgin, F., and Demirelli, K. (2012). Polymers Based on Methacrylate Bearing Coumarin Side Group: Synthesis via Free Radical Polymerization, Monomer Reactivity Ratios, Dielectric Behavior, and Thermal Stabilities, *ISRN Polymer Science*, Vol. 2012 352759. doi: 10.5402/2012/352759.

[16] Najjar, R. and Bigdeli, E. (2018). Synthesis of novel core-shells of PMMA with coumarin based liquid crystalline side chains and PMMA shell as electro-optical materials,

European Polymer Journal, Vol. 104 136-146. doi: https://doi.org/10.1016/j.eurpolymj.2018.05.012.

[17] Cazin, I., Rossegger, E., Guedes de la Cruz, G., Griesser, T., and Schlögl, S. (2021). Recent Advances in Functional Polymers Containing Coumarin Chromophores, *Polymers*, Vol. 13 (1), pp: 56.

[18] Karkkainen, A., Hormi, O., and Rantala, J., (2000). *Covalent bonding of coumarin molecules to sol-gel matrices for organic light-emitting device applications*, SPIE,

[19] Zhang, J., Zou, Q., and Tian, H. (2013). Photochromic materials: more than meets the eye, *Advanced Materials*, Vol. 25 (3), pp: 378-399.

[20] de Oliveira, A.D. and Beatrice, C.A.G. (2018). Polymer nanocomposites with different types of nanofiller, *Nanocomposites-Recent Evolutions*, Vol. 103-104.

[21] Bashir, T., (2013). *Conjugated polymer-based conductive fibers for smart textile applications*, Chalmers University of Technology,

[22] Cobos, M., González, B., Fernández, M.J., and Fernández, M.D. (2017). Chitosan–graphene oxide nanocomposites: Effect of graphene oxide nanosheets and glycerol plasticizer on thermal and mechanical properties, *Journal of Applied Polymer Science*, Vol. 134 (30), pp: 45092.

[23] Lojka, M., Lochman, B., Jankovský, O., Jiříčková, A., Sofer, Z., and Sedmidubský, D. (2019). Synthesis, Composition, and Properties of Partially Oxidized Graphite Oxides, *Materials (Basel, Switzerland)*, Vol. 12 (15), pp: 2367. doi: 10.3390/ma12152367.

[24] Ebnesajjad, S., *4 - Surface and Material Characterization Techniques*, in *Surface Treatment of Materials for Adhesion Bonding*, S. Ebnesajjad, Editor 2006, William Andrew Publishing: Norwich, NY. p. 43-75.

[25] Höhne, G., Hemminger, W.F., and Flammersheim, H.-J., (2013). *Differential scanning calorimetry*, Springer Science & Business Media,

[26] Bourahla, A., Saiter, J.M., and Vautier, C. (2001). Electrical conductivity of polymethyl-3selenophene, *Materials Chemistry and Physics*, Vol. 69 (1), pp: 163-165. doi: https://doi.org/10.1016/S0254-0584(00)00388-6.

[27] Alyamani, A. and Lemine, O., *FE-SEM characterization of some nanomaterial*, in *Scanning electron microscopy*2012, IntechOpen.

[28] Kaushik, M., Fraschini, C., Chauve, G., Putaux, J.-L., and Moores, A., *Transmission Electron Microscopy for the Characterization of Cellulose Nanocrystals*, in *The Transmission Electron Microscope - Theory and Applications*2015.

[29] Choe, H.-C. and Yeung, K. (2010). Nanotechnology in biomedical applications-A Review, *International Journal of Nano and Biomaterials*, Vol. 3 119-139. doi: 10.1504/IJNBM.2010.037801.

[30] *X-ray diffraction (XRD) basics and application*, 2020.

[31] Essaïdi, Z., Krupka, O., Iliopoulos, K., Champigny, E., Sahraoui, B., Sallé, M., and Gindre, D. (2013). Synthesis and functionalization of coumarin-containing copolymers for second order optical nonlinearities, *Optical Materials*, Vol. 35 (3), pp: 576-581. doi: https://doi.org/10.1016/j.optmat.2012.10.011.

[32] Ramani M R S C, A., Chanda, B., Velu, S., and Sivasanker, S. (1999). One-pot synthesis of coumarins. Catalysis by the solid base, calcined Mg-Al hydrotalcite, *Green Chem.*, Vol. 1 163-165. doi: 10.1039/A903173A.

[33] Sollka, L. and Lienkamp, K. (2021). Progress in the Free and Controlled Radical Homo- and Co-Polymerization of Itaconic Acid Derivatives: Toward Functional Polymers with Controlled Molar Mass Distribution and Architecture, *Macromolecular Rapid Communications*, Vol. 42 (4), pp: 2000546. doi: https://doi.org/10.1002/marc.202000546.

[34] Fomine, S., Rivera, E., Fomina, L., Ortiz, A., and Ogawa, T. (1998). Polymers from coumarines: 4. Design and synthesis of novel hyperbranched and comb-like coumarin-containing polymers, *Polymer*, Vol. 39 (15), pp: 3551-3558.

[35] Ayaz, N., Bezgin, F., and Demirelli, K. (2012). Polymers based on methacrylate bearing coumarin side group: synthesis via free radical polymerization, monomer reactivity ratios, dielectric behavior, and thermal stabilities, *International Scholarly Research Notices*, Vol. 2012.

[36] Ashenagar, S., Ziaee, F., and Jalilian, S.M. (2013). Calculation of reactivity ratios of methacrylic acid-ethyl acrylate copolymer by on-line quantitative 1 H NMR spectroscopy, *Iranian Polymer Journal*, Vol. 22 (9), pp: 635-639.

[37] Biryan, F., Pihtili, G., and Demirelli, K. (2020). Thermal studies and influence of the thermal decomposition on dielectric properties of a new coumarin copolymers, *Journal of Thermal Analysis and Calorimetry*, Vol. 139 (6), pp: 3871-3885. doi: 10.1007/s10973-019-08993-0.

[38] Park, S., Palai, A.K., Park, J., Jung, J.H., and Pyo, S. (2019). Synthesis and characterization of photo-crosslinkable coumarin-containing polymer dielectric for organic transistors, *Organic Electronics*, Vol. 66 169-174.

[39] Trenor, S.R., Long, T.E., and Love, B.J. (2004). Photoreversible chain extension of poly (ethylene glycol), *Macromolecular Chemistry and Physics*, Vol. 205 (6), pp: 715-723.

[40] Hummers Jr, W.S. and Offeman, R.E. (1958). Preparation of graphitic oxide, *Journal of the American Chemical Society*, Vol. 80 (6), pp: 1339-1339.

[41] Sali, S., Mackey, H.R., and Abdala, A.A. (2019). Effect of Graphene Oxide Synthesis Method on Properties and Performance of Polysulfone-Graphene Oxide Mixed Matrix Membranes, *Nanomaterials*, Vol. 9 (5), pp: 769.

[42] Wu, C., Li, J., Fan, Y., Xing, J., Gu, H., Zhou, Z., Lu, X., Zhang, Q., Wang, L., and Jiang, W. (2019). The effect of reduced graphene oxide on microstructure and thermoelectric properties of Nb-doped A-site-deficient SrTiO3 ceramics, *Journal of alloys and compounds*, Vol. 786 884-893.

[43] Xu, H., Yang, B., Wang, J., Guang, S., and Li, C. (2007). Preparation, Tg improvement, and thermal stability enhancement mechanism of soluble poly (methyl methacrylate) nanocomposites by incorporating octavinyl polyhedral oligomeric silsesquioxanes, *Journal of Polymer Science Part A: Polymer Chemistry*, Vol. 45 (22), pp: 5308-5317.

[44] Anet, R. (1962). The photodimers of coumarin and related compounds, *Canadian Journal of Chemistry*, Vol. 40 (7), pp: 1249-1257.

[45] Venkatesan, S., Ranjithkumar, B., Rajeshkumar, S., and Basha, K.A. (2014). Synthesis, characterization, thermal stability and antibacterial activity of coumarin based methacrylate copolymers, *Chinese Journal of Polymer Science*, Vol. 32 (10), pp: 1373-1380.

[46] Ling, J., Rong, M.Z., and Zhang, M.Q. (2012). Photo-stimulated self-healing polyurethane containing dihydroxyl coumarin derivatives, *Polymer*, Vol. 53 (13), pp: 2691-2698.

[47] López-Vilanova, L., Martinez, I., Corrales, T., and Catalina, F. (2014). Photoreversible crosslinking of poly-(ethylene-butyl-acrylate) copolymers functionalized with coumarin chromophores using microwave methodology, *Reactive and Functional Polymers*, Vol. 85 28-35.

[48] He, J. and Zhao, Y. (2011). Light-responsive polymer micelles, nano-and microgels based on the reversible photodimerization of coumarin, *Dyes and Pigments*, Vol. 89 (3), pp: 278-283.

[49] Hughes, T., Simon, G., and Saito, K. (2019). Photocuring of 4-arm coumarin-functionalised monomers to form highly photoreversible crosslinked epoxy coatings, *Polymer Chemistry*, Vol. 10 (17), pp: 2134-2142.

[50] Vyazovkin, S., Burnham, A.K., Criado, J.M., Pérez-Maqueda, L.A., Popescu, C., and Sbirrazzuoli, N. (2011). ICTAC Kinetics Committee recommendations for performing kinetic computations on thermal analysis data, *Thermochimica Acta*, Vol. 520 (1-2), pp: 1-19.[51] Kandare, E., Deng, H., Wang, D., and Hossenlopp, J.M. (2006). Thermal

stability and degradation kinetics of poly (methyl methacrylate)/layered copper hydroxy methacrylate composites, *Polymers for advanced technologies*, Vol. 17 (4), pp: 312-319.

[52] Laachachi, A., Cochez, M., Ferriol, M., Leroy, E., Cuesta, J.L., and Oget, N. (2004). Influence of Sb2O3 particles as filler on the thermal stability and flammability properties of poly (methyl methacrylate)(PMMA), *Polymer Degradation and Stability*, Vol. 85 (1), pp: 641-646.

[53] Baskaran, R., Selvasekarapandian, S., Hirankumar, G., and Bhuvaneswari, M. (2004). Dielectric and conductivity relaxations in PVAc based polymer electrolytes, *Ionics*, Vol. 10 (1-2), pp: 129-134.

[54] Shubha, A., Manohara, S., and Gerward, L. (2017). Influence of polyvinylpyrrolidone on optical, electrical, and dielectric properties of poly (2-ethyl-2-oxazoline)-polyvinylpyrrolidone blends, *Journal of Molecular Liquids*, Vol. 247 328-336.

[55] Ramya, C., Savitha, T., Selvasekarapandian, S., and Hirankumar, G. (2005). Transport mechanism of Cu-ion conducting PVA based solid-polymer electrolyte, *Ionics*, Vol. 11 (5-6), pp: 436-441.

[56] Tareev, B. and Tareev, B., *Physics of Dielectric Materials, Mir Publ*, 1979, Mascow.

[57] Thomas, P., Ashokbabu, A., and Vaish, R. (2019). Structural, thermal and dielectric properties and thermal degradation kinetics of nylon 11/CaCu 3 Ti 4 O 12 (CCTO) nanocomposites, *Journal of Thermal Analysis and Calorimetry*, Vol. 1-13.

[58] Ghosh, A. (1990). Transport properties of vanadium germanate glassy semiconductors, *Physical Review B*, Vol. 42 (9), pp: 5665.

[59] Imran, Z., Rasool, K., Batool, S., Ahmad, M., and Rafiq, M. (2015). Effect of different electrodes on the transport properties of ZnO nanofibers under humid environment, *AIP Advances*, Vol. 5 (11), pp: 117214.

[60] Gupta, K., Chakraborty, G., Jana, P., and Meikap, A. (2009). Direct current conductivity of polyaniline-cobalt chloride nanocomposite prepared by wet chemical route, Vol.

[61] Kahouli, A., Sylvestre, A., Jomni, F., Yangui, B., and Legrand, J. (2012). Experimental and theoretical study of AC electrical conduction mechanisms of semicrystalline parylene C thin films, *The Journal of Physical Chemistry A*, Vol. 116 (3), pp: 1051-1058.

[62] Prabu, M., Banu, I.S., Gobalakrishnan, S., and Chavali, M. (2013). Electrical and ferroelectric properties of undoped and La-doped PZT (52/48) electroceramics synthesized by sol–gel method, *Journal of alloys and compounds*, Vol. 551 200-207.

[63] Mohan, K.R., Achari, V., Rao, V., and Sharma, A. (2011). Electrical and optical properties of (PEMA/PVC) polymer blend electrolyte doped with NaClO4, *Polymer testing*, Vol. 30 (8), pp: 881-886.

APPENDICES

APPENDIX- 1

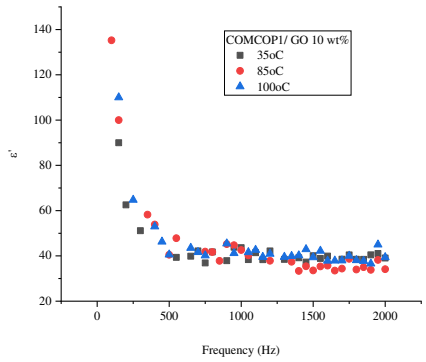

Figure A 1. dependence of dielectric constant on frequency for COMCOP1 composites loaded with 10 wt.% GO at different temperatures.

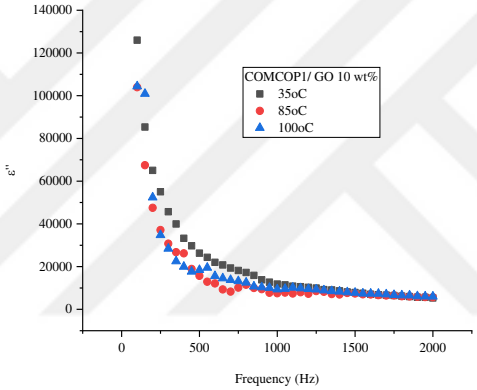

Figure A 2. dependence of dielectric loss on frequency for COMCOP1 composites loaded with 10 wt.% GO at different temperatures

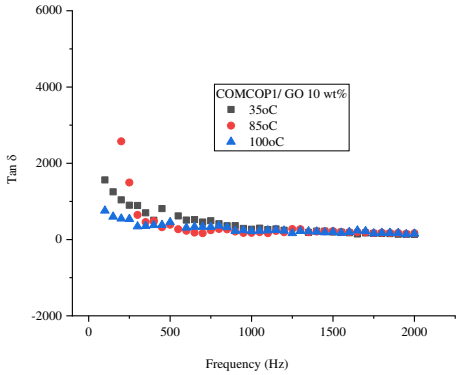

Figure A 3. tangent loss as a function of frequency for COMCOP1 composites loaded with 10 wt.% GO at different temperatures

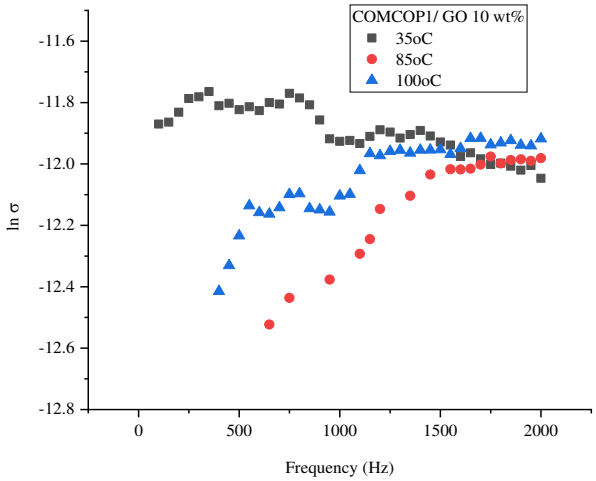

Figure A 4. variation of AC conductivity of COMCOP1 composites with frequency for 10 wt.% GO at different temperatures.

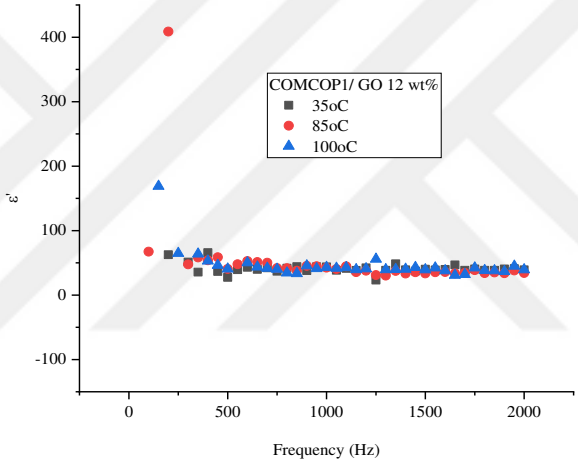

Figure A 5. dependence of dielectric constant on frequency for COMCOP1/ GO 12 wt.% composites at different temperatures

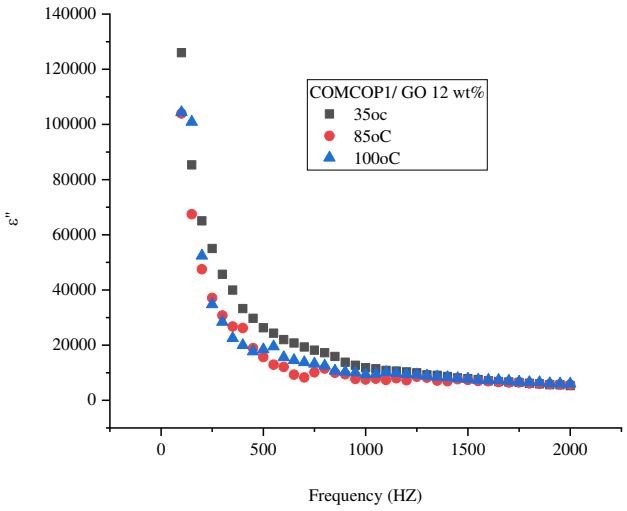

Figure A 6. dependence of dielectric loss on frequency for COMCOP1/ GO 12 wt.% composites at different temperatures

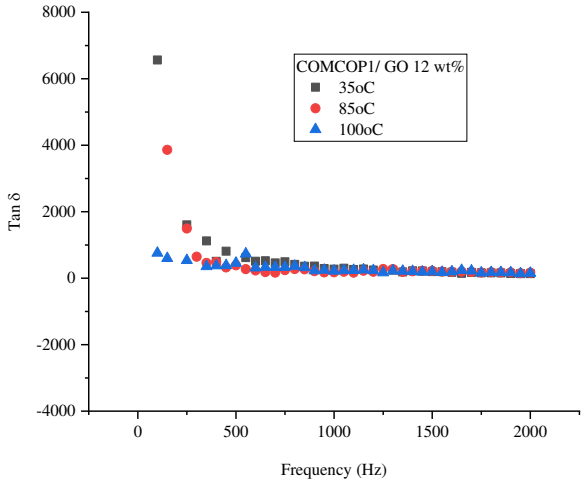

Figure A 7. Dependence of tangent loss on frequency for COMCOP1/GO 12 wt% composites at different temperatures

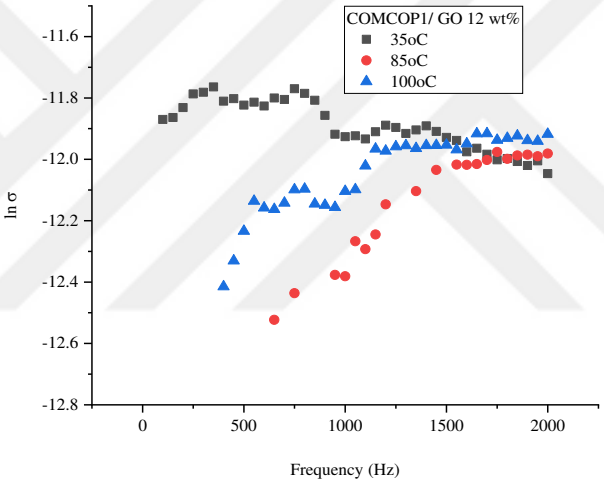

Figure A 8. variation of AC conductivity of COMCOP1/ GO 12 wt.% composites with frequency at different temperatures

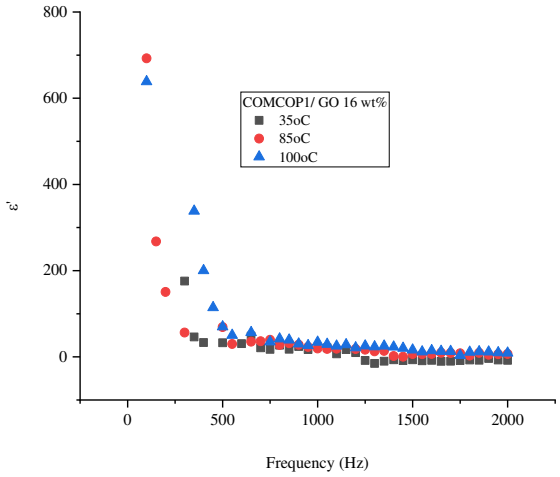

Figure A 9. dependence of dielectric constant on frequency for COMCOP1/ GO 16 wt.% composites at different temperatures

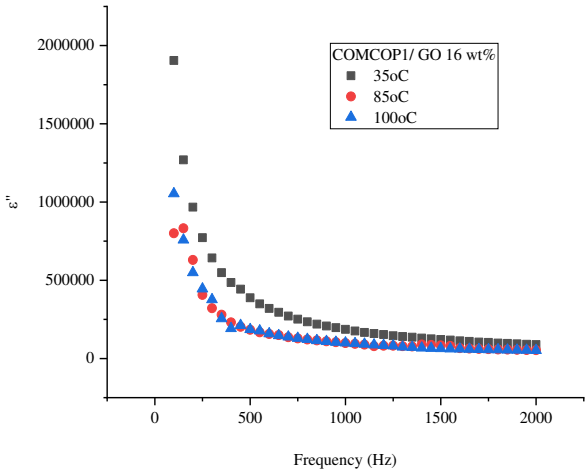

Figure A 10. dependence of dielectric loss on frequency for COMCOP1/ GO 16 wt.% composites at different temperatures

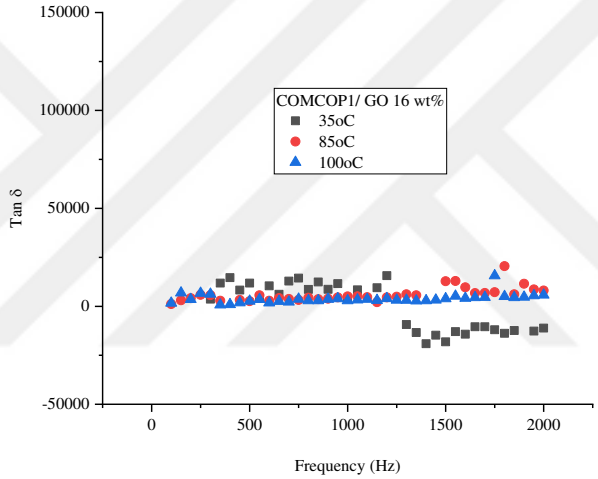

Figure A 11. dependence of tangent loss on frequency for COMCOP1/ GO 16 wt.% composites at different temperatures

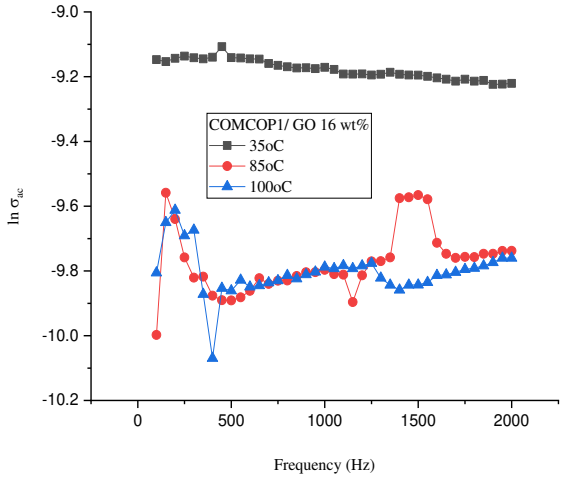

Figure A 12. Variation of AC conductivity of COMCOP1/ GO 16 wt% composites with frequency at different temperatures

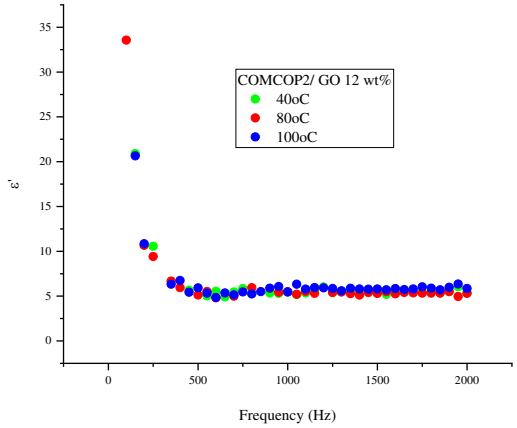

Figure A 13. dependence of dielectric constant on frequency for COMCOP2/ GO 12 wt.% at different temperatures

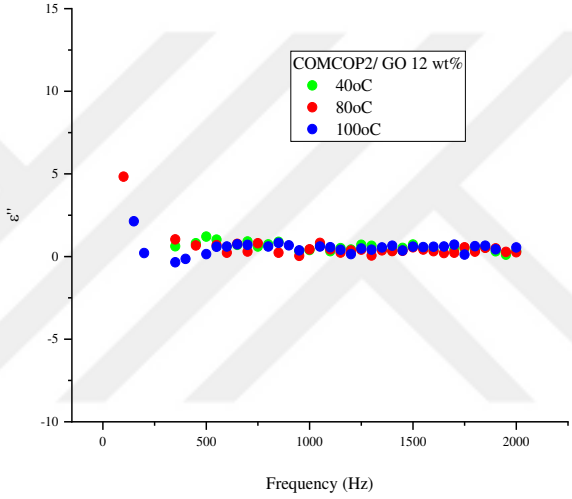

Figure A 14. dependence of dielectric loss on frequency for COMCOP2/ GO 12 wt.% at different temperatures

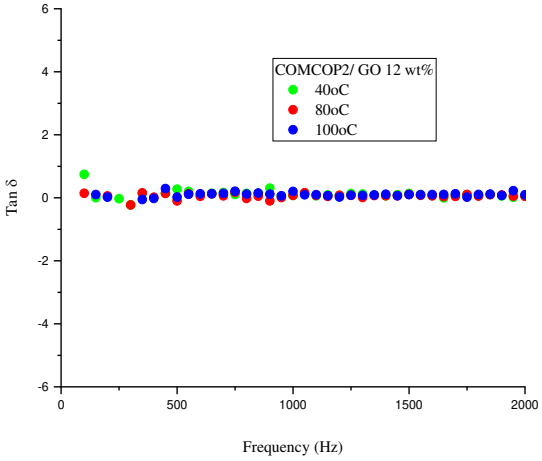

Figure A 15. dependence of tangent loss on frequency for COMCOP2/ GO 12 wt.% at different temperatures

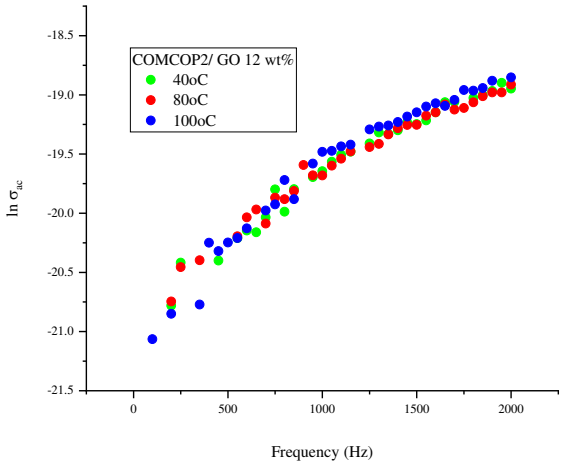

Figure A 16. variation of AC conductivity with frequency for COMCOP2/ GO 12 wt. % at different temperatures

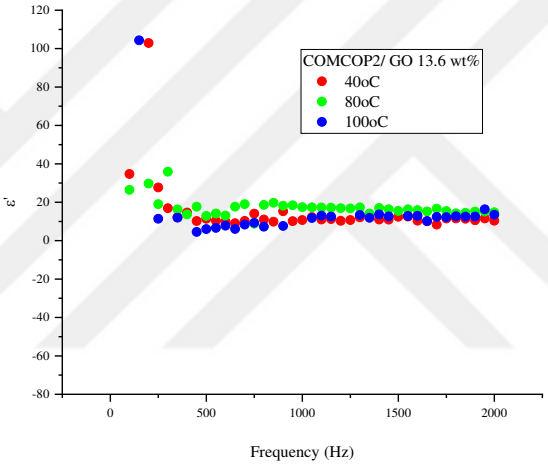

Figure A 17. dependence of dielectric constant on frequency for COMCOP2/ GO 13.6 wt.% at different temperatures

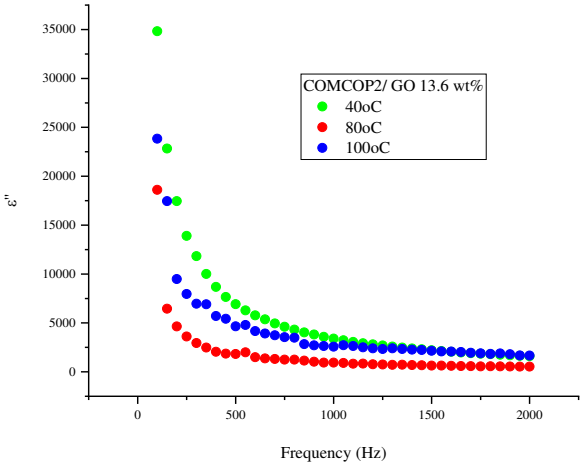

Figure A 18. dependence of dielectric loss on frequency for COMCOP2/ GO 13.6 wt.% at different temperatures

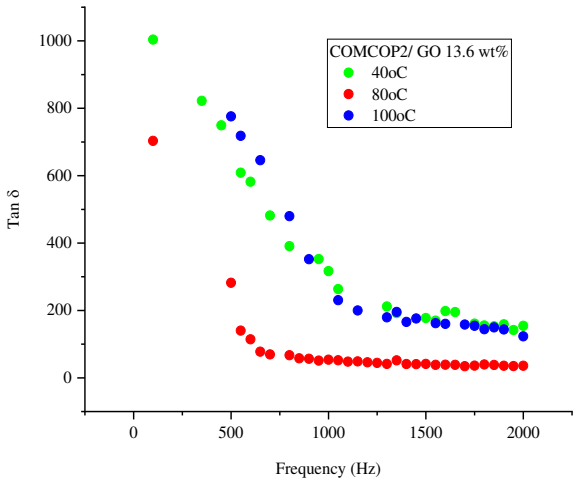

Figure A 19. dependence of tangent loss on frequency for COMCOP2/ GO 13.6 wt.% at different temperatures

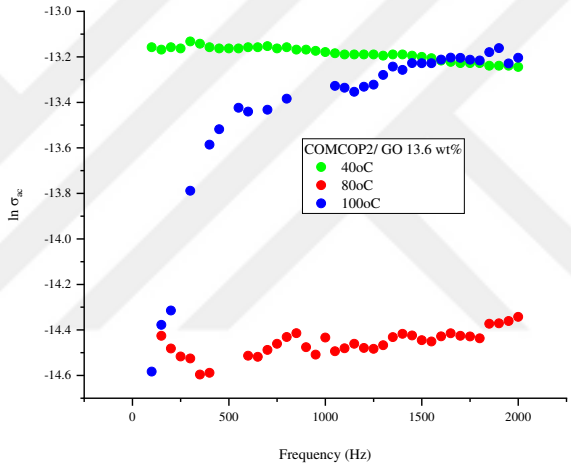

Figure A 20. Variation of AC conductivity with frequency for COMCOP2/ GO 13.6 wt.% at different temperatures

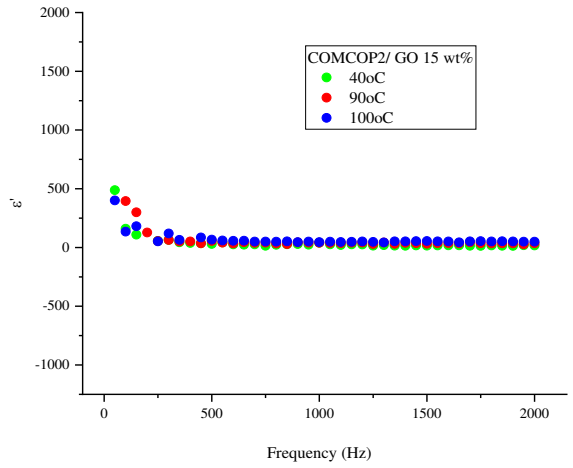

Figure A 21. Dependence of dielectric loss on frequency for COMCOP2/ GO 15 wt.% at different temperatures

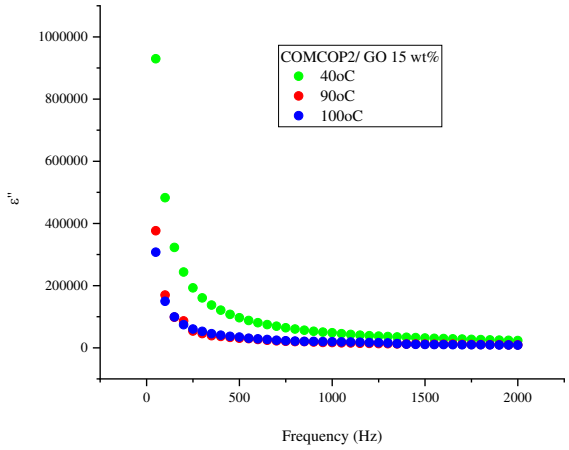

Figure A 22. Dependence of dielectric loss on frequency for COMCOP2/ GO 15 wt.% at different temperatures

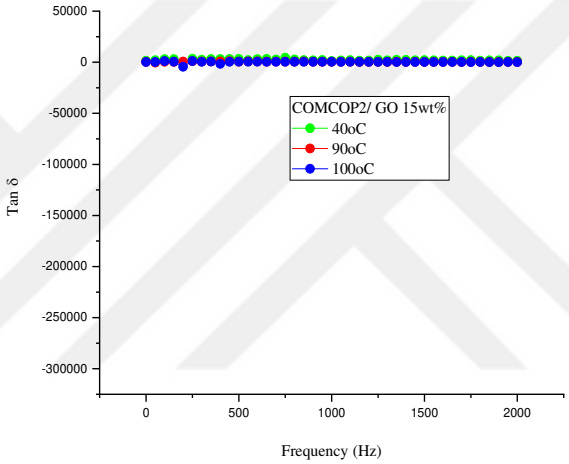

Figure A 23. Dependence of tangent loss on frequency for COMCOP2/ GO 15 wt.% at different temperatures

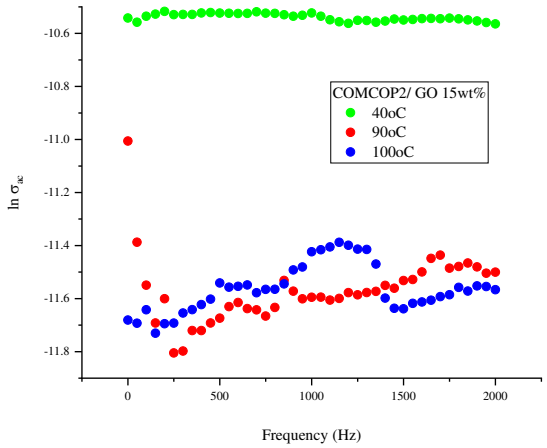

Figure A 24. Variation of AC conductivity with frequency for COMCOP2/ GO 15 wt.% at different temperatures

CURRICULUM VITAE

AbdulHaleem AbdulKareem AHMAD

[redacted]

[redacted]

[redacted]

[redacted]

[redacted]

ACADEMIC ACTIVITIES

Journal Papers and Conferences

1. **AHMAD Abdulhaleem A.**, Demirelli K. (2021) Effects of graphite oxide on thermal and electrical behaviors of coumarin based methacrylate copolymers: Its single-chain polymer molecule via intramolecular cyclobutane formation, *Journal of polymers for advanced technology* 2021

2. Demirelli K., **AHMAD Abdulhaleem A**. (2020) The effect of end group and graphene on dielectric properties and thermal degradation of poly(benzylmethacrylate) prepared by ATRP method, *Polymer Bulletin Journal, 2021*
3. **AHMAD, Abdulhaleem A.**, ABUBAKAR, Abdullahi Musa and DEMIRELLI K. Photodimerization and effects of graphite oxide loadings on the thermal behavior, electrical conductivity of a methacrylate copolymer system containing coumarin moieties. **MSNG Conference 2021**
4. ABUBAKAR, Abdullahi Musa, **AHMAD, Abdulhaleem A. 2021;** Synthesis, characterization and thermal stabilities of P(DEAMSt16%-co-St), linear copolymer precursor and SCPM-ball type CoPc. **PCFM Conference 2021**
5. ABUBAKAR, Abdullahi Musa, **AHMAD, Abdulhaleem A.** and DEMIRELLI K. 2021; Preparation of SCP ball-type CoPc and their Graphite oxide composites: Their characterization and electrical behaviors. **MSNG Conference 2021**